UNIVERSITA' DEGLI STUDI DI PAVIA

GHENT UNIVERSITY

Finite Element Analysis of self-expanding braided wirestent

by

Michele Conti

Supervisors: Prof. Pascal Verdonck (Ghent University)
Prof. Ferdinando Auricchio (Universita' degli Studi di Pavia)
Co-supervisor: Eng. Matthieu De Beule (Ghent University)

A Thesis submitted in Partial Fulfilment of the requirements
for the degree of Master in
Biomedical Engineering

Academic year 2006–2007

Acknowledgments

I would like to thank my supervisors Prof. Pascal Verdonck and Prof. Ferdinando Auricchio for the great opportunity which they have given to me and for their kindness. I also greatly appreciate the evaluable, essential support provided by Prof. Benedict Verhegghe, Eng. Matthieu De Beule, Phd student and Eng. Peter Mortier, PhD student. I gratefully acknowledge Dr. Kali Babu Katnam, Dr. Alessandro Reali, Denis Van Loo, Sofie Van Cauter for their valuable support and assistance.

Finite Element Analysis of self-expanding braided wirestent: a novel way to assess its mechanical response

Michele Conti

Supervisor(s): Prof. dr. ir. P. Verdonck, Prof. dr. ir. F. Auricchio

Abstract

Wire stents are a class of self-expandable stents braided from a set of ultra fine wires and currently manufactured in a wide range of braiding patterns (single or multilayer) and materials (e.g. phynox, nitinol, (biodegradable) polymers). Despite the promising clinical outcome of minimally invasive interventions with state-of-the-art stent(graft)s, some drawbacks of this procedure still need further attention (e.g. restenosis, stent migration, artery straightening, side branch covering,etc.) and require additional investigation. Finite Element Analysis (F.E.A.) offers interesting insights in the mechanical behavior of stents. In this study, we firstly provide an analytical validation of the finite element model proposed for a virtual benchmark test to determine the minimal diameter of the wire stent which can be reached by applying an axial load without (unwanted) plastic deformations of the wires. Moreover a second benchmark test is proposed to perform stable and accurate finite element simulations of the wire stent free expansion (i.e. when the stent is released from the catheter). Finally a simple simulation of the stent deployment in a straight vessel has been performed.

Keywords

pyFormex, wirestent, modeling, free expansion, Finite Element Analysis, von Mises stress

I. Introduction

A stent is an expandable tube-like device that is inserted into a natural conduit of the body to restore a disease-induced localized stenosis or aneurysm. Stents are classified as either balloon-expandable or self-expandable, based on the way how they are deployed. Balloon-expandable stents are deployed and plastically deformed at the intended delivery site as a result of a high pressure applied to the inner stent surface by inflation of the balloon. In contrast, self-expandable stents are constrained into a catheter; when the desired delivery site is reached the constraint is removed and the stent deploys. In both cases, the expansion of the stent partially or completely restores or diverts the fluid flow.

The aim of this thesis is to assess the mechanical behavior of the wire stent using a finite element model, built with pyFormex (an in-house developed open source program). In the non-deformed state, the geometry of the model is defined by the external diameter (D_{e0}=20 mm)and the length (L_0=80 mm). The stent consists of n=36 wires each of a diameter (d) of 170 μm, braided into a helical composition with 18 left-handed and 18 right-handed helices with an initial pitch angle (β_0) of 34° (see figure 1). The considered stent geometry is combined with different stent materials (i.e. phynox, nitinol and stainless steel).

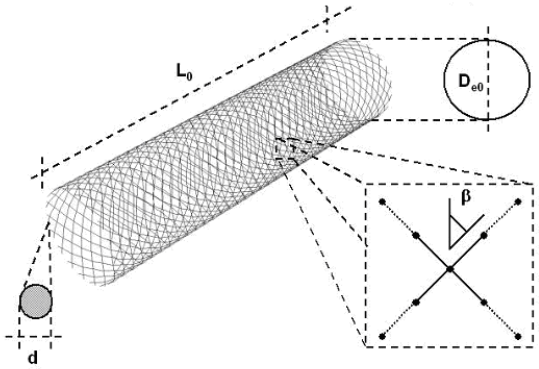

Fig. 1. pyFormex model of the Wallstent, Boston Scientific

M. Conti is with the Structural Mechanics Department, University of Pavia, Pavia, Italy. E-mail: Michele.Conti01@ateneopv.it. The thesis has been developed with Cardiovascular Mechanics and Biofluid Dynamics Research Group, Institute of Biomedical Technology (IBiTech), Ghent University, Ghent, Belgium.

II. Materials and Methods

A. Mechanical behavior of wire stents using different materials

In the first virtual benchmark test, the reduction of the stent diameter is modeled by applying an increasing axial load (**F**) resulting in an equivalent axial force (**nF**) on each wire on one end of the stent while the other end of the stent is constrained in both the tangential and axial direction. The action of the axial force (nF) results in bending (m_b) and twisting (m_t) moments acting on the wire. Due to the rotation costraint of the stent ends, the wires are subjected to additional bending and twisting resulting from the end moment M_0 (see figure 2-a). Defining the yield strength of the material σ_y, the maximum bending stress, according with von Mises criterion, should not exceed the σ_y in order to avoid plastic deformations. In fact the undesired plastic deformation could lead to problems in stent deployment out of the catheter. The von Mises equivalent stress σ_e in the stent wires is computed by analytical model based on previous works available in literature [1]-[2] and on the spring theory of Wahl[3] and compared with numerical results obtained by F.E.A. using the proposed model.

B. Free stent expansion

In the second virtual benchmark, we propose an innovative methodology to perform the wire stent free expansion as it exists out the catheter. In order to avoid the contact problem characterized by numerical instabilities and long (unpractical) simulation times involved in the simulation of the stent-catheter interaction, we study the variation of the stent radius as it exits out the catheter performing a different approach. In fact in our approach, radial displacement boundary conditions (BC) are applied on the node subsets to first reduce the stent diameter to the catheter size (i.e. 10 French or 3.4 mm diameter) and subsequently released as shown in figure 2(b).

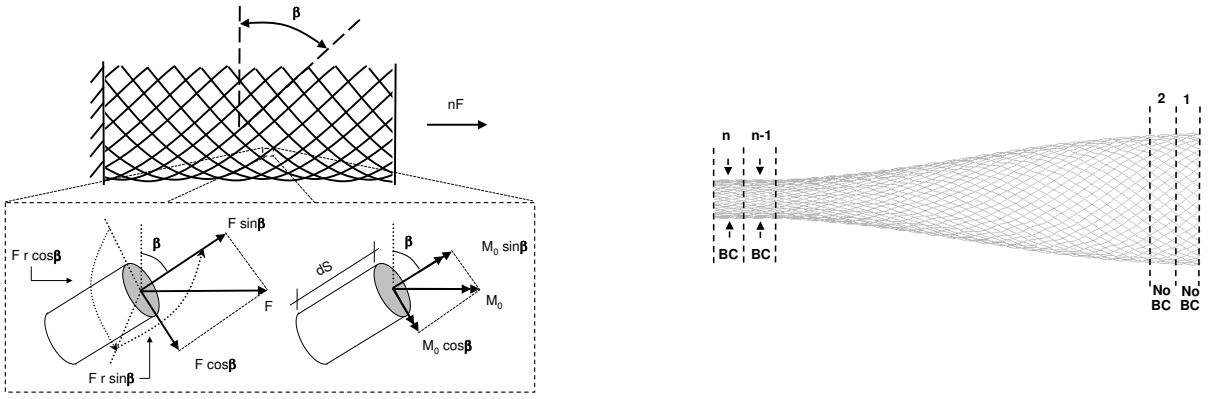

Fig. 2. a) Axial load of the wire stent; b) Stent deployment using BCs.

C. Stent vessel interaction

The numerical contact analysis of the stent-vessel interaction is performed following the approach proposed by of Lally et al.[4]. It is possible to perform a preopening of the vessel by an inner pressure increase and then perform the stent-vessel contact using the elastic equilibrium between the two bodies. Thus, the stent acts like a scaffold for the vessel. The vessel is modeled as a straight cylinder. An isotropic hyperelastic material is adopted to simulate the mechanical response of the vessel.

III. Results

Von Mises stress analysis: over the whole range of loading, the mechanical response of the phynox stent shows that Phynox behaves elastically and the data provided by the numerical simulation well fit the analytical approximation for the phynox stent, showing the accuracy of the proposed numerical model (see figure 3-a). The same analysis has been carried out for Nitinol and stainless steel. The Nitinol stent behaves elastically and its superelastic properties are not exploited. The use of stainless steel provides unrecoverable plastic deformations which comprimise the stent performance.

Stent deployment: the numerical results of the wire stent deployment simulations have been validated by comparison with experimental data reported by Wang and Ravi-Chandar [5] showing an excellent fit (see figure 2). In addition, the numerical simulations show an area of stress concentration at the tip of the catheter due to the high gradient of radial deformation (radius out the catheter=10 mm and radius inside the catheter=1.6 mm). Stent-vessel interaction: the contact analysis for the stent-vessel interaction provides many numerical problems and requires a big computational effort. Consequently further investigation are required to achieve reliable results.

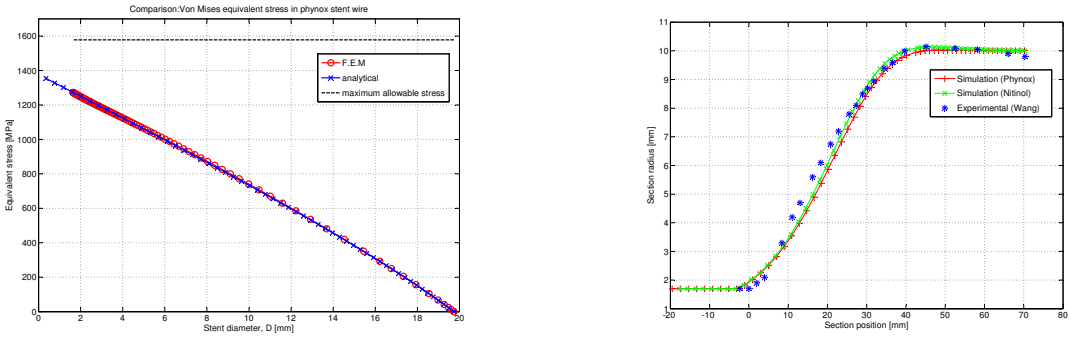

Fig. 3. a) von Mises stress in phynox stent wire; b) Stent deployment: Comparison between experimental and numerical data.

IV. Conclusions

Complex geometrical and finite element models of wire stents can quickly be built using the innovative pyFormex modeling tool. They can be used in finite element simulations for studying the mechanical behavior of the stent under complex mechanical loading conditions. The proposed benchmark tests and the developed pyFormex modeling strategy are a solid base for further study of the mechanical behavior of braided wire stents in real life conditions (e.g. patient-specific stent vessel interaction) and might be useful in the quest for the perfect braided stent.

References

[1] M. R. Jedwab and Clerc C. O. A study of the geometrical an mechanical properties of a self-expanding metallic stent - theory and experiment. *Journal of Applied Biomaterials*, 1993.

[2] R. Wang and K. Ravi-Chandar. Mechanical Response of a Metallic Aortic Stent-Part I: Pressure-Diameter Relationship. *Journal of Applied Mechanics*, 71:697, 2004.

[3] A.M. Wahl. *Mechanical Springs, 2nd edition*, pages 241–254. McGRAW-HILL BOOK COMPANY, 1963.

[4] C. Lally, F. Dolan, and P.J. Prendergast. Cardiovascular stent design and vessel stersses: a finite element analysis. *Journal of Biomechanics*, 2005.

[5] R. Wang and K. Ravi-Chandar. Mechanical Response of a Metallic Aortic Stent-Part II: A Beam-on-Elastic Foundation Model. *Journal of Applied Mechanics*, 71:706, 2004.

Contents

Part I

Literature

Chapter 1

Stents and their applications

1.1 Introduction: the device

A stent is an expandable tube-like device that is inserted into a natural conduit of the body to restore a disease-induced localized stenosis or aneurysm. Nowadays, the non-(or minimal-)invasivity of many clinical procedures is a requirement in a very wide range of medical activities and it is the new frontier in the research of medical devices design. In some clinical fields, such as cardiovascular applications, stents are playing a role of strategic importance because, thanks to their unique features, they allow to overcome a wide range of technical and design problems related to miniaturization. Therefore, a stent provides an excellent answer to the increasing trend for less invasive and therefore less traumatic procedures.

A stent is very often used with or in substitution of PTA (Percutaneous Transluminal Angioplasty). In fact this technique has shown many drawbacks as vessel dissection and elastic recoil [1]. Thus the use of the stent has two main goals:

- short term effect: to avoid the effects of intimal dissection and the elastic recoil;
- long term effect: to avoid restenosis due to the neointimal hyperplasia.

Dotter first introduced the idea of using stents in percutaneous applications in 1969 so, clearly, many improvements have been done up to now in the device design and in the stenting procedure. Also many clinical trials have been performed to assess the effectiveness of this procedure [2] and many efforts to improve the long-term outcomes are still required [3].

One of the main indications is that the investigation of the stenting procedure involves many fields of knowledge and, thus, a multi disciplinary approach. In fact it is necessary to understand the physiologic reaction of the vessel to the injury induced by a stent. The study of the material and the geometrical properties of the stent can provide useful indications on its performance and on its interaction with the target vessel. Biomechanics, by its characteristic multi-disciplinary approach, may provide the right key to investigate these devices. One of the major engineering aspects of this problem involves the stent design, besides materials, coatings, etc. The inescapable biomechanic requirements for the stent can be summarized as follows:

- good contour-ability to obtain an adequate fixation to the duct's wall,
- adequate resistance against the elastic recoil;
- resistance to fatigue due to the pulsatile flow and/or body kinematics;
- high size minimization of the device to make easier the percutaneous procedure;

- low thrombogenicity;
- high biocompability.

From a mechanical point of view, stents can be classified as:

- **balloon-expanding**;
- **self-expanding**.

This classification is based on the way how they are deployed. Balloon-expanding stents are deployed and plastically deformed applying a high pressure to their inner surface by a balloon. Instead Self-expanding stents are constrained into a catheter imposing a diameter reduction and when the desired delivery site is reached, the constraint is removed and the stent elastically deploys. Clearly, both devices have the same goal but a very different mechanical behavior.

In this chapter, we will provide a brief discussion on the features of these types of stent highlighting their differences. Then we will focus the attention on the Wallstent® (Boston Scientific/Schneider, Inc., Minneapolis, MN), the main object of our investigation. We will present the application fields of this device and the main drawbacks related to its use.

1.2 Self-expanding and Balloon-expanding stents

1.2.1 Balloon-expanding (BX) stents

As previously said, the expansion of the BX stent is achieved by the balloon inflation which provides plastic deformation of the stent. A common use of BX stents is the stenting of coronary vessels. In this procedure, as shown in Fig. 1.1(a-c), a PTCA[1] is performed; then if the PTCA leads residual plaque dissection or if a high elastic recoil takes place, a BX stent is applied. Thus, the BX stent is mounted on a folded angioplasty balloon and expanded to the desired diameter by inflation of the balloon. Subsequently, the balloon is deflated and removed, leaving the stent at the targeted site (see Fig. 1.1(a-c)).
BX stents can be divided into two groups:

- coil design;
- tube design.

Coil design stents, shown in Fig.1.2(a), incorporate a continuous wound wire as in Wiktor stent (Medtronic Inc., Minneapolis, MN) or a series of flat sheet coils as in Gianturco-Roubin stent (Cook, Inc.,Bloomington, IN). They have a large strut width; a gap and no connections between struts provide them high flexibility. However, the design lacks radial strength, and the wide gap allows tissue damage since the tissue prolapses between the wire elements.
Tube design stents are cut from a steel tube, i.e. Palmatz-Schatz stent (Johnson & Johnson/Cordis Corporation) or obtained from a metal sheet which is rolled and welded, i.e. NIR stent (Medinol Ltd, Tel Aviv, Israel) [5]. The Palmatz stent (Cordis, Johnson & Johnson, Miami, FL) made from 316L steel can be considered as the first tubular stent (see Fig. 1.3(a)). This stent is manufactured through laser

[1] Percutaneous Transluminal Coronary Angioplasty

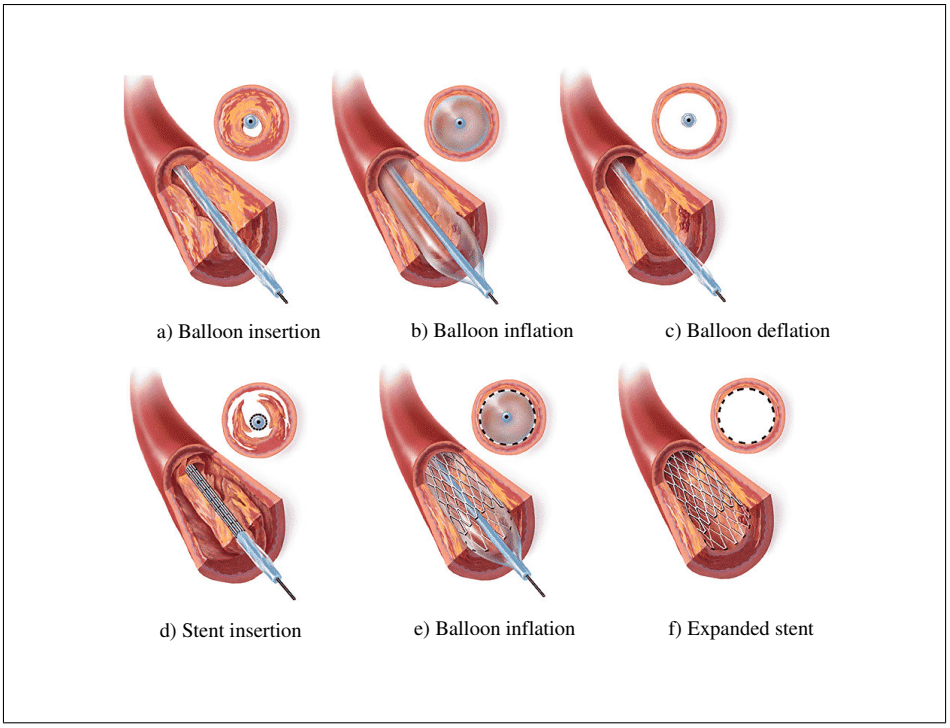

Figure 1.1: PTA and BX stent's deployment [4]

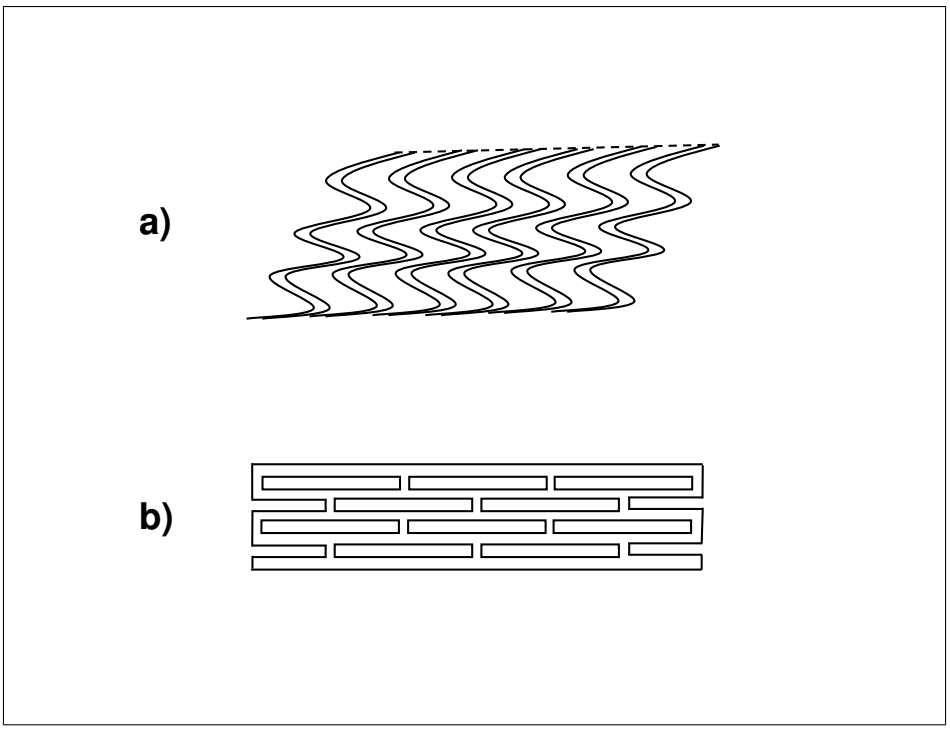

Figure 1.2: Coil (a) and tube design (b).

cutting (thus, without weldings) and has a tubular shape with rectangular holes. After deployment the holes assume rhomboidal shape. As it has limited flexibility, the design has been modified in the Palmatz-Schatz (Palmatz with an articulated join) for coronary applications, as shown in Fig. 1.3(b). Both stents have been the topic of many clinical studies in the years after their introduction.

The different design (coil/tube) leads to different mechanical behavior. In fact an investigation of the mechanical properties (strength, elasticity and plasticity) of the expandable stents shows that, under all types of stress, the Palmaz stent has a higher resistance but is completely inelastic while the Gianturco stent shows a lower resistances but is completely elastic [6].

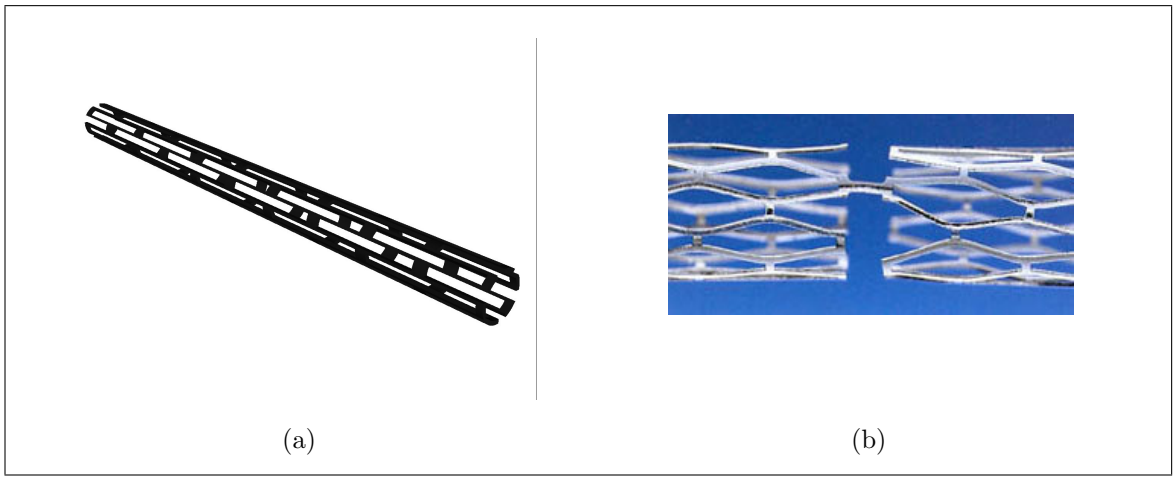

(a) (b)

Figure 1.3: Palmaz stent (a) and expanded Palmaz Schatz stent(b)

1.2.2 Self-expanding (SX) stents

Self-expanding stents do not require a balloon and expand by a spring mechanism triggered when the device is unloaded from a constraining delivery catheter (see Fig. 1.4(a)), or by resuming a preset configuration triggered by thermal memory at body temperature using the shape memory effect of Nitinol (see Fig. 1.4(b)). The final diameter of the stent-vessel system is the result of the elastic equilibrium between the duct elastic recoil and the stent radial strength.

A PTA can be performed before the stent implant to allow a pre-dilatation of the vessel and to improve the final gain of vessel lume. But the experimental studies suggest that direct stenting can be used in angioplasty sessions with a favorable outcome without previous PTA, since it results in less intimal hyperplasia. However it is necessary to consider the ability of the self-expanding stent to open the atherosclerotic lesion [7].
Many different types of SX stent designs are available in the market. In the following, we will provide a brief overview of self-expanding stent designs. This overview is clearly not complete since herein it has only the goal of showing the differences between the various designs. SX stent design can be classified as:

1. wire-based stent design;
2. sheet-based stent design;
3. tube-based stent design.

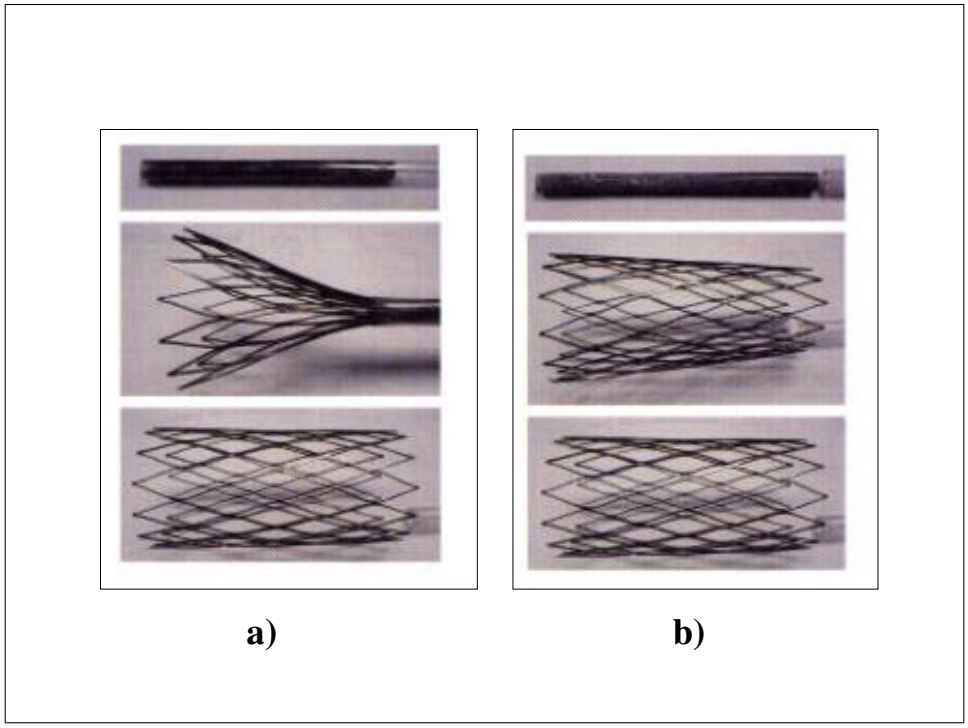

Figure 1.4: Expansion of SX stents:(a)elastic expansion by constrain remove;(b)thermal expansion by temperature increase.

In the first type is included the **Wallstent** (Boston Scientific/Schneider, Inc., Minneapolis, MN), shown in Fig. 1.5(a) that it is made of stainless steel woven monofilaments, the **IntraCoil** stent (IntraTherapeutics Inc., St. Paul, MN), shown in Fig. 1.5(b) which uses the thermal shape memory of Nitinol to recover its shape once it reaches body temperature, the **Cragg** stent (Mintec, Bahamas Islands) consisting of a sinusoidal coil with peak-to-valley suture connections for vascular and non vascular applications (see Fig.1.5(c)). Another nitinol stent, the Boston Scientific Symphony stent is made of a single strand of nitinol configured to form a tubular implant of hexagonal cell patterns, as shown in Fig. 1.5(d).
The sheet-based stents designs are based on the idea to roll a sheet, previously laser-cut, and weld or fix it at specific struts (see Fig. 1.6) [8].
As in the case of BX stents, laser technology plays a very important role because the demand for smaller delivery systems requires stents to be smaller in their delivery condition, not only in outside diameter but also in strut thickness to accommodate the size reduction. The combination of this technology and the introduction of the Nitinol provides many different tube-based stent designs. In Fig. 1.7 some commercially available SX laser-cut tubular nitinol stents are shown.
Because of their intrinsic characteristics SX and BX stents behave differently and accordingly the interaction with the vessel wall is different: BX stents resist the balloon expansion process and dictate the vessel expansion while SX stents assist it. The market share of SX stents is growing thanks to their use for peripheral applications, where their peculiar features, like kink resistance and trackability, are required. In renal and coronary stenting the BX are still preferred to the SX because experience has shown that BX stents recoil less than SX stents when placed in calcified lesions [10].

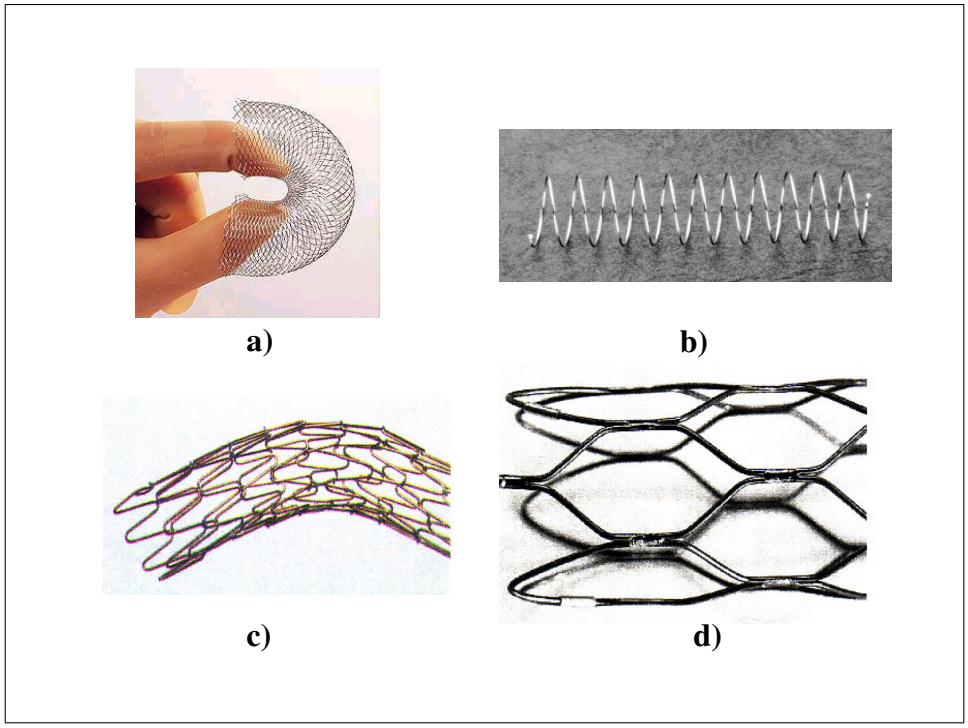

Figure 1.5: Wire-based stent designs.

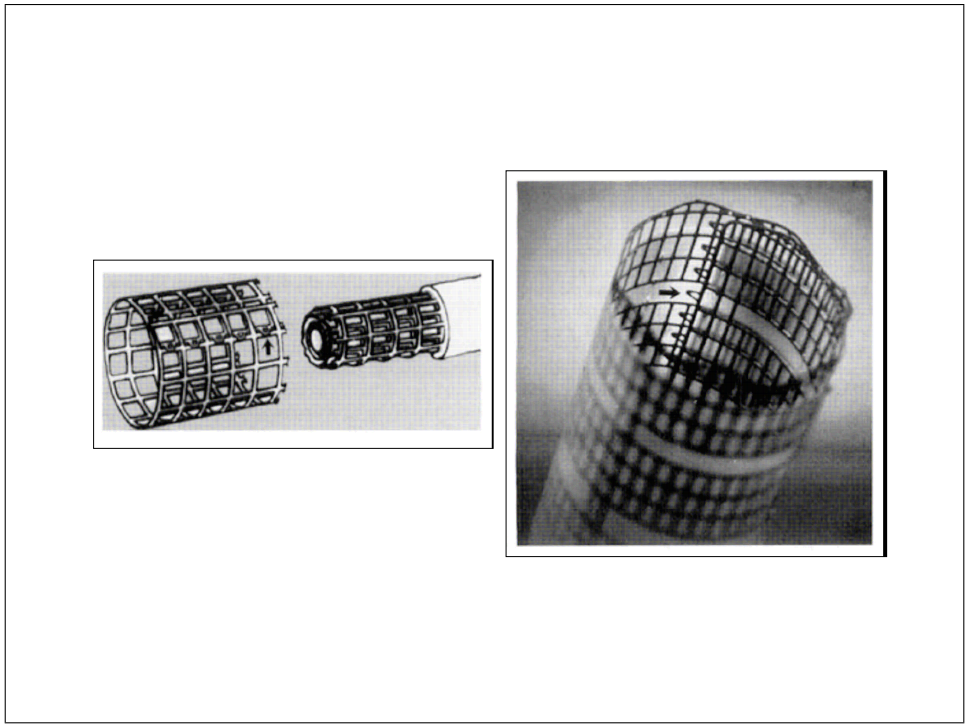

Figure 1.6: SX nitinol coiled-sheet stent (EndoTex) [8]

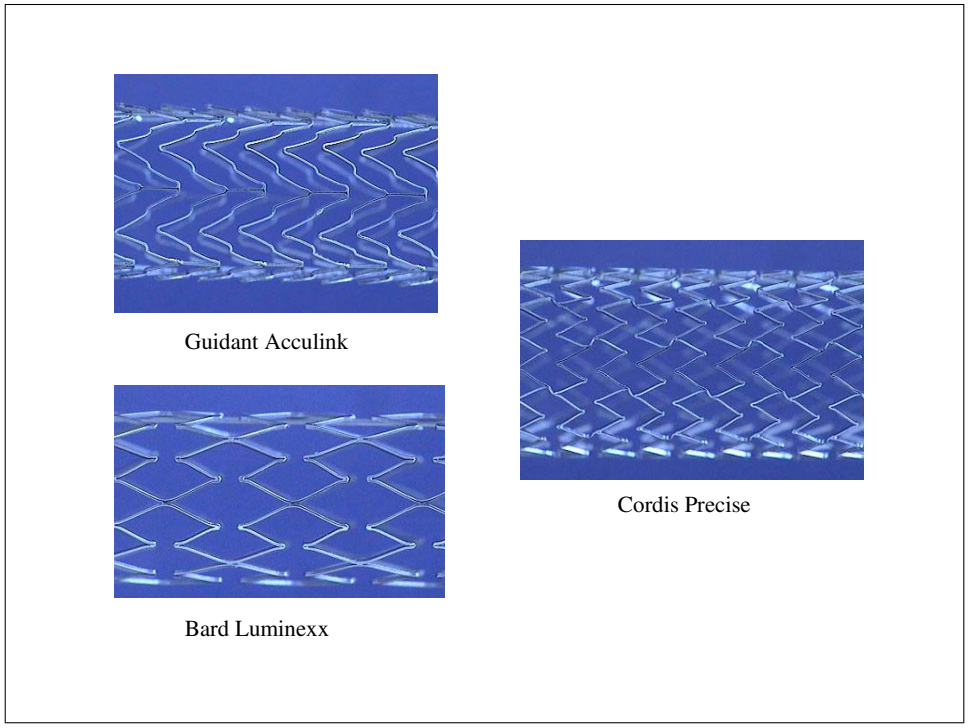

Figure 1.7: Overview of Nitinol SX stents [9].

1.3 Balloon-expandable superelastic stents

As previously illustrated, both BX and SX stents have limitations. As a consequence, efforts have been made to combine the features of BX and SX stents, creating a balloon-expandable superelastic stent. At least, two approaches have been proposed. The first approach is based on the idea to add an extra constraint to a SX stent. Theriault et al. [11] propose the developing of a Nitinol stent with a progressive expansion device made of polyethylene, allowing smooth and gradual contact between the stent and the arterys wall by creep effect (see Fig. 1.8). In the second approach, proposed by Besselink (U.S. Pat. No. 6,488,702), the stent design proposes a Nitinol SX stent modified in order to produce two stable states:

- closed (see Fig. 1.9(a));
- open (see Fig. 1.9(b)).

The balloon inflation is used to start the destabilization of constrained shape so that the stent snaps to its open configuration.

1.4 The Wallstent

In this section, we will focus the discussion on the main object of our investigation: the Wallstent. It is defined as a SX metallic endoprothesis made of filaments braided in a criss-cross pattern to form a tubular mesh configuration. Its deployment is performed using its elastic behavior. In fact applying a constraint, the braided wire stent with a certain diameter at the expanded configuration, is inserted into a catheter with a smaller diameter to perform the percutaneous implantantation. When the

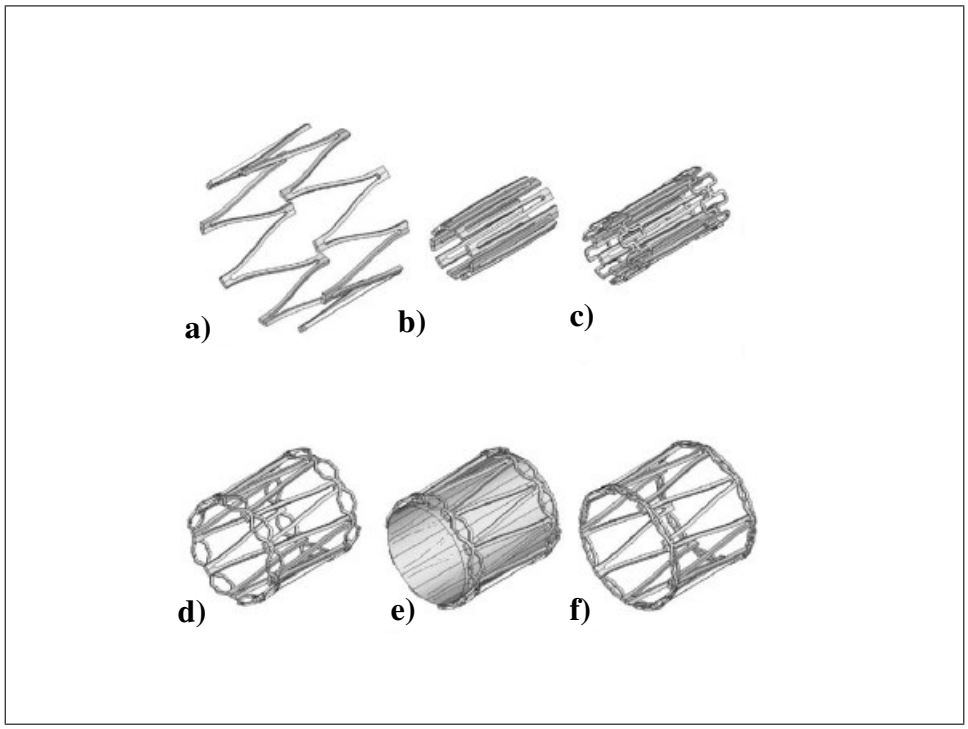

Figure 1.8: Position of stent at principal steps of the simulation by Theriault et al. [11]. From the initial shape of stent (a) to the creep of rings after 28 days (f).

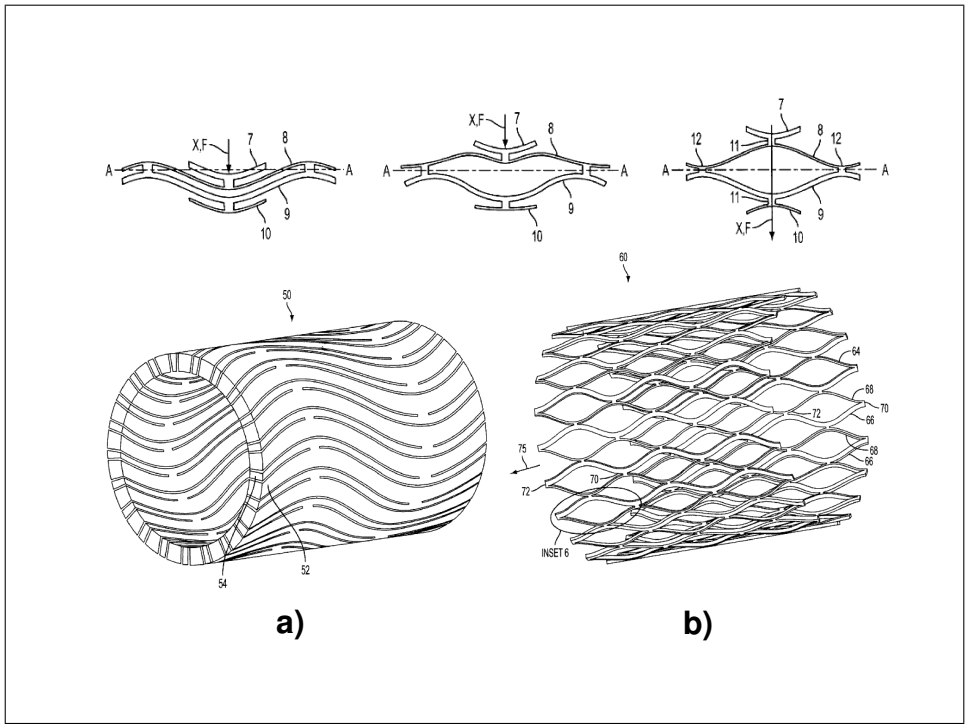

Figure 1.9: Bi-stable stent:a) closed configuration; b) open configuration.

delivery site is reached constraints are released and the stent elastically deploys. Fig. 1.10 illustrates the Wallstent® and the UNISTEP™ delivery system [12].
The Wallstent is mounted between two coaxial catheters. The exterior tube serves to constrain the stent. Retraction of the external tube allows the partial stent expansion [13](see Fig. 1.11).

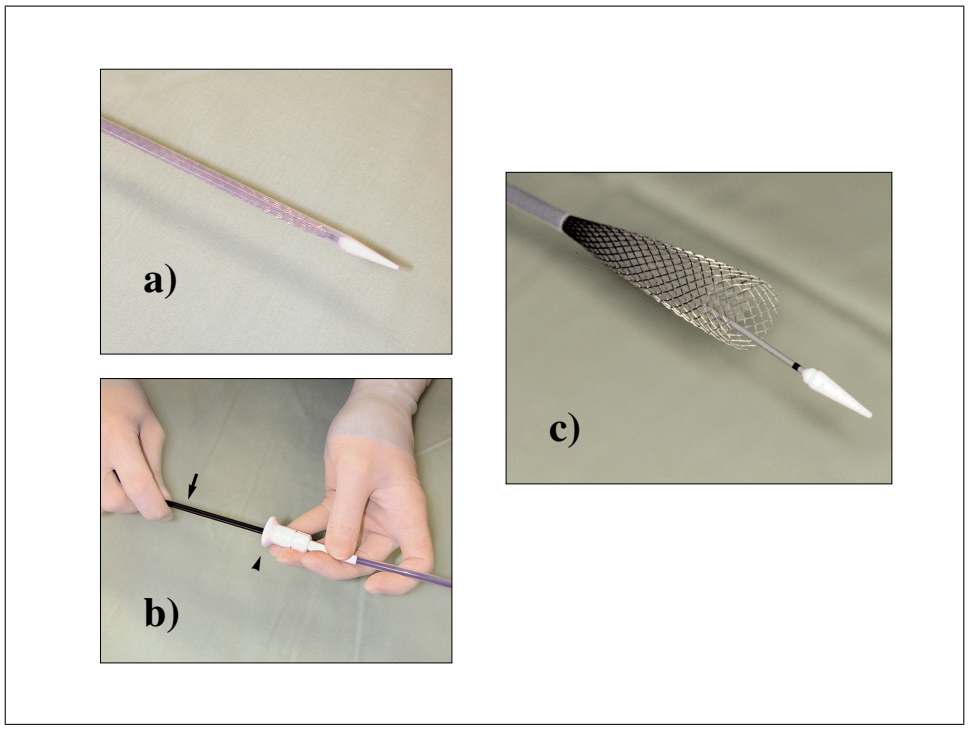

Figure 1.11: (a)Wallstent before deployment;(b) the inner tube s held fixed while the outer sheath is withdrawn in order to push out the stent(c).

1.4.1 Wallstent applications

Braided stents tend to be very flexible, having the ability to be placed in tortuous anatomy, still maintaining patency. Many cases are present in clinical literature about the successful use of SX braided wire stents such as the Wallstent®(Boston Scientific Corporation, Massachusetts, USA) or Urolume® (AMS, Minnesota, USA). A first application is to treat carotid artery stenosis [14] and to exclude subclavian and other peripheral artery aneurysms from the pulsatile blood flow [15]. These implants are also used to reopen collapsed airways and to treat obstructing (tracheo)bronchial lesions [16]. In addition, they can be used for the palliation of symptoms provided by malignant lesions or (benign) stenoses in the esophagus and gastrointestinal tract [17] and urethral strictures. More recently, a partially deployed Wallstent has even been used as a temporary inferior vena cava filtration device during coil embolization of high-flow arteriovenous fistula [18].

1.5 Covered stents and Stent-Grafts

Nowadays, the minimization of the percutaneous technique has opened interesting scenarios and new frontiers also for covered stents and stent-grafts. The goal of covered stents in vascular applications is to re-built a physiological lumen in order to exclude the blood flow in diseased vessels such as

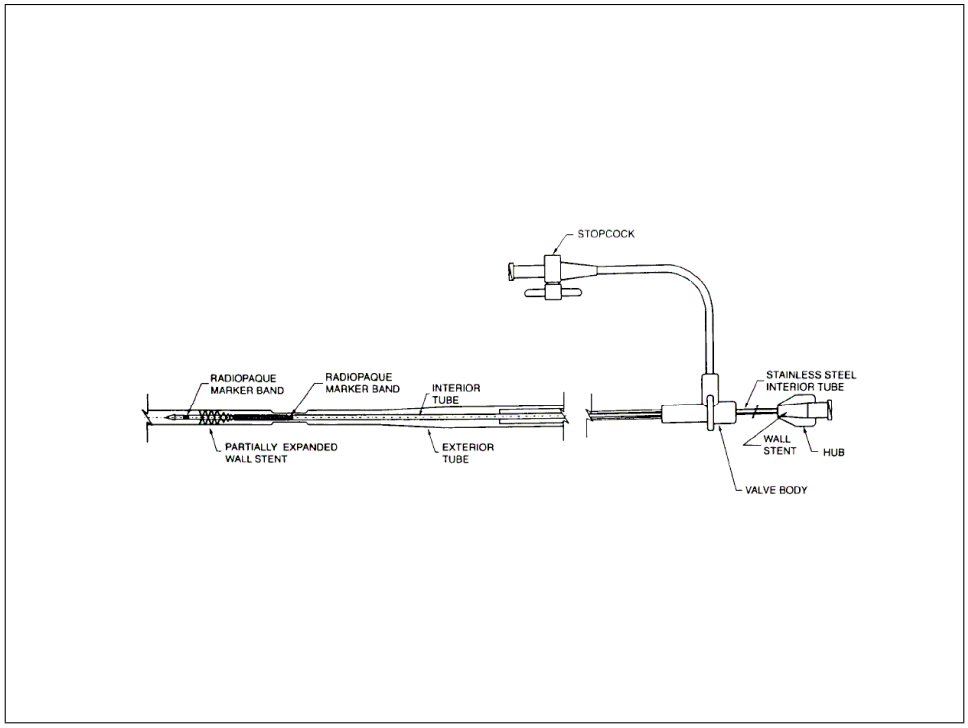

Figure 1.10: Wallstent® and UNISTEP™ delivery system.

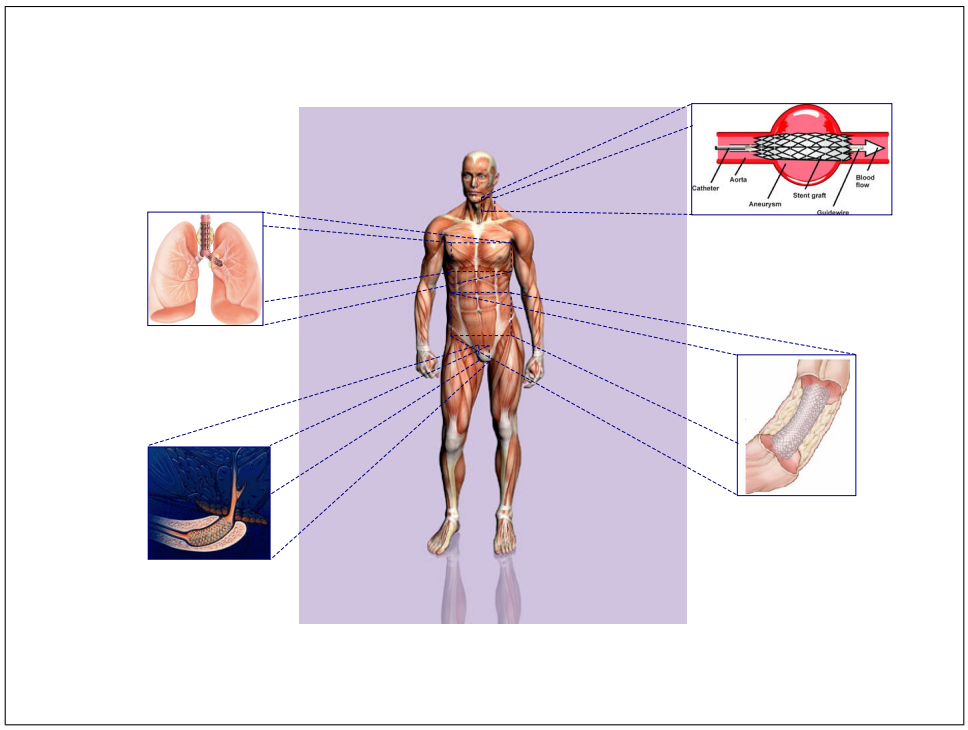

Figure 1.12: Application of the Wallstent and its graft.

aneurysms, pseudo-aneurysms or vascular fistulas [19]. In this way, in an aneurysm it is possible to avoid the risk of the vessel rupture and in an arteriovenous fistula to restore normal hemodynamic conditions (see Fig. 1.13).

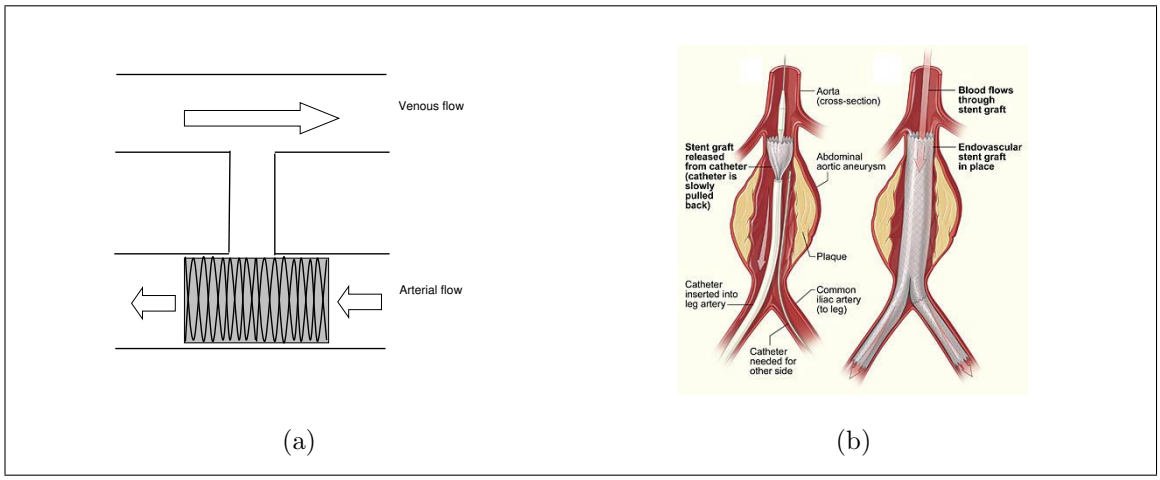

Figure 1.13: Covered stent's application scheme in arteriovenous fistula (a) and abdominal aortic aneurysm (b).

In extra-vascular applications, the covering of the SX stents (see Fig. 1.14) is useful to reduce the failure rate due to the neointimal cellular growth between the stent wire leading to a re-occlusion [20].

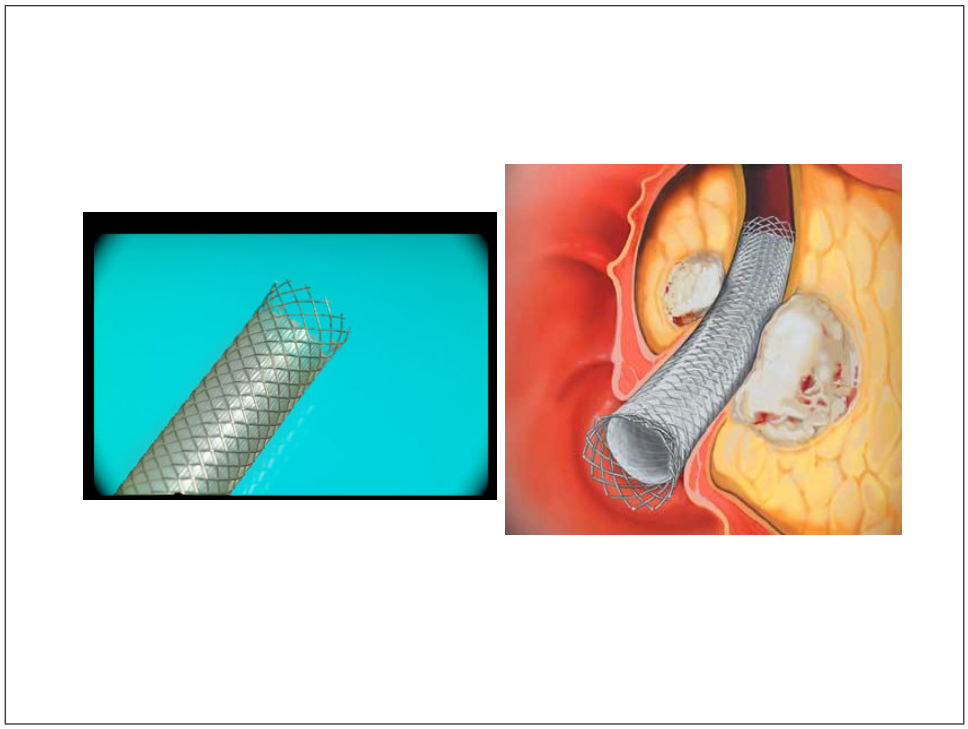

Figure 1.14: Covered Wallstent [21].

1.6 Wire stent drawbacks

As previously introduced, wire stents have a very wide application field and many clinical studies can be found in literature, but drawbacks in its use are still present. The main problems in wire stent applications are:

- restenosis [22] (see Fig. 1.15) ;
- inflammation provided by body immune response;
- hyperplasia, the abnormal growth of the cells between the wires;
- stent migration, a complication of stent placement, in which the stent is displaced proximally or distally [23].

Stent implantation was developed to overcome the acute recoil and high restenosis rate of balloon angioplasty (PTA), but they may lead to chronic in-stent restenosis related to specific factors regarding patient, stent, lesion and procedural characteristics. After stent implantation, the mechanism of restenosis is principally neointimal hyperplasia, as stents resist arterial remodeling. The significant correlation between the degree of arterial injury caused by metallic wire coils and the resultant neointimal thickness and lumen stenosis at the stented site has been established by animal studies [24], although inflammation and related subsequent release of growth factors after arterial injury has been implicated as one of the major contributing mechanisms of restenosis [25]. The stent migration is closely connected to the stent anchorage to the body duct. Stent migration is also a result of the radial stent displacement provided by the pulsatile kinematics of the duct.

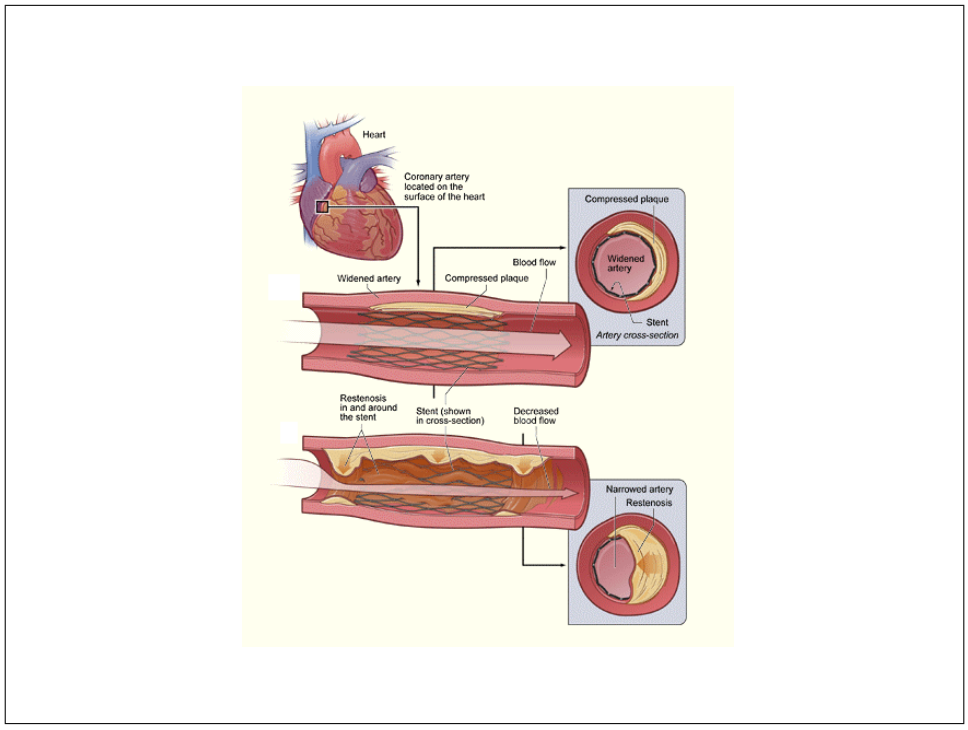

Figure 1.15: In-stent restenosis.

Chapter 2

Stent materials

The correct choice of the stent material is an essential step of stent design process as well as for every other medical device. In this chapter, we want to provide the current stent metal options available and discuss the influence of their features on this choice. The stent material choice is a symbiosis between the required mechanical properties (flexibility, ability to support the duct wall, ability to expand, ...) and the biocompatibility.

2.1 Biocompatibility

It is not easy to provide a unique definition of biocompatibility. In fact the interaction of a material with the body involves many factors and a single test is not able to define whether a material is biocompatible or not. Here, we consider the biocompatibility of a stent. This device is (in general[1]) a long-term implanted device so its biocompatibility can be defined as the property of the device to perform its task, not providing any undesirable local or systemic effects in the host body. A biocompatible material may not lead to a toxic or harmful immunological response. The way to assess the biocompatibility or the tissue reaction is to test the substances firstly *in vitro* then *in vivo*. The usual response of the host to an implant includes:

- trauma;
- inflammation;
- the immune system reaction;
- eventual healing or scarring [26].

The biocompatibility of the metals is directly related to their ability to resist to the aggression of biological fluids. In fact the biological fluids have a well-known corrosive action. The corrosion has consequences on the mechanical properties of the metal implant and a toxicological action since it leads the release of metallic ions in the body. The anti-corrosion features of the metals can be improved applying ad hoc technologies acting on the chemical stability of the device surface (i.e. passivation) and on the surface geometry (i.e. electrochemical polishing).

The evaluation of the biocompatibility requires a well define procedure which starts investigating the chemical behavior of the sole metal and concludes with the implant set in the body host. In fact the *in vitro* tests involve the cytotoxicity (i.e. the quality of being toxic to cells; examples of toxic agents are a chemical substance or an immune cell) of the material but they are not able to assess the cell interaction with the surface properties of the material. For this reason, it is necessary to perform *in vivo* tests on animals (i.e. pigs, dogs and sheeps) having features comparable to the human body. The final phase of the testing is the implant of the device into the human body during clinical trials [26].

[1] The new generation of biodegradable stents are good candidates for short term implants

2.2 Current metallic stent materials

The stent market is a very interesting research field also from the point of view of material science, the discovery of a new material can lead to a sudden wide and rapid (r)evolution as e.g. happened with Nitinol and polymeric materials. Furthermore, the rapid influx of the new stent material requires well understanding of the relative strengths and weaknesses of the various materials. In the following, we will discuss the mechanical and chemical properties, highlighting their role in the stent design, of the following materials:

- Stainless steel;
- Gold;
- Cobalt Chromium alloys;
- Magnesium;
- Nitinol.

2.2.1 Stainless steel (SS)

Steel is an iron alloy. It includes 2% of carbonium(C) (at most). The stainless steels are specific types of steel which well resist to the chemical agents. It is includes chromium(Cr) (more than 10%) and nickel(Ni). By the crystal microstructure, the SSs can be classified as:

- martensitic SSs;
- austenitic SSs;
- ferritic SSs.

Here, we will focus the attention on the austenitic SSs which are the most important class of materials for medical device applications and most BX stents, which are based on the metal plastic deformation, are stainless steel made (SS). This types of SSs are interesting because they propose a good compromise among corrosion resistance, strength, formability, weld ability, and cost [27]. They are also non magnetic allowing magnetic resonance imaging (MRI) of the device. The first austenitic SS used in the medical application was the Type 302 but it became obsolete since its scarce corrosion resistance [28]. Nowadays the most widely used SS is the Type 316L, a variation of Type 316 including molybdenum, which provides more resistance to the salt water: the Type 316L contains less carbon than Type 316 as shown in the Table 2.1.

Type	C	Cr	Ni	other alloying elements
316	0.1%(max)	16-18%	10-14%	Mo:2-3%
316L	0.03%(max)	16-18%	10-14%	Mo:2-3%

Table 2.1: Composition of austenitic stainless steels Type 316 and 316L [28].

2.2.2 Gold

Gold has a high radiopacity, biocompatibility and chemical inertia and is therefore well suited for medical applications. Gold markers are used in hybrid devices to improve the radiopacity and to allow precise positioning of the stent. Gold coating also improves stent visibility under fluoroscopy. The visibility is particularly valuable for precise stent placement during renal artery stenting (RAS). Hovewer, there is conflicting evidence regarding restenosis with gold-coated stents. In fact Gold-coated renal stents had a substantially higher rate of restenosis than stainless steel stents [29]. Of course, it is necessary to take into account many factors; an interesting *in vitro* comparison of stainless steel and gold surfaces, using platelet reactivity as an index, shows that the stainless steel faired better under some conditions, while under other conditions, gold is superior [30].

2.2.3 Cobalt-Chromium alloys

ASTM F1058

The cobalt-chromium-nickel-molybdenum-iron alloy, ASTM F1058, nowadays has many trademark names as Phynox™ [31] or Elgiloy® [32]. This alloy is well suited for coil and flat springs and generally for applications in which high fatigue strength and corrosion resistance are required [33]. This alloy can be classified as a cobalt based superalloy. Nominally it contains:

- 40% cobalt;
- 20% chromium;
- 15.5% nickel;
- 7% molibdenum;
- 2% manganese;
- 0.15% carbon
- balance iron.

It is used to produce pacemaker lead conductors, porcine heart valve stents, vena cava filters and neurosurgical clips. Thanks to its non-magnetic characteristics this alloy can be safely imaged using magnetic resonance. This cobalt alloy has a high yield strength and high elastic and shear moduli; it shows excellent fatigue properties. These mechanical properties make it an ideal material for medical implants which utilize spring designs, such as self-expanding stent endoprothesis, which require high yield strength and fatigue resistance. The Table 2.2 shows the mechanical properties of wire that was cold drawn to 65% reduction in cross-sectional area as the final forming operation and then age-hardened[2]. The cold worked and age hardened cobalt alloy has high tensile strength and modulus than cold worked 316L SS and Ni-Ti .

Cobalt chromium L605

In the last years, Cobalt based alloys play a growing role in the BX stents [34]. In opposition to the previously mentioned vascular applications (i.e. pacing leads, stent graft, SX stents, etc.), this alloy in

[2]Age-hardening: a process of aging that increases hardness and strength and usually decreases ductility.

Property	ASTM F1058 No Age Hard.	65% C. W. With Age Hard.	316L SS	Ni-Ti
Yield strength, 0.2% offset (MPa)	1650	2450	–	643
Ultimate tensile strength (MPa)	2050	2700	1800	1564
Elongation (%)	≥2	≈1	–	14
Elastic modulus, E (MPa)	174000	206000	193000	47000
Shear modulus, G (MPa)	73000	81000	69000	25000

Table 2.2: Typical mechanical properties of implant alloy wires [33].

BX stents is used in the annealed conditions to facilitate the plastic deformation during the expansion. The Type L605, a variant of Co-Cr alloy, thanks to its mechanical properties appears particular interesting for BX stents. In fact comparing this variant with the other Co-Cr alloys (Phynox/Elgiloy, MP35N), it stands out with higher density and elastic modulus, bringing a comparative advantage in stent for radiopacity and recoil. Moreover, the use of Co-Cr alloys in BX stents allows stent designs with thinner struts (than SS made) thanks to their tensile properties. The thinner struts allow a lower profile, smaller stent volume and high flexibility. The strut size can influence also the host reaction in fact a randomized trial demonstrates that coronary stents with thinner struts are associated with a reduced risk for angiographic and clinical restenosis [35].

2.2.4 Magnesium

The research of new stent materials is also producing some novel alternative materials for innovative stent construction as the aluminum/magnesium alloy made coronary stents. The stent based on a magnesium alloy allows controlled corrosion with release to the vessel wall and the blood stream of a natural body component such as magnesium [36]. The biocorrosion implies that the degradation products are removed by cellular activity in the biological environment. Thus, the idea is to use the bioabsorbable stent to:

- prevent of acute or subacute recoil occurring mainly in the first days after the implant;
- deliver antiproliferative drugs to prevent smooth muscle cell proliferation which takes place in the first 2-3 weeks after the implant;
- overcome the limitations related to the permanent metallic stents (i.e. chronic inflammation, late stent thrombosis, prolonged antiplatelet therapy, artifacts in MSCT[3] and MRI[4], etc.).

The first approach in bioabsorbable stent was the use of biodegradable polymers. Firstly, most of these polymers have been demonstrated to induce a marked inflammatory reaction within the coronary artery with subsequent neointimal thickening, which was not expected on the basis of *in vitro* tests. The reaction may be due to a combination of parent polymer compound, biodegradation products, and possibly implant geometry [37]. The following use a more biocompatible polymers such as PLLA (poly-L-lactic acid) reduces these physiological reactions [38] but drawbacks in the stent mechanical behavior appeared. Thus, the use of metallic magnesium alloy stents are attractive. They can offer vessel integrity and relative high degradation rate. A recent study shows that the magnesium

[3] multislice-computed tomography
[4] magnetic resonance imaging

alloy stents are safe and are associated with less neo-intimal formation than stainless steel stent [39]. However, reduced neointimal growth does not result in larger lumen and only one design of SS stent has been involved in the investigation.

2.2.5 Nitinol

Nitinol alloys exhibit a combination of properties which make these alloys particularly suited for medical devices like SX stents. Many works are present in scientific literature about Nitinol and many scientific fields are involved in the research about this material. Here we want to discuss briefly the mechanical behavior of this material and how it can be used in medical applications. Finally, a brief discussion of constitutive material models and its numerical implementation will be carried out.

Material properties

Nitinol is an equiatomic or near-equiatomic intermetallic compound of nickel and titanium produced for the first time by W. J. Buehler in the 1960's [40]. The martensitic transformation, a solid phase change, leads to nitinol two interesting properties:

- shape memory effect (SME), as shown in Fig. 2.1(a), the material can be deformed at one temperature (from A to C) but when heated or cooled, return to their original shape by thermal shape transformation (from D to A);
- superelasticity (SE), as shown in Fig. 2.1(b), in this case, after a initial linear increase in stress with strain, a small further force induces considerable deformation (B' to C'), defining the so-called loading plateau; but when the force is removed, a rapid decrease of stress takes place until the a lower plateau (from C' to D'), where the strain is recovered with a small decrease in stress (from D' to A'), finally the last strain recover takes place linearly.

The superelastic behavior leads an hysteresis in the stress-strain curve.
In order to understand the mechanical behavior of Nitinol and its capabilities, it is necessary to consider its atomic structure. The nitinol behavior depends on two different crystallographic phases:

- the austenitic phase that is stable at high temperature;
- the martensitic phase that is stable at low temperature.

In the austenitic phase, the crystal structure is well defined and it has a cube-like shape (see Fig.2.2(a)) providing high strength.

In the martensitic phase, atomic microstructure is defined by a self-accommodating arrangement composed of alternative zig-zag like layers of variants, as shown in the model in Fig. 2.2(b). The material is soft and ductile.

The transformation from austenite to martensite, or vice versa, can be thermically or mechanically triggered.

Let us consider the SME. Fig. 2.3 shows the scheme of the crystal structure's transformation in the one-way SMA and the changing shape of a specimen with one-way SME. When the austenite phase (see Fig. 2.3(a)) is cooled at lower temperature transforms in martensite, with self-accommodating arrangement configuration called multi-variant martensite (see Fig. 2.3(b)). Thanks to its ductility and softness

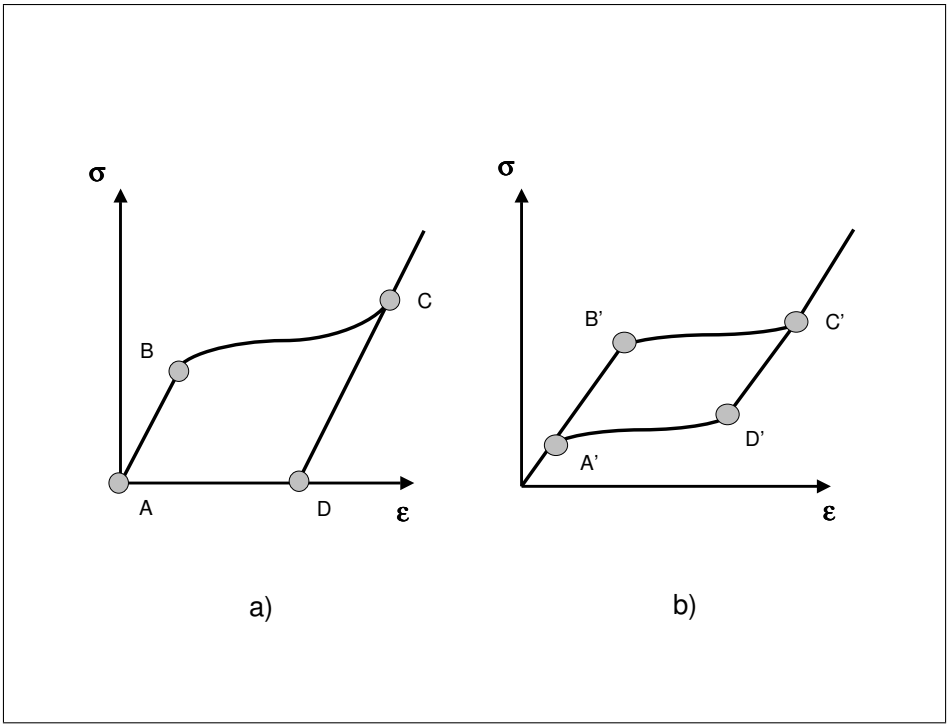

Figure 2.1: SME (a) and SE (b).

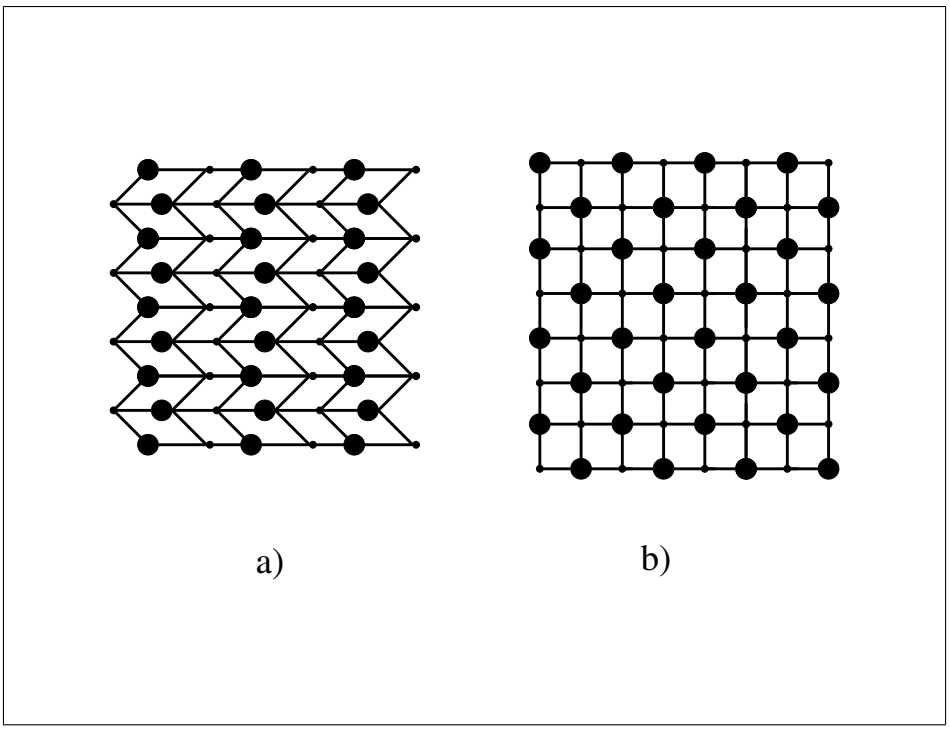

Figure 2.2: Atomic structure models of Nitinol's crystal.

in the martensitic phase, Nitinol can easily be deformed in the desired shape, switching the atomic configuration from twinned (multi-variant martensite) to de-twinned (single-variant martensite) (see Fig. 2.3(b)-Fig. 2.3(c)). Since the martensite in this phase is stable when the stress is removed a residual deformation takes place. On re-heating, the crystal structures start to change recovering its original shape. In one-way SME, re-cooling the material, the austenite transforms in multi-variant martensite instead in two-way SME, the re-cooling provides to come back from austenite to single-variant austenite.
The temperatures which define the phase change are called transformation temperature. It is possible to define four transformation temperatures:

- A_s: the temperature at which the transformation from martensite to austenite begins on heating;
- A_f: the temperature at which the transformation from martensite to austenite finishes on heating;
- M_s: the temperature at which the transformation from austenite to martensite begins on cooling;
- A_f: the temperature at which the transformation from austenite to martensite finishes on cooling.

The Fig. 2.4 shows the temperature range for the martensite-to-austenite transformation and vice versa. The temperature range for the martensite-to-austenite transformation on heating is somewhat higher than that for the reverse transformation upon cooling [41]. This difference on heating and cooling leads an hysteresis. The transformation temperatures and so the hysteresis depend on material composition, amount of cold-work and heat treatment [42].
Now, let us consider the SE. We suppose to work in a temperature range above A_f. In this condition the austenite is stable but it is possible to induce martensitic transformation. In fact in this case, the phase transformation is mechanically triggered. When the material is loaded beyond a certain stress the phase transformation takes place (see Fig. 2.5). The transformation produces a substantial amount of strain, which on unloading is reversible. This behavior is defined superelastic because transformation strains are large (of the order of 6%) compared to elastic strains in typical metals. The transformation stress tresholds increase with the work temperature. Alloy composition, material processing, and ambient temperature greatly affect the superelastic properties of the material [43].
Phase transformation from austenite to martensite results in macroscopic deformation which can be split into shear strain and volume strain. When transformation is solely due to the change of temperature, martensitic twin structures form to compensate the microscopic shear strains induced by different martensitic variants. On the macroscopic scale, the net shear strain is zero. By contrast, stress-induced martensitic transformation will result in a stress-biased macroscopic shear strain as well as a volume transformation strain [44].

2.2.6 Biocompatibility of Nitinol

Beyond the mechanical properties of Nitinol also its biocompatibility facilitate its use in medical applications. In fact Nitinol consists of about 50 at.% Ni (balance Ti), which is known to provoke severe toxicological and allergic responses. Despite this potential risk, good biocompatibility is documented [45] because any release of Ni is efficiently blocked by a thin titanium oxide layer formed

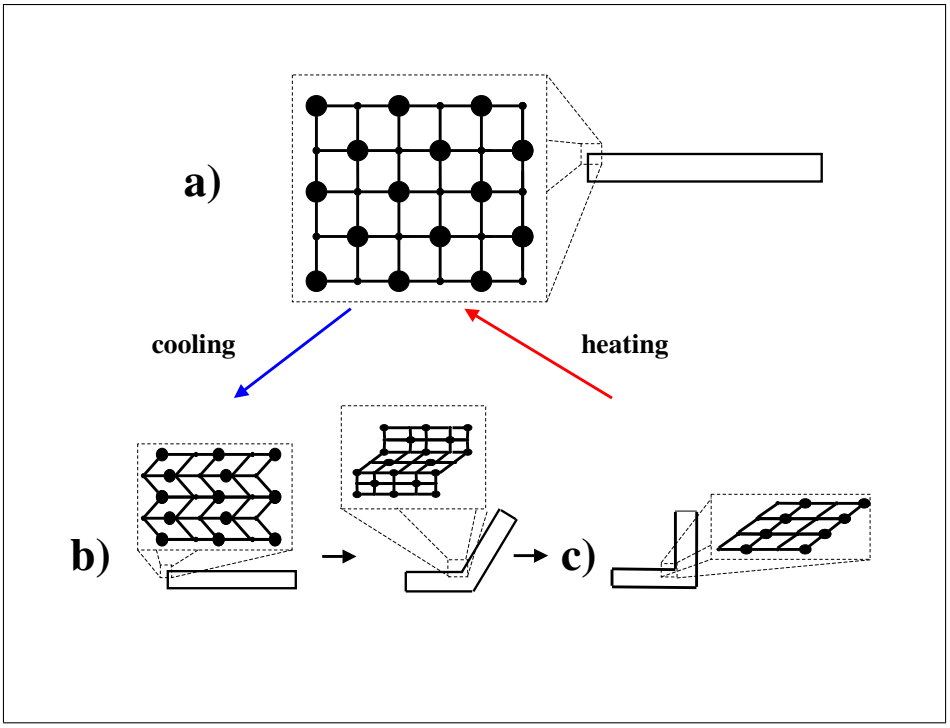

Figure 2.3: One way SME.

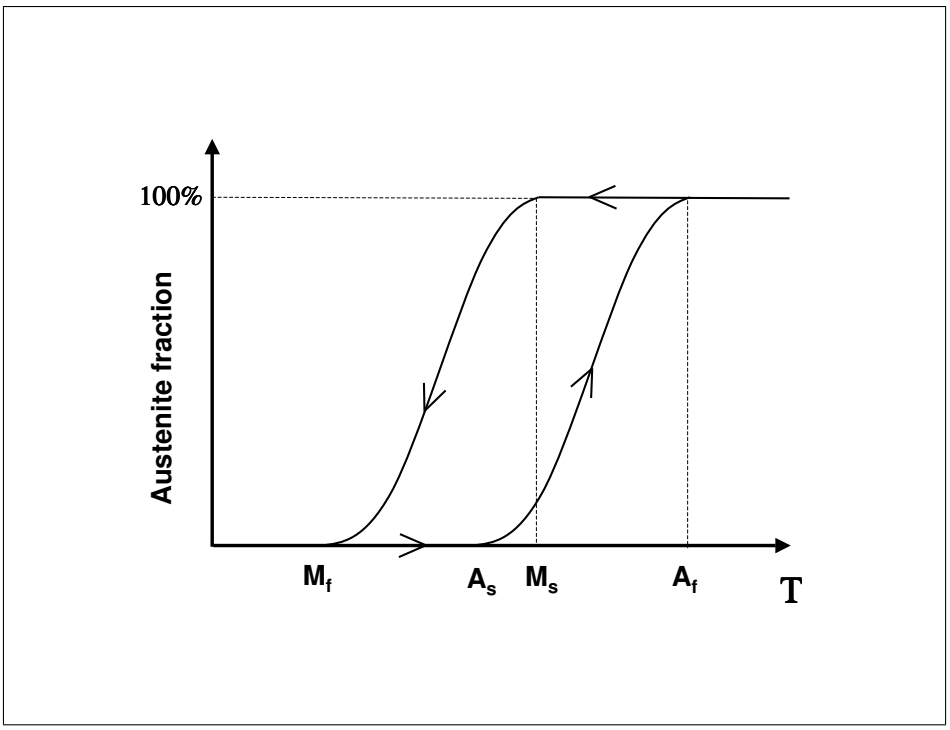

Figure 2.4: Transformation temperatures.

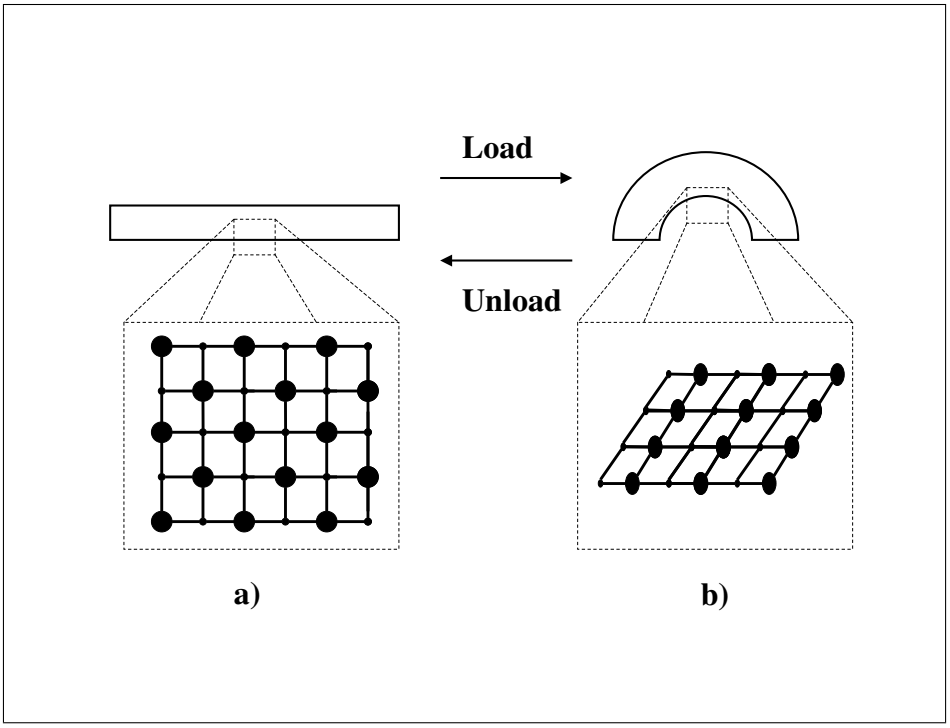

Figure 2.5: Scheme of SE phase transformation.

naturally or artificially at the surface of Nitinol medical products. Various methods of surface modification (i.e. electro polishing and passivation) can affect the structure of the layer and so the nitinol biocompatibility [46].

Certainly, the introduction of Nitinol in medical field has opened wide scenarios, leading a sort of revolution in the medical devices [5]. Probably, nitinol SX stents are the best illustration of this phenomenon. In fact, lastly, the interest in SX stents is increasing and Nitinol is playing a key role in this growth [47]. SX nitinol stents, in the open configuration, are manufactured with a diameter slightly larger than the target vessel. They are easily inserted in the delivery system at or below room temperature. In the delivery system the stent is constrained by retractable sheath and when the desired site is reached the sheath is removed and the nitinol stent expands conforming itself to the vessel wall [48]. The Fig. 2.6 shows the biased stiffness [49], a device feature based on the hysteretic superelastic behavior of Nitinol:

- firstly, the stent is crimped in the delivery system (from A to B);
- when the sheath is withdrawn, the stent expands following the unloading path of the stress-strain curve and reaching the point C;
- the diameter of the stent in the point C is obtained by the elastic equilibrium between the stent and the vessel wall and the stent provides a small chronic outward force (COF) against it;
- if the stent lumen is reduced by external forces or spasms, the stent reacts with a larger radial resistive force (RRF) (curve from C to D).

[5] An overview of nitinol medical devices are provided in Appendix A

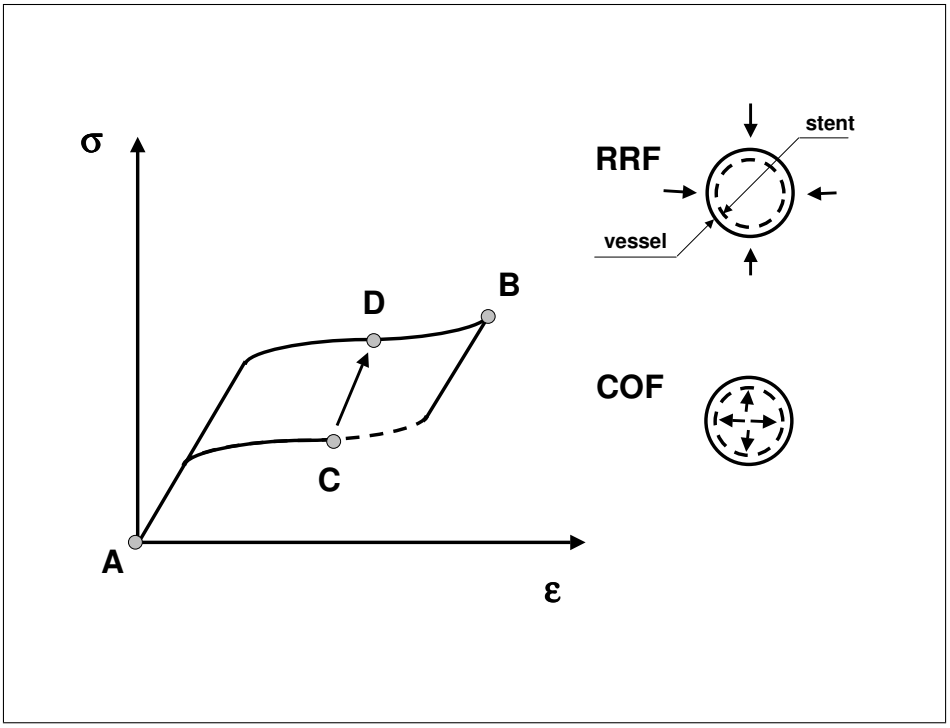

Figure 2.6: Bias stiffness in nitinol stent.

Since the fatigue resistance is an essential feature of the ideal stent, specifically in the superficial applications, the Nitinol can lead a high improvement in this direction, since it high fatigue resistance [10]. The fatigue experienced by a stent must be distinguished in pulsatile (due to the blood pulse pressure) fatigue and flexural fatigue. The newer, more stent flexible generations, can experience also axial fatigue deformations. Clearly, the fatigue analysis of a stent inserted in a coronary vessel or other very complex environmental (such as carotid or polipteal artery) is very hard to carry out. Such type of investigations involves physical testing and finite element stress analysis [50]. However the **in-vivo** fatigue behavior of nitinol stents has not been well understood and more efforts are still required.

2.2.7 An engineering model of Nitinol

Since we want to simulate the SE of Nitinol using the commercial code ABAQUS, we will briefly explain the theory on which the material subroutine is based in this section. Surely, the creation of a robust material model to numerically implement the superelastic behavior of Nitinol requires to understand the thermodynamic process involved and the macroscopic effects. The polycrystalline material model based on the microscopic behavior of a single crystal have been shown excellent agreement with experimental data [51]. However, the approach based on microscopic behavior of the material is not really practical from an engineering point of view. An engineering constitutive equation must include the following features:

- influence of the initial conditions (T,σ) on phase transformation;
- different stress thresholds for each phase transformation to perform the hysteresis;
- the reversibility of the phase transformation by thermo-mechanical cycles.

Most of the mechanical testing data available is uniaxial since Nitinol is typically available as relatively thin wires and tubes. The uniaxial superelastic behavior is relately easy to reproduce yet it is more difficult to produce a model that represents Nitinol's 3-D stress strain behavior. Several models have been developed in order to describe this complex behavior [52], [53], [54], [55],. Since the numerical implementation of the nitinol superelasticity is beyond the scope of this thesis, in the following we will provide only a brief discussion on the user material routine (Umat/Nitinol) implemented in the commercial finite element code Abaqus [56]. This subroutine is based following the model proposed by Auricchio and Taylor [54], [53]. Assuming a small strain regime, the total strain ϵ is decomposed into two parts: a purely linear elastic component ϵ^{el} and a transformation component ϵ^{tr}, which is also the internal variable. The model is a Mechanism Based Continuum Mechanics Model based on generalized plasticity (MCMMGP). The generalized plasticity theory by Lubliner [57] introduces the new concept, separating the yielding and limiting functions thus the associative evolution law for ϵ^{tr} is:

$$\dot{\epsilon^{tr}} = \dot{\xi}\partial F/\partial\sigma \tag{2.1}$$

$$F^S \leq F \leq F^F \tag{2.2}$$

where ξ is the martensite fraction and F is a limiting function. The intensity of the transformation follows a stress potential law:

$$\dot{\xi} = f(\sigma, \xi)\dot{F} \tag{2.3}$$

Moreover since there is a volume increase associated with the transformation, a Drucker-Prager approach is adopted for the limiting function:

$$F = \bar{\sigma} - ptan\beta + CT \tag{2.4}$$

where $\bar{\sigma}$ are the Mises equivalent stress, p the pressure stress and T the temperature.

Part II

Numerical simulations

Chapter 3

Mechanical behavior of wire stents using different materials

3.1 Introduction

Many works regarding the investigation of the mechanical behavior of balloon-expanding stents and the stent-vessel interaction are present in literature. Finite Element Analysis (F.E.A.) is the main tool to perform this investigation [58] [59]. All these studies show the power and the usefulness of the finite element approach for non-linear complex problems. Instead, regarding wire stents, only analytical models are present in literature and the F.E.A. of this kind of devices is totally missing. This is very surprising because the braided wire stent has a very wide application field, experiencing several different complex loading conditions. So, for this reason, the F.E.A. seems very suitable for this kind of problem, in fact this approach allows, once built a correct and validated model, to change easily the geometrical and material parameters, as its application on balloon-expanding stents' investigation has shown. The main reason for this lack in scientific effort could be due to the complexity of the wire stent modeling because of its geometrical structure. The classical CAD approach to build the geometrical model does not provide an adequate methodology for this type of complex structures.

In this chapter, we will discuss the investigation of the mechanical properties of the wire stent using the F.E. model created by the innovative approach provided by pyFormex, a script based method to build geometrical structures.

Firstly, we will provide a brief review of previous works in available in scientific literature about wire stent mechanical behavior.

Secondly, we will discuss the geometrical model of wirestent using pyFormex.

Finally, we will investigate the von Mises stress in stent wires when an axial load is applied on the stent. The numerical results will be validated by an analytical model of wirestent based on the previous works and on the Wahl's spring theory [60]. The impact of different stent materials (i.e. Phynox, Nitinol, stainless steel) on the stent mechanical response and a possible (practical) use of this investigation will be also discussed.

3.2 Previous works in literature about wire stent mechanical behavior

As already mentioned, there are no F.E.A. of wire stent available in literature. In contrast there are a few analytical models. The reading of the following studies has been done keeping in mind that

an analytical model could be an excellent benchmark for the validation of the numerical results or for more accurate and advanced numerical approaches; particularly when experimental data are not available. This section will provide an overview of the analytical wire stent models, which are currently present in literature and each subsection briefly will summarize and highlight the key aspects, in our point of view, of following articles:

- A Study of the Geometrical and Mechanical Properties of a Self-Expanding Metallic Stent Theory and Experiment by Jedwad and Clerc [61];
- Mechanical Response of a Metallic Aortic Stent-Part I: Pressure-Diameter Relationship by Ravi-Chandar and Wang [62];
- Mechanical Response of a Metallic Aortic StentPart II: A Beam-on-Elastic Foundation Model by Ravi-Chandar and Wang [63].

3.2.1 A Study of the Geometrical and Mechanical Properties of a Self-Expanding Metallic Stent - Theory and Experiment

The authors, Jedwab and Clerc [61], developed a mathematical model of a self-expanding metallic stent with the goal of computing several geometrical and mechanical properties of it. The theoretical model is based on four main assumptions:

1. the stent is a combination of a number of independent open-coiled helical springs undergoing large deformations;
2. the extremities of the stent are not free to rotate due to the friction between the stent wires in the crossing points;
3. the springs experience only elastic deformation;
4. the springs have large ratio D/d.

D is the stent average diameter and d is the stent wire diameter. Under these conditions, they may use the equation for open-coiled helical springs given by Wahl [60]. Considering an axial force F acting on the stent, it leads to an elongation of the stent and a change in the pitch angle β (see Fig. 3.1). So they obtained an analytical relation between the axial force and the initial and the current pitch angle after assigning the material properties.

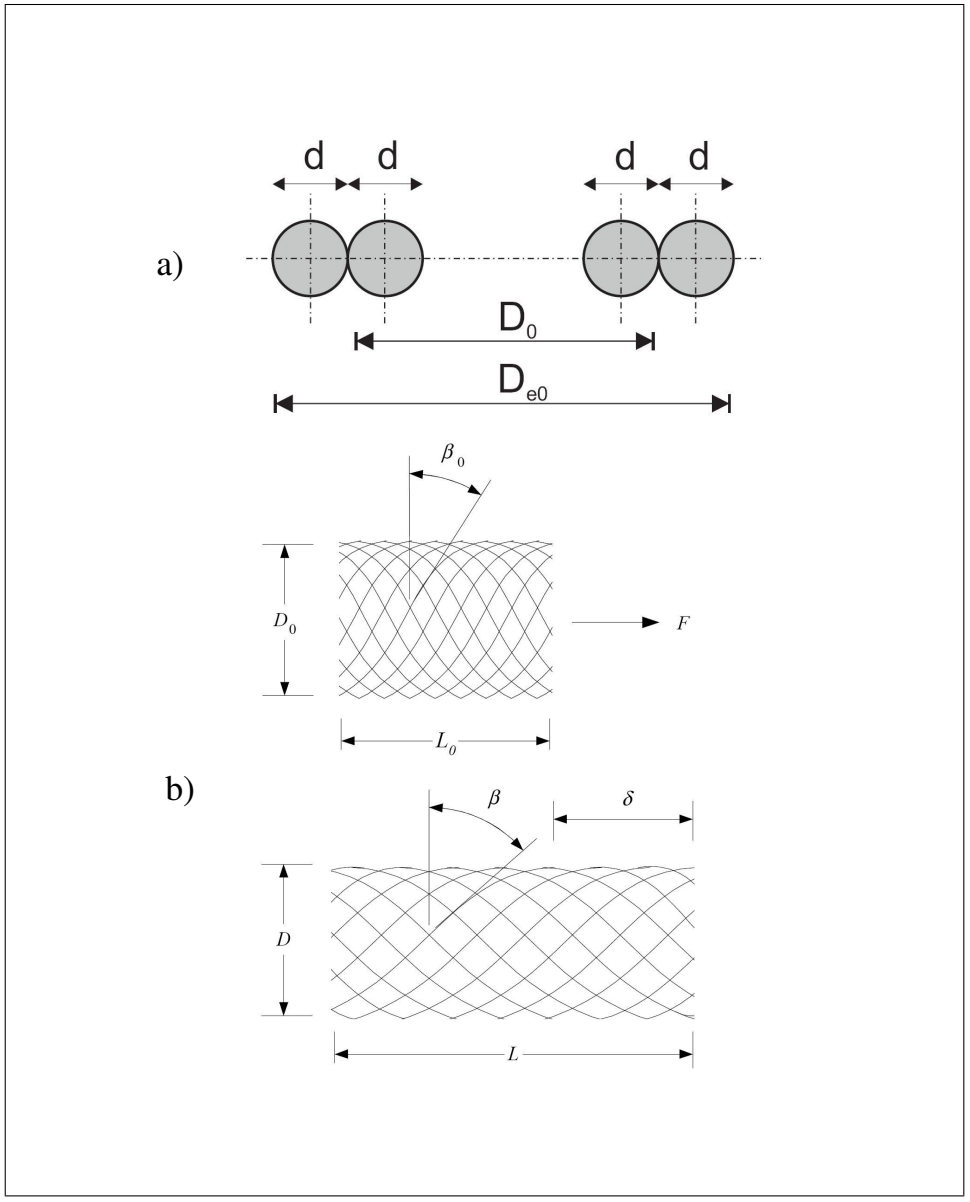

Figure 3.1: Stent geometry (a) and stent elongation under the action of a load F (b) by Jedwab [61]

The analytical model has been validated with data provided by experiments, performed by the authors, on a Phynox wire stent. The experimental results show good agreement with the theory and thus with the analytical model. Now, will be focused our attention on the following equation[1] which shows the relation between the axial force acting on the stent and the geometrical parameters:

$$F = 2\,n \left[\frac{GI_p}{K_3} \left(\frac{2\,\sin\beta}{K_3} - K_1 \right) - \frac{EI\,\tan\beta}{K_3} \left(\frac{2\,\cos\beta}{K_3} - K_2 \right) \right] \tag{3.1}$$

where K_1, K_2, K_3 are constants given by:

$$K_1 = \frac{\sin 2\beta_0}{D_0} \qquad K_2 = \frac{2\cos^2\beta_0}{D_0} \qquad K_3 = \frac{D_0}{\cos\beta_0} \tag{3.2}$$

[1]Equation corrected by Kim Van Loo [64]

n the number of wires, I and I_p are the wire moment of inertia and polar moment of inertia, respectively, E is Young's modulus of elasticity,G the rigidity modulus, D_0 the initial average stent diameter (see Fig. 3.1), related to the initial stent external diameter D_{e0} by:

$$D_0 = D_{e0} - 2d \tag{3.3}$$

β_0 is the initial pitch angle (see Fig. 3.1).
Keeping in mind the following geometrical relations :

$$D = \frac{D_0 \cos\beta}{\cos\beta_0} \qquad R_0 = \frac{D_0}{2} \qquad R = \frac{D}{2} \tag{3.4}$$

Equation 3.1 can be written as an explicit function of the current pitch angle β and the initial pitch angle β_0:

$$F = n\left[\frac{GI_p\cos\beta}{R}\left(\frac{2\sin\beta\cos\beta}{R} - \frac{2\sin\beta_0\ \cos\beta_0}{R_0}\right) - \frac{EI\sin\beta}{R}\left(\frac{2\cos^2\beta}{R} - \frac{2\cos^2\beta_0}{R_0}\right)\right] \tag{3.5}$$

So the force F_{wire} acting on each wire is given by:

$$F_{wire} = F/n \tag{3.6}$$

where n is the number of wires. Furthermore, the authors provides an analytical computation of the von Mises stress in the stent wires as shown in Fig. 3.2.

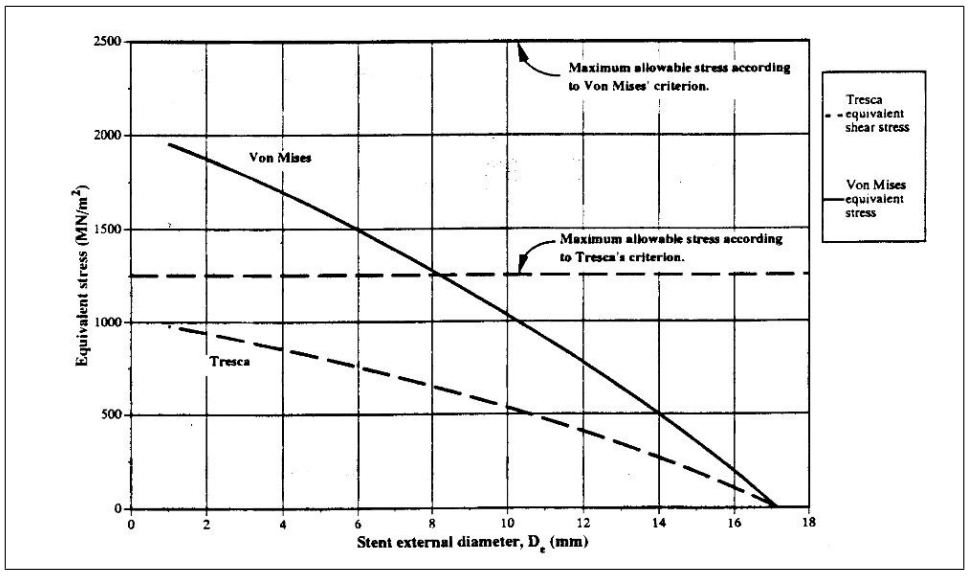

Figure 3.2: Equivalent Tresca and Von Mises stress versus stent external diameter D_e by Jedwab [61]

3.2.2 Mechanical Response of a Metallic Aortic Stent - Part I: Pressure-Diameter Relationship

The authors, Ravi-Chandar and Wang [62], experimentally explored the mechanical response of a metallic aortic stent undergoing an internal or external pressure, applied using a polyethylene bag (see Fig. 3.3-Fig. 3.4). They developed also an analytical model, based on the slender rod theory,

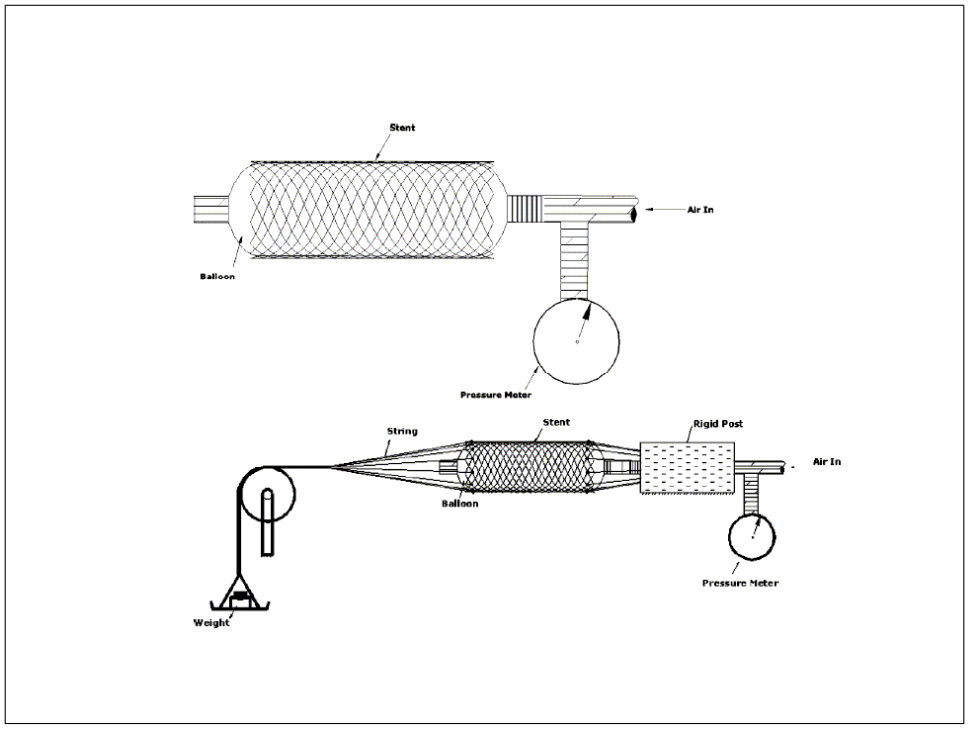

Figure 3.3: a) Schematic representation of a stent under internal pressure produced by compressed air-filled polyethylene bag by Wang and Ravi-Chandar [62].

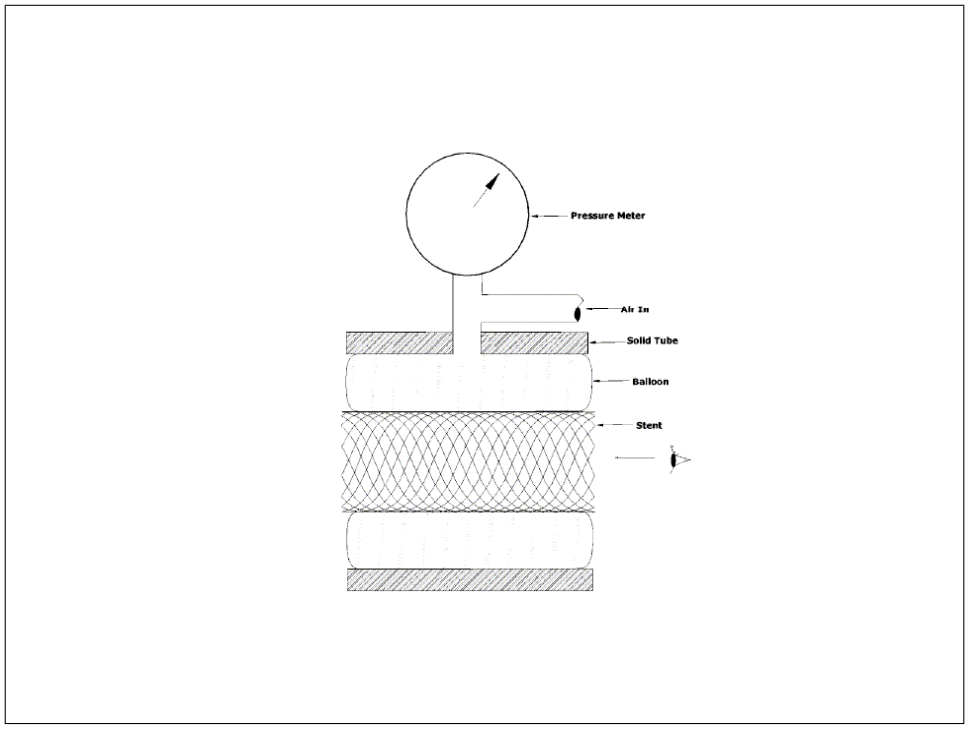

Figure 3.4: Schematic representation of a stent under external pressure produced by a compressed air-filled polyethylene bag by Wang and Ravi-Chandar [62].

able to catch the stent pressure-diameter relationship. The mathematical model was validated using the data obtained from the experimental test.
We now want to highlight the similarities of this mathematical model with the work of Jedwab (see section 3.2.1). For this reason, there are some aspects that are necessary to emphasize:

- the stent does not experience an axial load (as in Jedwad's approacf) but a lateral pressure is provided by the polyethylene bag;
- it is necessary to consider the equilibrium of a spring under pressure on the lateral sides;
- the frictional resistance between the wires dictates the following geometric constraint:

$$\frac{r}{\cos\alpha} = \frac{r_0}{\cos\alpha_0} \tag{3.7}$$

Defining q as the load per unit of length along the wire which results from the pressure p in the stent, r as the radius of the helix, and α as the pitch angle, the components of the forces and moments acting on the stent wire can be assumed as shown in Fig. 3.5.
The authors denote F_z the external force along the axis of the helix that is supplied by the end constraints. Clearly F_z is zero if the stent/helix is free is free to expand/contact axially. The introduction of a nonzero F_z allows the calculation of the axial force necessary if the stent is to maintained at some final length due to the end constrain. Considering p in function of q the authors describe the axial force F_z as a function of the lateral pressure p and the pitch angle α:

$$\begin{aligned} F_z \quad = \quad & \frac{2\pi r^2 \sin^2\alpha}{n\cos^2\alpha} p - \left[\frac{GI_p \cos\alpha}{r} \left(\frac{2\sin\alpha\cos\alpha}{r} - \frac{2\sin\alpha_0\ \cos\alpha_0}{r_0} \right) + \right. \\ & \left. - \frac{EI\sin\alpha}{r} \left(\frac{2\cos^2\alpha}{r} - \frac{2\cos^2\alpha_0}{r_0} \right) \right] \end{aligned} \tag{3.8}$$

If p is zero, equation 3.8 is equal to equation 3.6, showing the agreement between the analytical model of Ravi-Chandar and Jedwab.
The Fig. 3.6 and Fig. 3.7 show the variation of the stent diameter D and the variation of the stent length over the complete range of pressure p used in the experiments of Ravi-Chandar and Wang [62]. In these plots the markers define the experimental data and the line the results obtained using the proposed analytical model. It is interesting to highlight that the experimental results show three regimes in the response of the Wallstent:

- the first limiting state takes place when the is fully collapsed as when it is inserted in the catheter: the diameter D is about 4 mm and the length is almost the double than the undeformed stent length;
- the second limit state takes place at fully expanded condition when the length is a minimum and the maximum possible diameter;
- an intermediate state connecting the limiting state.

At both the limiting states, the stiffness is quite high; it means that a large change in pressure provides a small change in the diameter. Instead in the intermediate state the stiffness is quite small and so a small change in pressure provides a significant change in diameter.

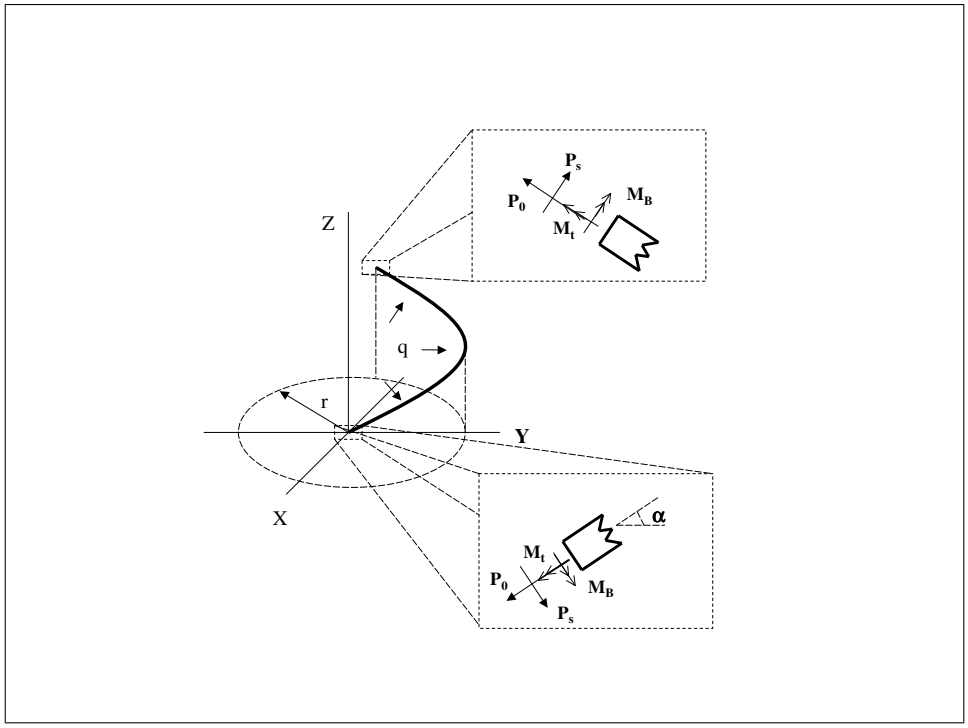

Figure 3.5: Free-body diagram on one-half turn of one wire in the stent.

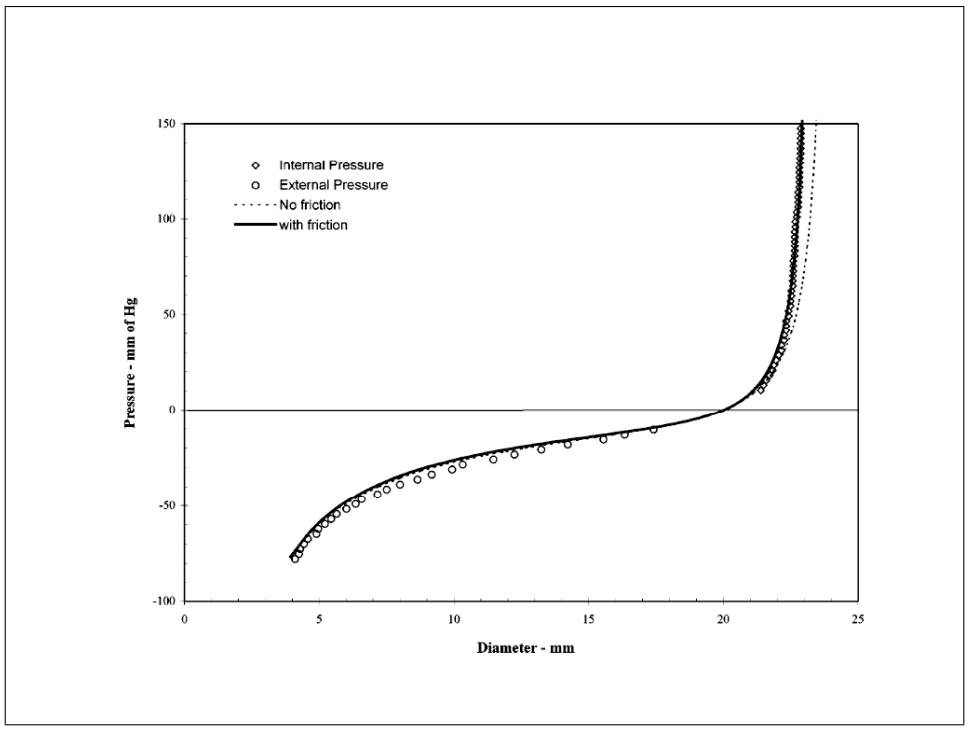

Figure 3.6: Variation of the diameter of the stent with pressure in Ravi-Chandar and Wang [62].

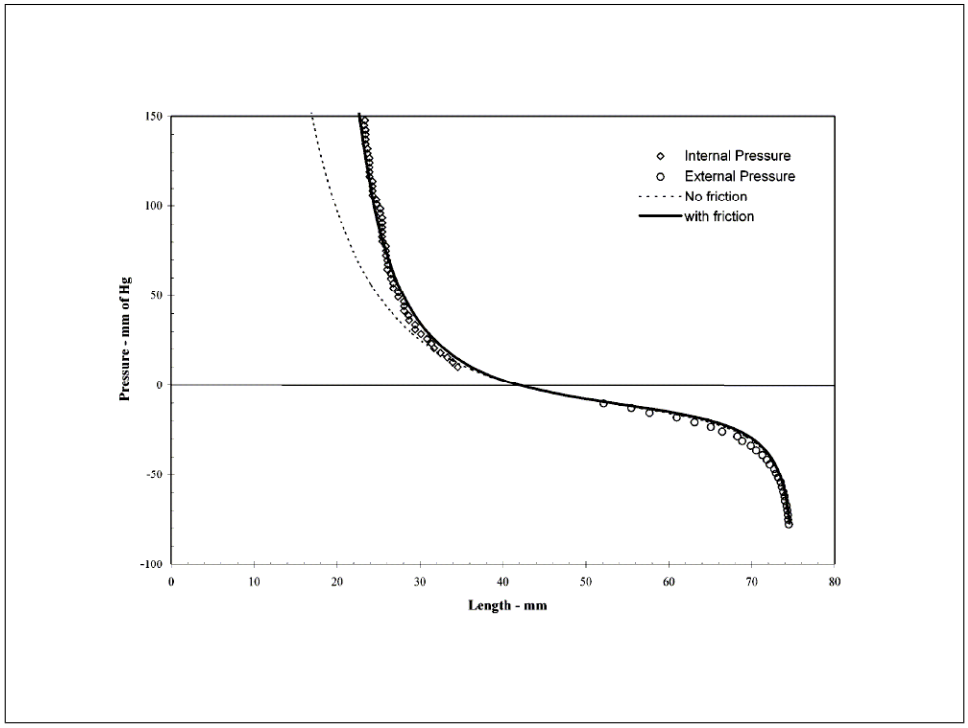

Figure 3.7: Variation of the length of the stent with pressure in Ravi-Chandar and Wang [62].

3.2.3 Mechanical Response of a Metallic Aortic Stent Part II: A Beam-on-Elastic Foundation Model

The authors, Ravi-Chandar and Wang [63], in this paper, propose an analytical model of the response of a metallic stent subjected to axisymmetric loading conditions over its length and to different boundary conditions. This model is necessary because these conditions introduce bending stresses in the stent which the analytical model of the stent proposed in the previous work is not able to catch (see section 3.2.2). The model is developed as an analytical approach to evaluate the coupled response of the stent and the blood vessel or in other complex loading situations as when the stent exits the catheter. Here, we will focus our attention on this last point, neglecting the analytical formulas, only considering the comparison between the results obtained from the model and the experimental data from a photograph of a stent exiting the catheter showed in Fig. 3.8.

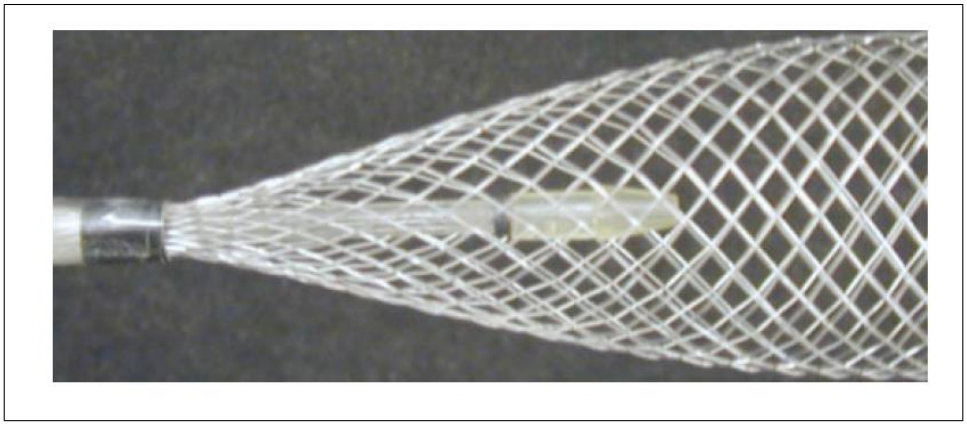

Figure 3.8: Picture of a stent partially released from the catheter

The catheter imposes fixed boundary conditions on the part of the stent inside the catheter (radius of the stent equal to internal radius of the catheter) and the outside part is free (no BCs). Fig. 3.9 shows the variation of the stent radius as function of the stent length.

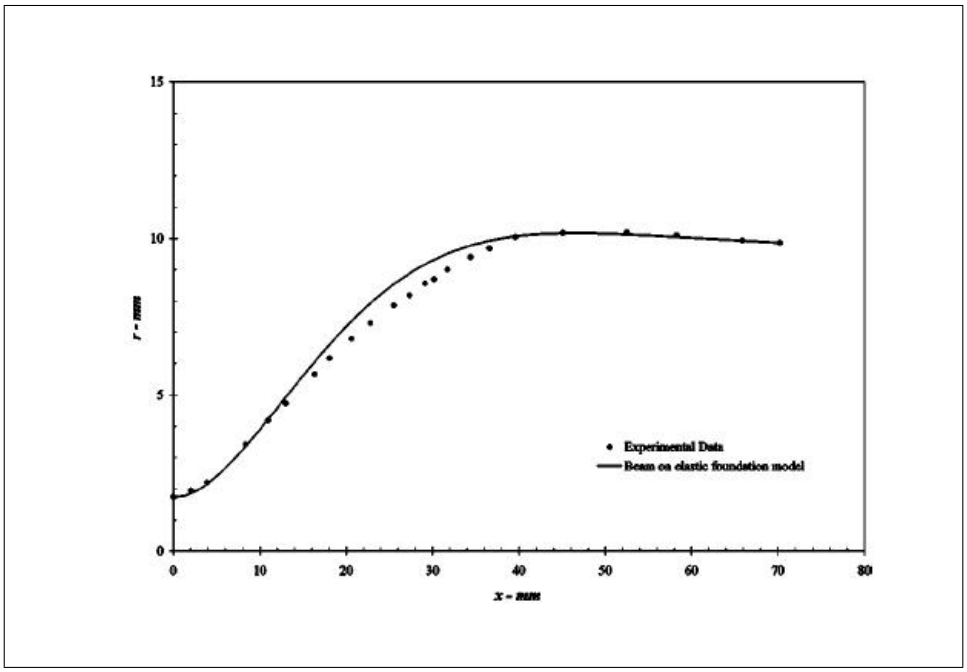

Figure 3.9: Comparison of the measured data with the predictions of the analytical model from the variation of the stent radius along the stent length

3.3 PyFormex: a novel way to build a geometrical model

Since the previous considerations (section 3.1), it is clear that a F.E. model of a braided wire stent (e.g. Wallstent) could open a wide and very interesting scenario of investigations. So our idea is to study the mechanical behavior of such wire stent and the stresses inside its wires using the stent model created by pyFormex. PyFormex [65] is an innovative and creative platform based on Python

scripting language and is currently under development at Ghent University. It provides a powerful tool to build geometrically complex structures by a sequence of mathematical transformations. In fact, the geometrical structure of the stent model is obtained implementing the following four operations (see Fig. 3.10):

1. creation of a planar base module of two crossing wires;
2. extending the base module with a mirrored and translated copy;
3. replicating the base module in both directions of the base plane;
4. rolling the planar grid into a cylinder.

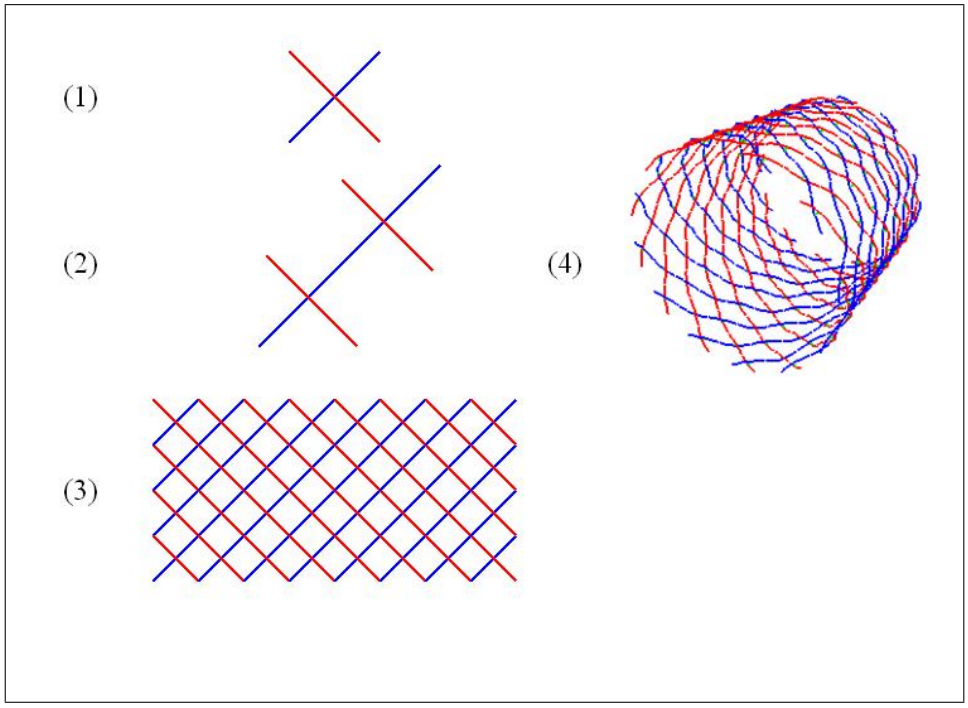

Figure 3.10: PyFormex wire stent model generation.

The model is defined by the following geometrical parameters (Fig. 3.11):

- stent external diameter (D_{e0});
- stent length (L_0);
- wire diameter (d);
- number of wires (n);
- pitch angle (β).

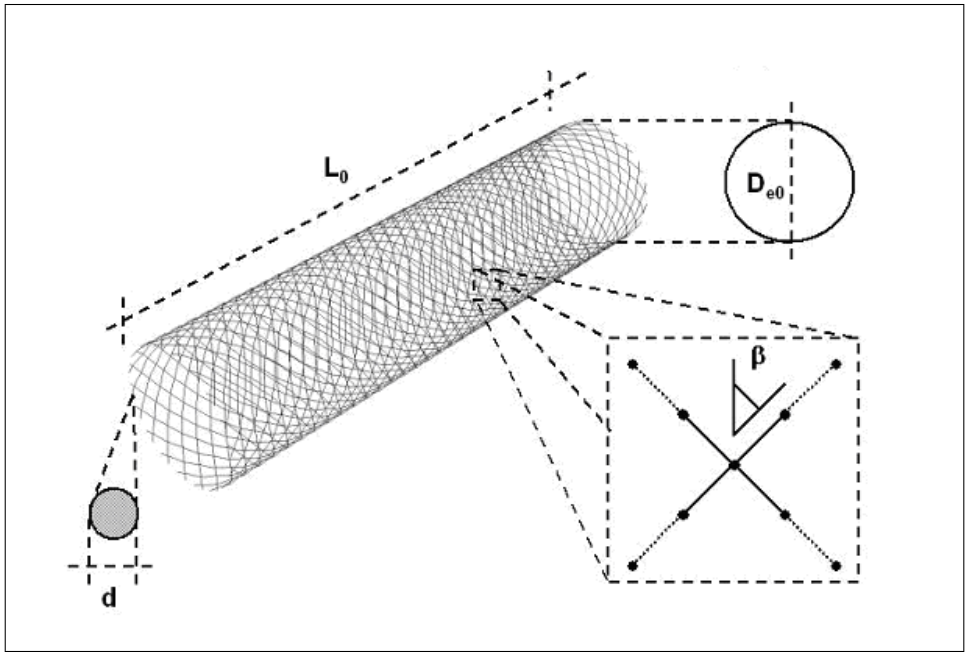

Figure 3.11: PyFormex wire stent geometrical parameters.

Usually, in an engineering model, modeling problems in which two different parts are connected in some way can be an enormous challenge. The connection can be simple or complicated, depending on the constraint between the parts. There can be a kinematic constraint that transmits the velocity of one part to another one or more complicated constraints that involve force-displacement/velocity laws in the relative motion of the parts. To avoid numerical instabilities in the simulations related to contact modeling, connectors are used to implement the contact between all the crossing wires in the wire stent model.

As our problem is fully three dimensional, thus we chose the 3d connector element CONN3D2 which connect two nodes in the space. Moreover, we chose a basic connection component (JOIN). Connection type JOIN makes the position of two nodes the same (e.g. the position of node **b** equal to that of node **a**) [66]. If the two nodes are not coincident initially, the Cartesian coordinates of node **b** relative to node **a** are fixed (see Fig. 3.12). The constraint force in the JOIN connection acts in the three local directions at node **a** and is defined as following:

$$\bar{f} = f_1 e_1^a + f_2 e_2^a + f_3 e_3^a \tag{3.9}$$

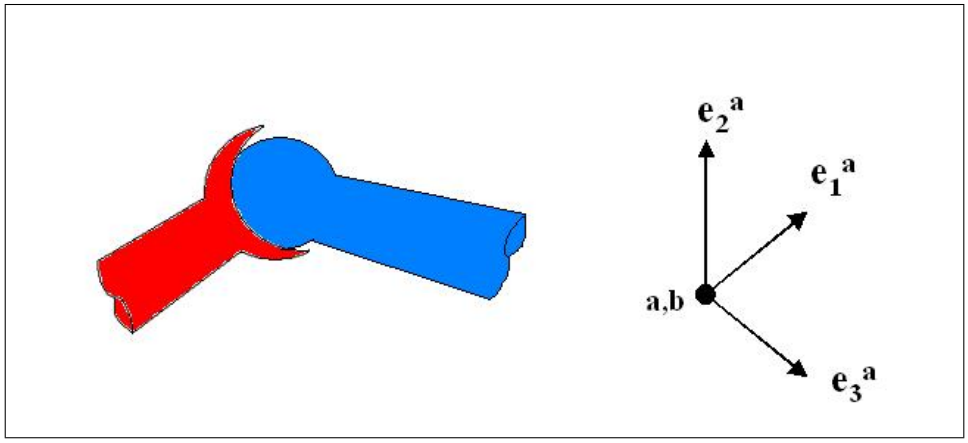

Figure 3.12: Connection type JOIN.

As shown in Fig. 3.13 the connectors are used to maintain a fixed distance between the wires in the crossing points.

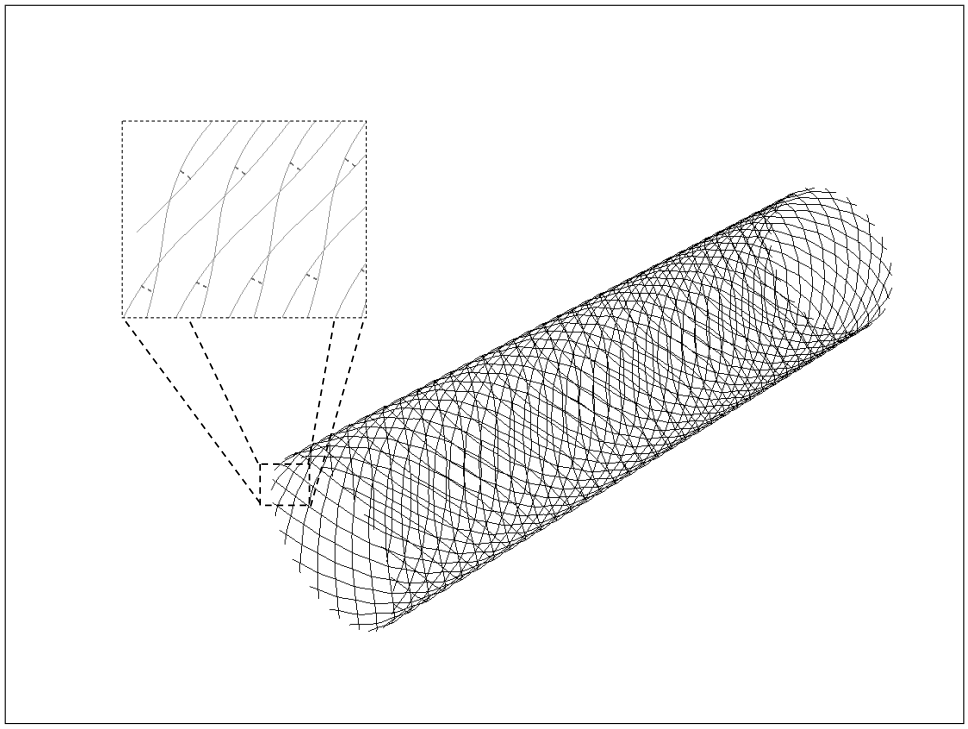

Figure 3.13: Connectors in Wallstent model.

The use of the connector elements allows a realistic curvature in the wire shape in the crossing points.

3.3.1 Geometrical properties of the adopted wire stent F. E. model

The parameters defining the wire stent model geometry used in our F.E.A. are summarized in the Table 3.1:

Table 3.1: Geometrical parameters of the investigated Wallstent

n	Number of wires	36
d	Diameter of stent wire	170 μm
β_0	Pitch angle of the helix at undeformed state	34°
D_{e0}	stent external diameter	20 mm
L_0	Length of the stent	80 mm

3.4 von Mises equivalent stress in the stent wire

3.4.1 Stent wire: the elements

Once the geometrical model is created, it can be imported into a (commercial) numeric solver code in order to implement the material properties and compute its mechanical response to various loading conditions. In our investigation we use the F.E. solver ABAQUS [56]. The mesh of the finite element model is created automatically by PyFormex in the pre-processing phase in which the stent geometrical features are defined. The next step in the F.E. modeling consists in the element choice.

Since that the complex stent structure is wire based, two main assumptions can be done:

- the problem is fully three dimensional;
- the length of the stent wires is significantly greater than the cross-sectional dimensions.

Thus, the beam element seems the more suitable element to model this structure. We want also underline that the structure is complex and that its mechanical behavior is not a priori well known. In the following, we will discuss briefly the beam element and its feature.

The beam elements are based on the beam theory which is the one-dimensional approximation of a three-dimensional continuum. The approximation and consequently the reduction in dimensionality is a direct result of slenderness assumptions: the dimensions of the cross-section are small compared to typical dimensions along the axis of the beam. The axial dimension must be interpreted as a global dimension and not as the element length. Thus the axial dimension can be referred to distance between supports or distance between gross changes in cross-section or wavelength of the highest vibration mode of interest [66]. In ABAQUS a 3D beam element is a one-dimensional line element in three-dimensional space that has stiffness associated with deformation of the beam's axis. These deformations consist of:

- axial stretch;
- curvature change (bending);
- torsion.

Moreover, beam elements offer additional flexibility associated with transverse shear deformation between the beam's axis and its cross-section directions (Timoschenko-type formulation). The main advantage of beam elements is that they are geometrically simple and have few degrees of freedom. This simplicity is achieved by assuming that the member's deformation can be estimated entirely from variables that are functions of position along the beam axis only. Thus, it is important to judge

whether such one-dimensional modeling is appropriate. The fundamental assumption used is that the beam section (i.e. the intersection of the beam with a plane that is perpendicular to the beam axis) cannot deform in its own plane. The beam elements, available in beam element library of ABQ/STD can be divided in two families:

- Euler-Bernoulli-type beams;
- Timoschenko-type beams.

Euler-Bernoulli(slender) beam elements do not allow for transverse shear deformation; plane sections initially normal to the beam's axis remain plane and normal to the beam axis. They should be used only to model slender beams: the beam's cross-sectional dimensions should be small compared to typical distances along its axis. For beams made of uniform material, typical dimensions in the cross-section should be less than about 1/15 of typical axial distances for transverse shear flexibility to be negligible. The ratio of cross-section dimension to typical axial distance is called the slenderness ratio. The Euler-Bernoulli beam elements use cubic interpolation functions, which makes them reasonably accurate for cases involving distributed loading along the beam.

Timoshenko beam elements (as B31) allow for transverse shear deformation. They can be used for thick as well as slender beams. ABAQUS assumes a linear elastic response with fixed modulus of Timoshenko beams in the transverse shear behavior. So it is independent of the response of the beam section to axial stretching and bending.

We adopt three-dimensional linear beam elements (b31) based on the Timoshenko's formulation with a circular cross-section profile.

3.4.2 Materials

Since the goal of this chapter is to highlight and understand the relation between the stent material properties and the stress in the stent wires, several materials will be taken into account. We will refer, when possible, to experimental data or data provided in literature to characterize the behavior of these materials. We will also label the materials in order to avoid confusion when referred to.

Phynox

In the following investigation Phynox is assumed as an (ideal) elasto-plastic material with mechanical properties defined by the following engineering constants:

E	Young's module	220000 MPa
ν	Poisson's ratio	0.33
σ_y	Yielding stress	1578 MPa

Nitinol

The nitinol super-elastic mechanical behavior (see section 2.2.5), implemented using the UMAT subroutine in ABAQUS, is based on the uniaxial behavior shown in Fig. 3.14:

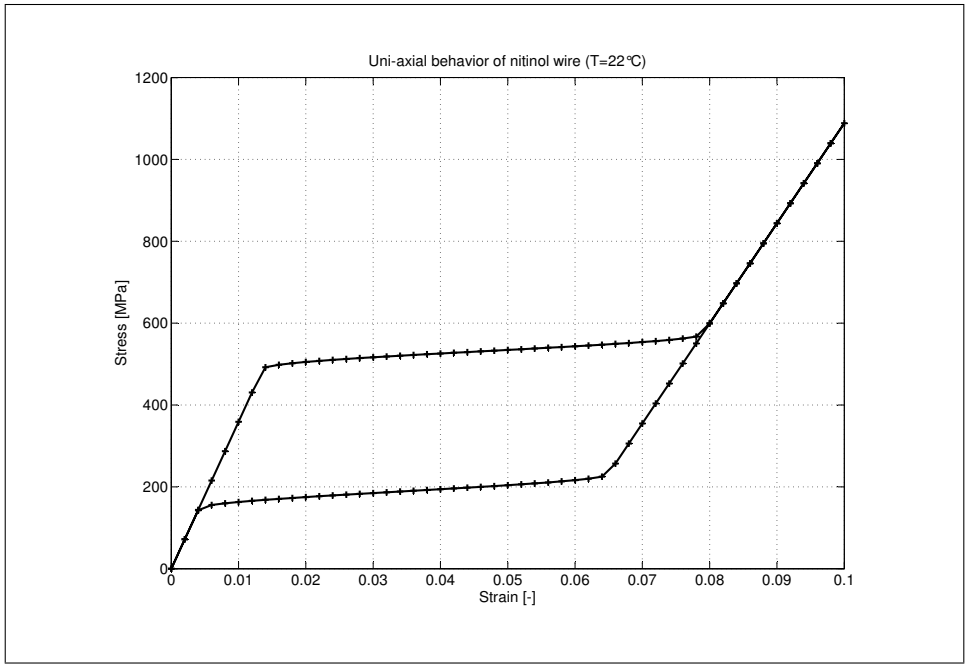

Figure 3.14: Stress-strain curve of Nitinol

We refer to the uniaxial behavior of a nitinol wire provided by Pelton [67](Fig. 3.15(a)-(b)).

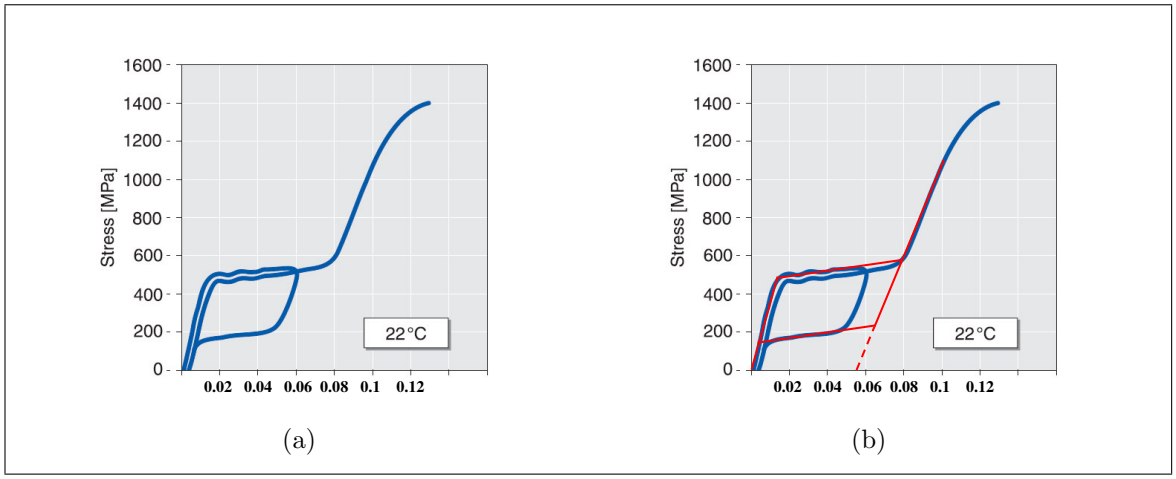

Figure 3.15: (a)Stress-strain curve of a nitinol wire under axial load in Pelton et al. [67];b) Nitinol material parameters obtained by the stress-strain curve considered.

Table 3.2 shows the values of the parameters used as input to Umat/Super-elasticity (Fig. 3.16).

Table 3.2: Parameters in Abaqus' Umat

Parameter	Description	Value
E_A	Austenite elasticity	35877 MPa
ν_A	Austenite Poisson's Ratio	0.33
E_M	Martensite elasticity	24462 MPa
ν_B	Martensite Poisson's Ratio	0.33
ϵ^L	Transformation strain	0.0555
$(\partial\sigma/\partial T)_L$	$(\partial\sigma/\partial T)$ loading	6.7
σ_L^S	Start of transformation loading	489 MPa
σ_L^E	End of transformation loading	572 MPa
T_0	Temperature	22° C
$(\partial\sigma/\partial T)_U$	$(\partial\sigma/\partial T)$ unloading	6.7
σ_U^S	Start of transformation unloading	230 MPa
σ_U^E	End of transformation unloading	147 MPa
σ_{CL}^E	Start of transformation stress (loading in compression)	–
ϵ_V^L	Volumetric transformation strain	–

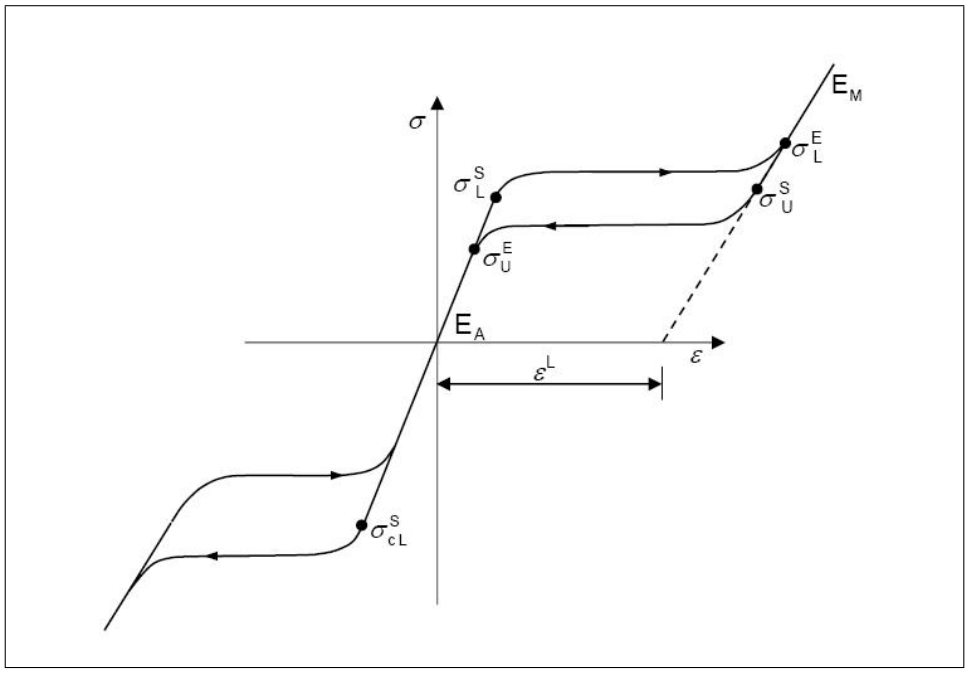

Figure 3.16: Nitinol super-elastic behavior in Umat subroutine.

The uniaxial behavior has been obtained simulating a uniaxial test (displacement driven) in 2 direction as shown in Fig.3.17.

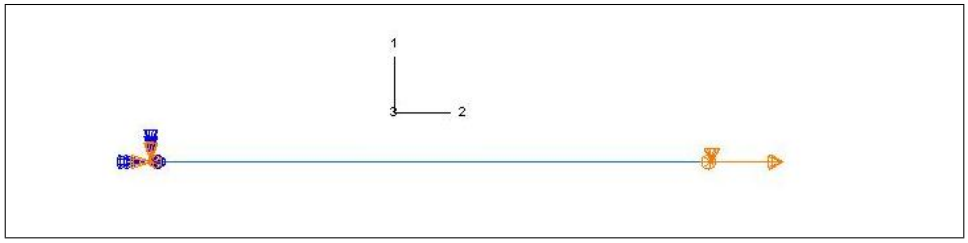

Figure 3.17: Uniaxial test for a nitinol wire.

Table 3.3: Wire geometrical properties

Length(L)	10 mm
Section's profile	Circular(r=0.5642 mm; Area=1 mm^2

The use of the Umat subroutine requires to define the transverse shear stiffness. Usually, ABAQUS calculates the transverse shear stiffness values required in the element formulation but the default shear stiffness values are not calculated in some cases if estimates of shear moduli are unavailable during the preprocessing stage of input; for example, when the material behavior is defined by user subroutine UMAT, UHYPEL, UHYPER, or VUMAT . In such cases the transverse shear stiffness must be defined. So when we use the UMAT for nitinol, we will define the transverse shear stiffness as follows:

- $K_{\alpha 3}$=kGA with $\alpha = 1, 2$;

where **G** is the elastic shear modulus or moduli and **A** is the cross-sectional area of the beam section and **k** is a constant. For circular section **k** is defined as 0.89 [66].

Stainless steel Type 316L

In the following investigation Stainless steel (SS) Type 316L is assumed as an (ideal) elasto-plastic material with mechanical properties defined by the following engineering constants [68]:

E	Young's module	201000 MPa
ν	Poisson's ratio	0.33
σ_y	Yielding stress	330 MPa

3.4.3 The analytical model

Let us consider the reduction of the stent diameter. In one end of the stent, a force nF acting along the longitudinal axis of stent is applied while the other end of the stent is constrained in both the tangential and axial direction, allowing only radial displacements.. The action of the force provides a stent elongation and a changing of the pitch angle β (see Fig.3.18).

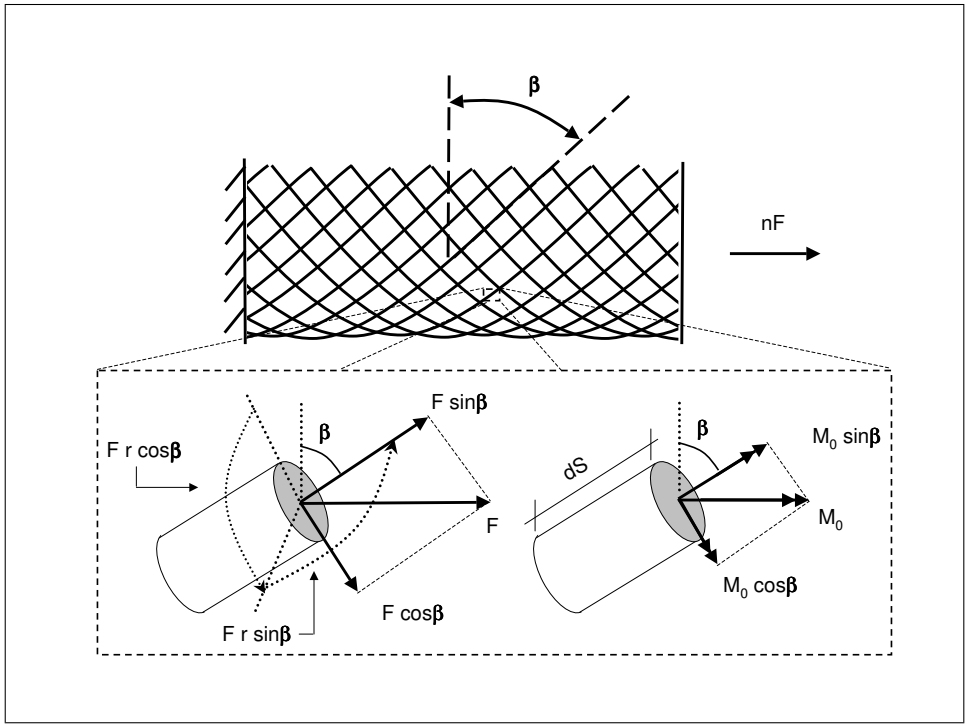

Figure 3.18: Axial force in the wire stent and resulting forces and moments over the wire.

As proposed by Jedwab (see section 3.2.1), we consider the stent as a combination of a number n of independent open-coiled helical springs undergoing large rotation with ends fixed against rotation since the friction between the wires in the crossing points. Under these conditions the analytical model is based on the Wahl's spring theory for springs with ends fixed against rotation. The initial average stent diameter D_0 is related to the initial stent diameter D_{e0} by:

$$D_0 = D_{e0} - 2d \tag{3.10}$$

$$D = \frac{D_0 cos\beta}{cos\beta_0} \tag{3.11}$$

Where D_0 an D are, respectively, the initial and the current average stent diameter. Consequently the initial and current average radius are r_0=$\frac{D_0}{2}$ and r=$\frac{D}{2}$. The moment M_0 and the load F acting on a single wire (Fig. 3.18) are defined as:

$$F = \frac{GI_p cos\beta}{r}\left(\frac{sin\beta cos\beta}{r} - \frac{sin\beta_0 cos\beta_0}{r_0}\right) - \frac{EIsin\beta}{r}\left(\frac{cos^2\beta}{r} - \frac{cos^2\beta_0}{r_0}\right) \tag{3.12}$$

$$M_0 = GI_p sin\beta\left(\frac{sin\beta cos\beta}{r} - \frac{sin\beta_0 cos\beta_0}{r_0}\right) + EIcos\beta\left(\frac{cos^2\beta}{r} - \frac{cos^2\beta_0}{r_0}\right) \tag{3.13}$$

Finally, considering that F and M_0 act simultaneously, the bending moment m_b and the twisting moment m_t acting on the element A of length dS are:

$$m_b = M_0 cos\beta - Frsin\beta = F_1 = EIsin\beta\left(\frac{cos^2\beta}{r} - \frac{cos^2\beta_0}{r_0}\right) \tag{3.14}$$

$$m_t = M_0 sin\beta - Frcos\beta = F_2 = GI_p\left(\frac{sin\beta cos\beta}{r} - \frac{sin\beta_0 cos\beta_0}{r_0}\right) \tag{3.15}$$

So defining the shear and the bending stress [60]:

$$\tau = \frac{16 m_t}{\pi d^3} \tag{3.16}$$

$$\sigma = \frac{32 m_b}{\pi d^3} \tag{3.17}$$

The Von Mises equivalent stress σ_e is given by:

$$\sigma_e = \sqrt{\sigma^2 + 3\tau^2} \tag{3.18}$$

Defining the yield strength of the material σ_y, the maximum bending stress, according with von Mises criterion, should not exceed the σ_y in order to avoid plastic deformations. In fact the undesired plastic deformation could lead to problems in stent deployment out of the catheter.

The analytical computation of the von Mises stress is performed implementing the proposed model in Matlab (see Appendix B). The array containing the pitch angle is used as input. The pitch angle goes from 34° to 89°.

3.4.4 F.E. approach

Proposed method for stent axial loading

In the numerical simulation the reduction of the stent diameter is modeled by applying a concentrate load on one end of each stent wire. The force F increases smoothly from 0 to 0.6 N. The other end of the stent is constrained in both the tangential and axial direction, allowing only radial displacements. The action of the concentrate force provides a stent elongation and a changing of the pitch angle β. The von Mises equivalent stresses computed by finite element model will be compared with the analytical results to provide an analytical validation of the finite element model.

Output

The output MISESMAX in the five nodes of the F.E. model were considered (see Fig. 3.19(a)) and the average of the numerical results was performed in order to consider the non uniform distribution of the deformation along the stent. MISESMAX provides, for a beam element, the maximum von Mises stress among all the section points (points 3, 7, 11, and 15) in the cross-section.
In ABAQUS, several default integration points are used in the beam in space (circular profile): 3 points in radial direction, 8 along the circumference (17 total; trapezoidal rule). Instead, default stress output points, in the integration during the analysis are on the intersection of the surface with the 1- and 2-axes (points 3, 7, 11, and 15 above for default integration) (Fig. 3.19(b)).

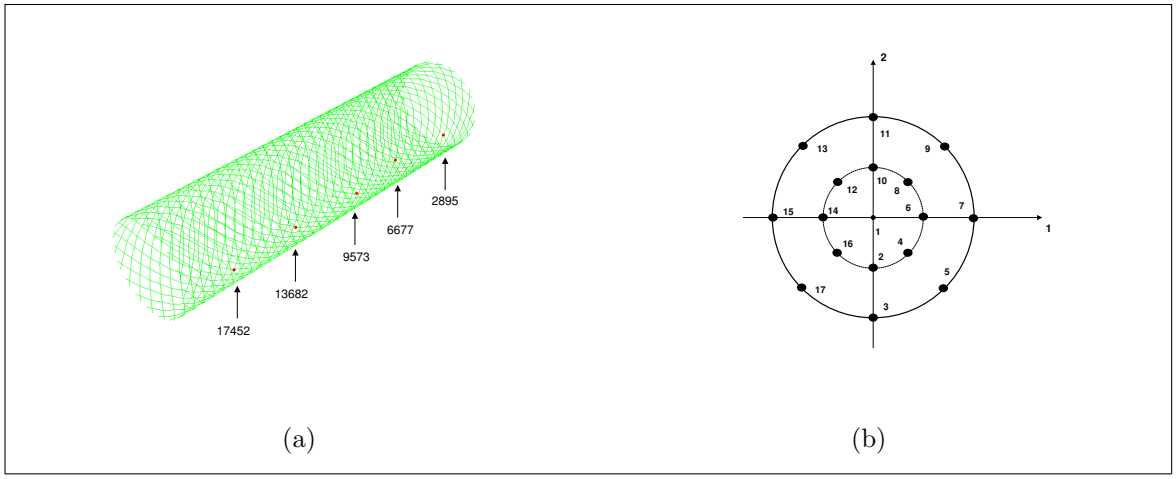

Figure 3.19: Integration points in beam circular section (a) and output nodes in F.E. model (b)

3.4.5 Results

VNM equivalent stress in phynox stent wire

Plotting the equivalent von Mises stress in function of the stent diameter, there is a good match between the data from F.E.M. and the data from the analytical model using phynox material properties, as shown in Fig. 3.20.

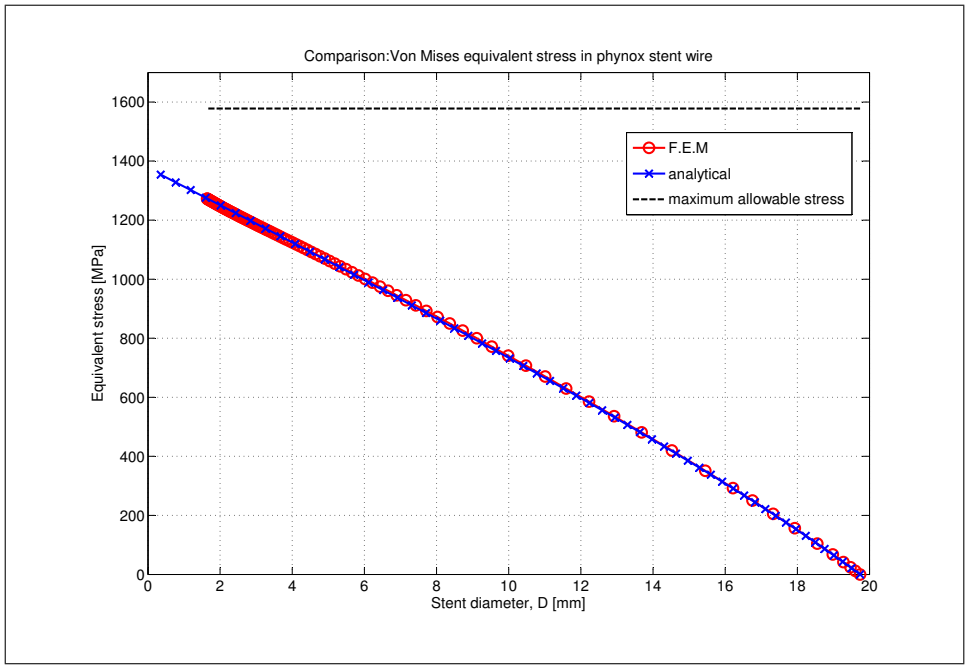

Figure 3.20: VNM stress in phynox stent wire.

Computing, analytically, the VNM stress for the phynox stent wire we obtained, as expected, that VNM equivalent stress is proportionally related to the wire diameter as shown in Fig. 3.21.

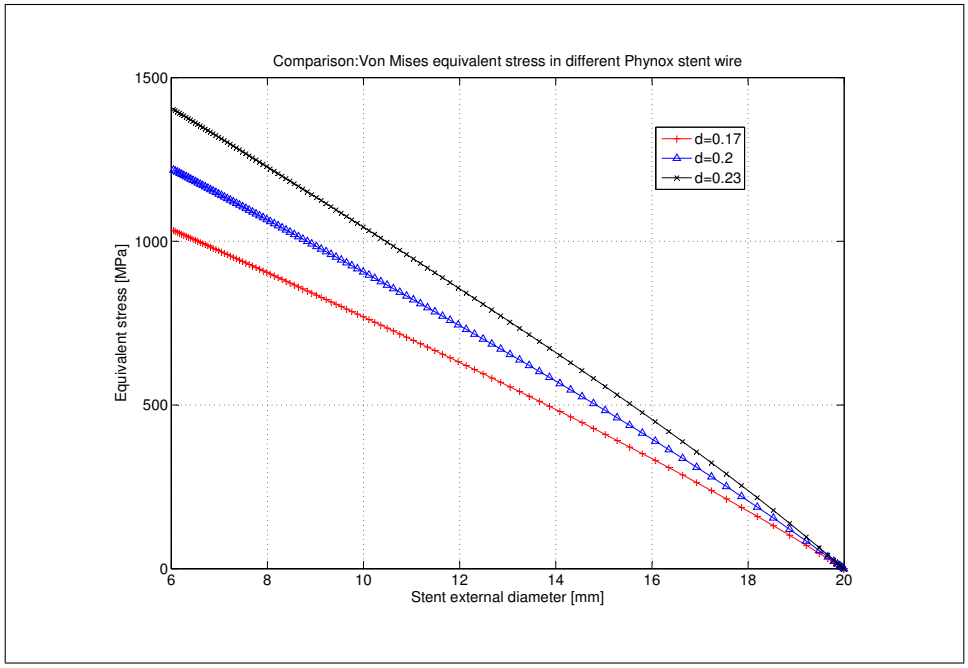

Figure 3.21: VNM stress in phynox stent wire with different diameters.

VNM equivalent stress in nitinol stent wire

Referring to Fig. 3.22, which shows the equivalent von Mises stress in nitiniol stent wires as function of the stent diameter, it is possible to observe that:

- applying the same axial force applied on the phynox stent it is possible to reach a smaller diameter (less than 2 mm);
- the numerical data well match the analytical data;
- a discrepancy takes place when the stent diameter gets less than 4 mm and the equivalent stresses have a sudden increase when stent diameter gets less than 2 mm;
- since the maximum allowable stress according with the von Mises criterion is not reached, Nitinol, in this case, behaves as an elastic material adn its superleastic behavior is not exploited.

The variation of the stent diameter D with the axial force axial force nF acting the whole stent during the axial load (see Fig. 3.18) is shown in Fig. 3.23 and in Fig. 3.24. The variation is computed using the material properties of Phynox (see Fig. 3.23) and the material properties of Nitinol (see Fig. 3.24).
The curves suggest that during the stretch of the stent there is a limiting state corresponding to a fully collapsed condition (i.e. stent inserted in the catheter) according with the results obtained by Ravi-Chandar and Wang [62] (see section 3.2.2). At the limiting state the axial stiffness of the stent is high, implying that a large change in axial force provides a very small change in diameter since that the stent wires are not more able to accommodate their axial elongation. The limiting state does not depend by the material properties.
The limiting state takes place at diameter less than 2 mm. Clearly, since the different elastic moduli of the two materials (E_{Phynox} (220GPa) is almost 7 times higher than $E_{Nitinol}$ (35.877 GPa)), an

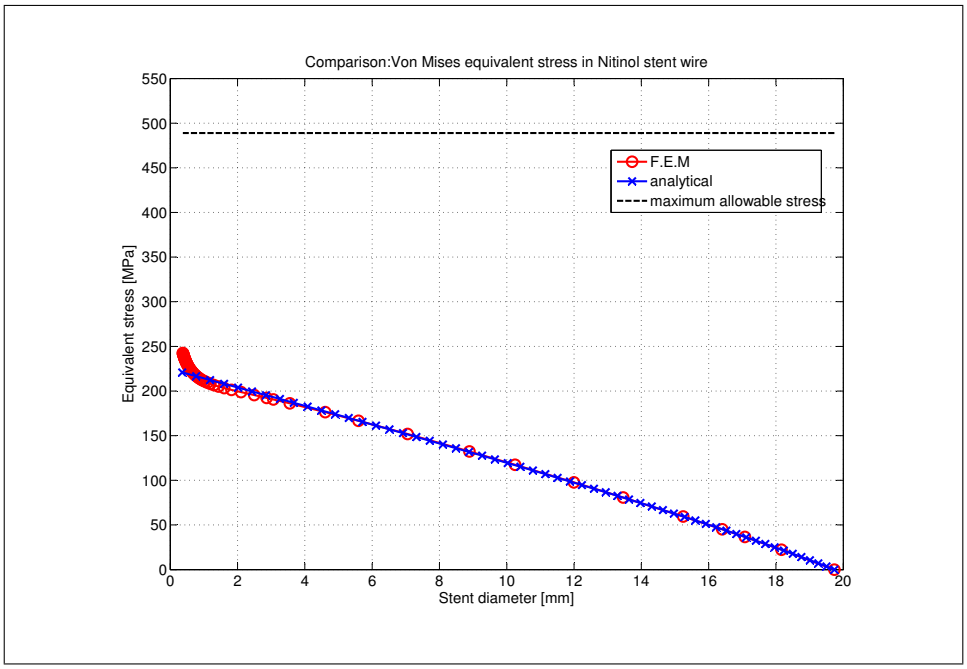

Figure 3.22: VNM stress in Nitinol stent wire.

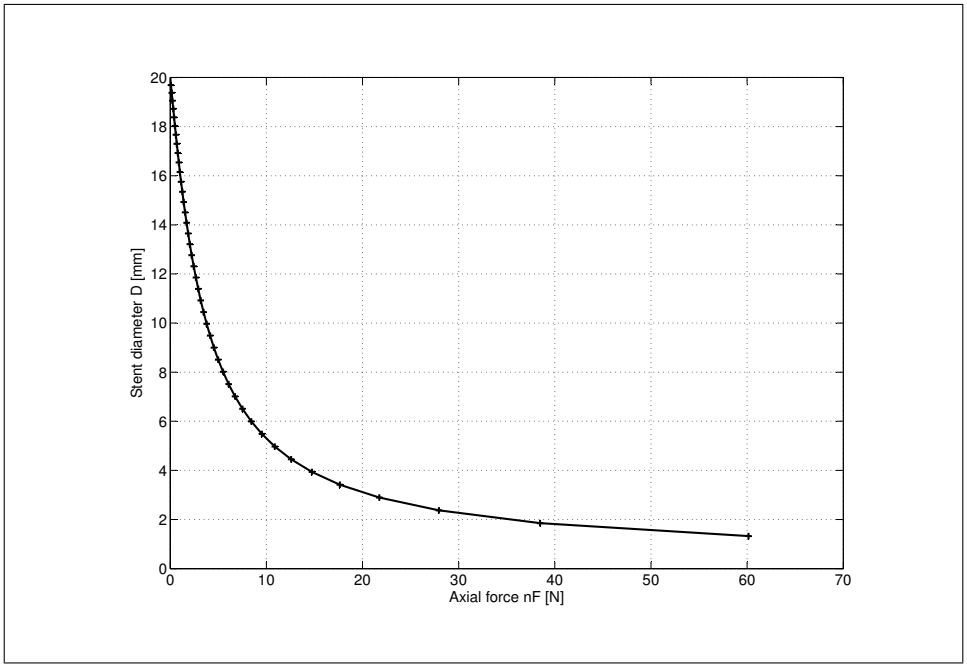

Figure 3.23: Variation of the diameter D with the axial load nF using Phynox.

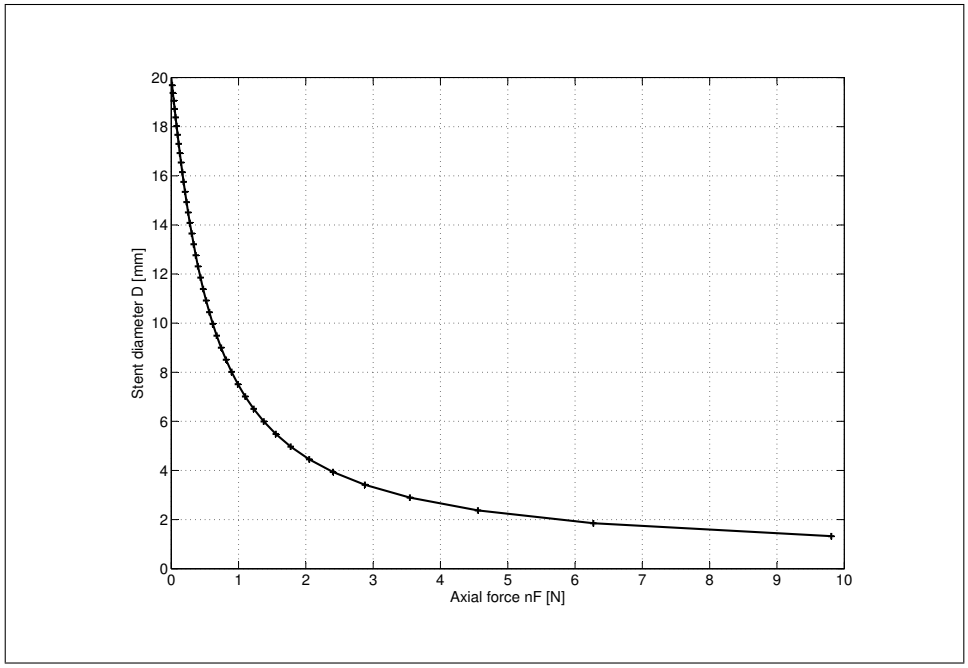

Figure 3.24: Variation of the diameter D with the axial load nF using Nitinol.

higher axial force is required to achieve the limiting state using Phynox (about 35.5 N) than Nitinol (about 5.5 N).

VNM equivalent stress in stainless steel stent wire

The Fig. 3.25 shows the von Mises equivalent stress during the axial loading and unloading phase of the stent using Phynox and stainless steel type 316L. Comparing the mechanical response provided by the two materials, it is possible to notice that the equivalent VNM stress, using SS 316L, exceeds the yield stress and a residual stress (244 MPa) occurs when the load is released, in contrast using Phynox, the stent recovers elastically the original diameter. The plastic deformations leads an incomplete recovering of the original undeformed shape; the final stent diameter is about 12 mm, it means that the the stent recovers only the 55% of the original diameter (i.e. 20 mm).
Fig. 3.26 shows the the von Mises equivalent stress in the stent wires stainless steel 316L made when two different loading-unloading paths are performed. In the fist loading case (solid line with marker + in Fig. 3.26), the stent diameter is reduced to almost zero by axial load ($\|F\|$=0.6 N) and then the stent is unloaded releasing the load. In the second loading case (solid line with circular marker in Fig. 3.26) the stent diameter is reduced to 3 mm by axial load ($\|F\|$=0.14 N) and then the stent is unloaded releasing the load. It is possible to notice that the residual radial deformation depends by the entity of the loading path, in fact in the second loading case the final stent diameter is 12.2 mm (61% of stent diameter recovering) in contrast in the first case the final stent diameter is 9.8 mm (49% of stent diameter recovering)

Residual stress are the almost same for both case (239 Mpa in the first case-219 in second case).
It is necessary to underline that the obtained numerical data with elasto-plastic material are not analytically validated. Hovewer they could be consider reliable since the excellent results achieved for the analytical validation of the elastic behavior.

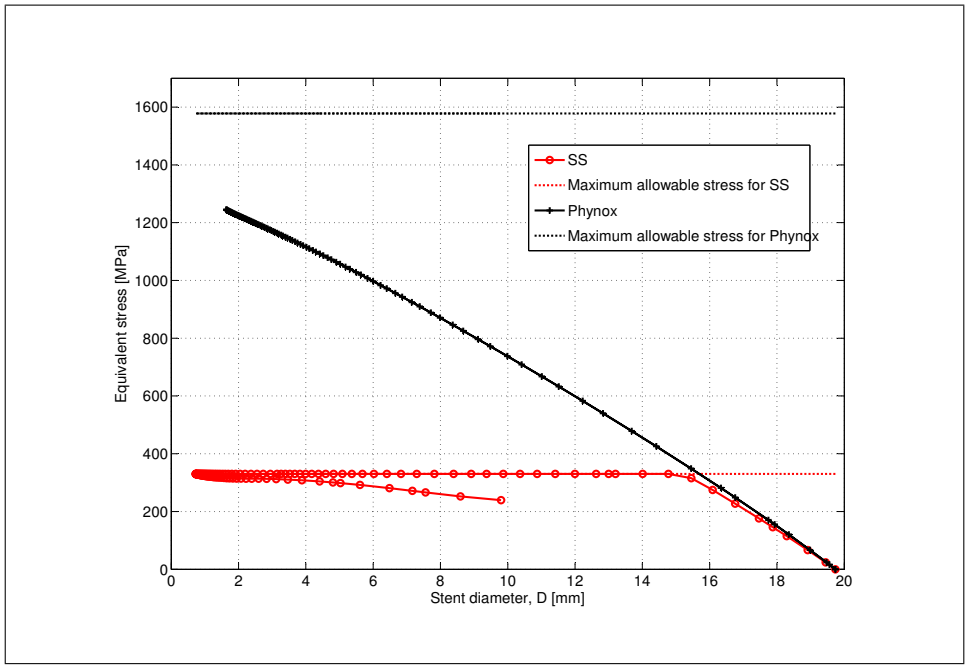

Figure 3.25: Axial loading and unloading of the stent: von Mises equivalent stress in stent wires using Phynox and stainless steel.

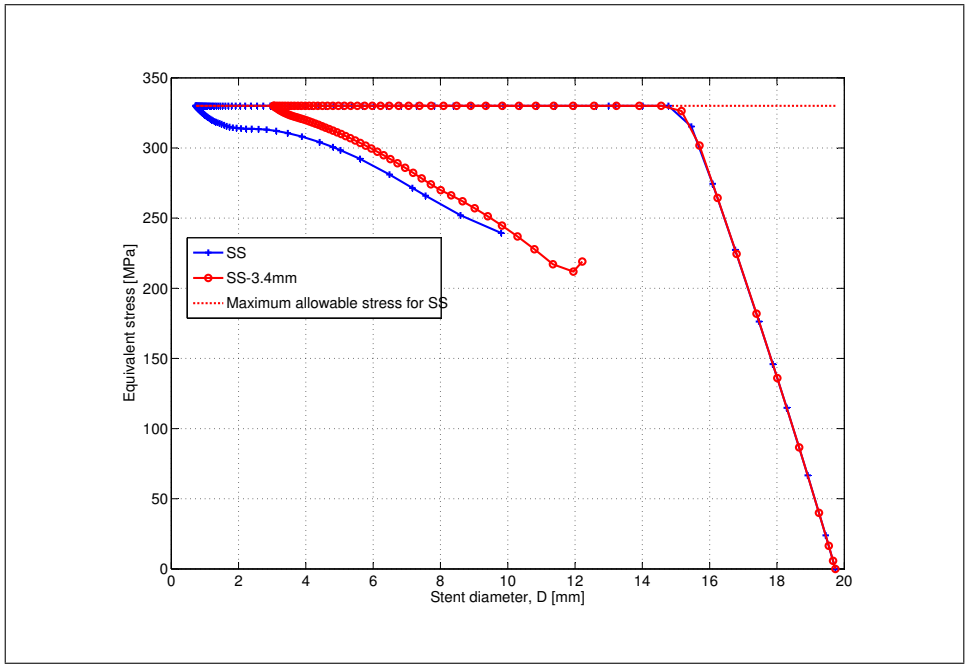

Figure 3.26: Axial loading and unloading of the stainless steel stent: two different loading paths.

3.4.6 VNM stress and catheter size

The numerical computation of the von Mises equivalent stress can be a useful approach to define the smallest catheter diameter when the mechanical and geometrical properties of the wire stent are defined. So computing the von Mises stress for phynox stent with a wire diameter of 0.17 mm and with the other geometrical properties defined in the Table 3.1 is possible to reach a stent diameter of 2.5 mm without plastic deformation, as shown in Fig. 3.20. So it seems feasible to reduce the actually used catheter size from 10 F (i.e. 3.4 mm) [21] to 7.5 F (i.e. 2.5 mm).

The Nitinol, in this case, works only in the elastic region so it is possible to say that the stent behaves elastically and its superelastic behavior is not exploited.

The use of stainless steel as stent material, for the assumed cases of loading and assumed geometry , provides unrecoverable plastic deformations which compromises the stent performance.

However it is necessary, in this discussion, to take into account that the reduction of the catheter diameter can influence:

- the required force to release the stent from the catheter, since the friction action between stent and catheter;
- the kink resistance of the stent-catheter system.

Chapter 4

Free stent expansion

The investigation of the wire stent can not leave the stent deployment out of consideration. In this section,firstly, we will discuss the delivery system of the Wallstent® and then we will propose an innovative and stable method to perform numerical simulations of wire stent free expansion and we will discuss the mechanical response.

4.1 The Wallstent and the Unistep delivery system

The goal of this section is:

- to provide a view on the state of the art of the SX wire stent as Wallstent® and its delivery system;
- to explore the idea on which is based the deployment of the wire stent.

Let us consider the Wallstent® Endoprothesis distributed by Boston Scientific Scimed Inc. [21] (see Fig. 4.1). The stent is combined with a Unistep™ delivery system. The main device features proposed by the manufacturer [21] are:

- high recapture-ability: this features allows a perfect stent placement even if it is not quite right the first time. The Wallstent® Endoprothesis is recapturable even when up to 87% deployed;
- high radiopacity;
- high flexibility: the flexible stent and shaft facilitates access, tracking and smooth crossing of lesions, even in the most challenging anatomies;
- conformability: unique tapering design allows optimal apposition in tortuous or tapered vessels.

In the device description provided by the manufacturer it is also highlight that the new delivery system (i.e. Unistep delivery system™) offers reduced profile and increased flexibility. This shows clearly the essential role of the delivery system in the stent performance and the usefulness of a F.E. simulation of the stent free expansion. The usefulness of the F.E. analysis is also underlined by the FDA approval requirements for the medical devices (see document Summary of Safety and effectiveness [69]).

The Unistep delivery system™ is a recent commercial embodiment of various stent delivery system design. For this reason, in order to understand the idea on which is based the wire stent deployment, let us consider the delivery system proposed by Burton et al. described in the U.S. Patent NO. 5,026,377. In the following we will refer to Fig. 4.2, which shows a side elevation, partly in section , of the delivery system proposed in the patent, labeling numerically the different parts of system according with this picture. Thus, the delivery system consists in the following components:

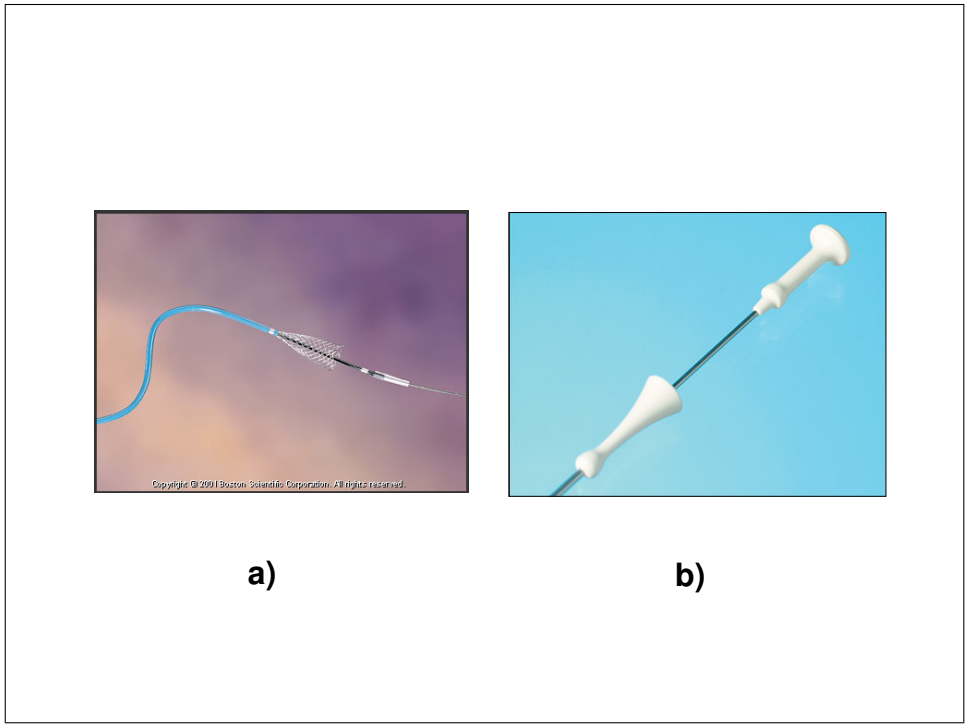

Figure 4.1: a) Wallstent Endoprothesis [21]; b) proximal part of the Unistep delivery system [21].

- an outer sleeve (1) having a handle (2) at its proximal end[1];
- an hollow core (5) disposed axially within the outer sleeve (1) having an handle (6) at its proximal end;
- the distal end (7) of the hollow core (5) has a stepped up diameter to favor a smooth diameter transition during the insertion in the body channel;
- a guide wire (8): the core is hollow to allow the insertion of a guide wire (8) in order to perform a precise set of the device in body duct;
- a grip member (9): it is attached at the distal end of the core: it is the most significant feature of the instrument, in fact is to enable both deployment and retraction of the stent (10).

The grip member, attached at the distal end of the core, may be a sleeve or coating having a larger diameter than the remainder of the core. The suitable materials for member grip are silicone rubber or polyurethane. The grip member has circumferential gaps (12, 13) closed its distal and proximal part to allow the stent ends accommodation in the constrained configuration.

The stent is constrained between the grip member (9) and the outer sleeve (1). The deployment of the SX is performed holding fixed the inner core (5) and at same time withdrawing the outer sleeve providing a relative slip motion between two parts.

[1]The term proximal means the end or part nearest to the operator and consequently the term distal means the end or the part furthest of the operator (3 in Fig.4.2)

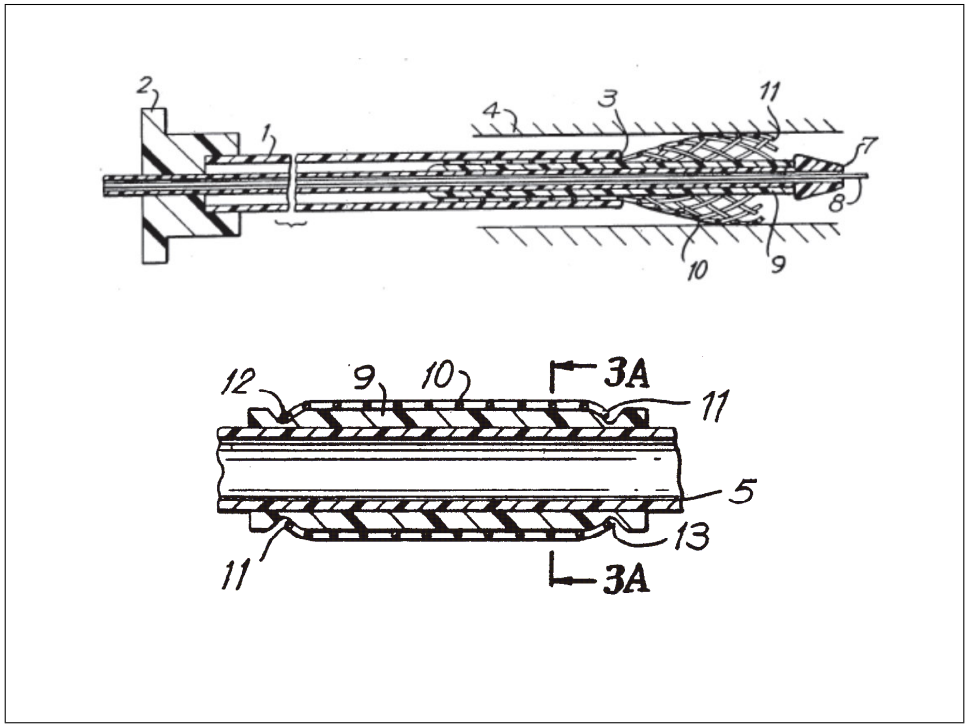

Figure 4.2: Drawings from U.S. Patent NO. 5,026,377. On top) Stent deployment system; on bottom) grip member.

To allow an easy stent deployment is necessary that the inner surface of the outer sleeve (1) is made from low friction material and it is necessary to provide a sufficient gap clearance between the grip member (9) and the outer sleeve (1).

4.2 The standard approach: stent-catheter interaction

The (at first sight) obvious way to simulate the stent deployment out of the catheter should be to consider the actual interaction between the wire stent and the catheter. For this reason, we design the F.E. model of the catheter as an discrete cylindrical rigid body. The idea is to perform a simulation including the stent insertion into the catheter and the free stent expansion performing, numerically, the stent catheter interaction. The scheme in Fig. 4.3 shows the main steps of the numerical simulation.

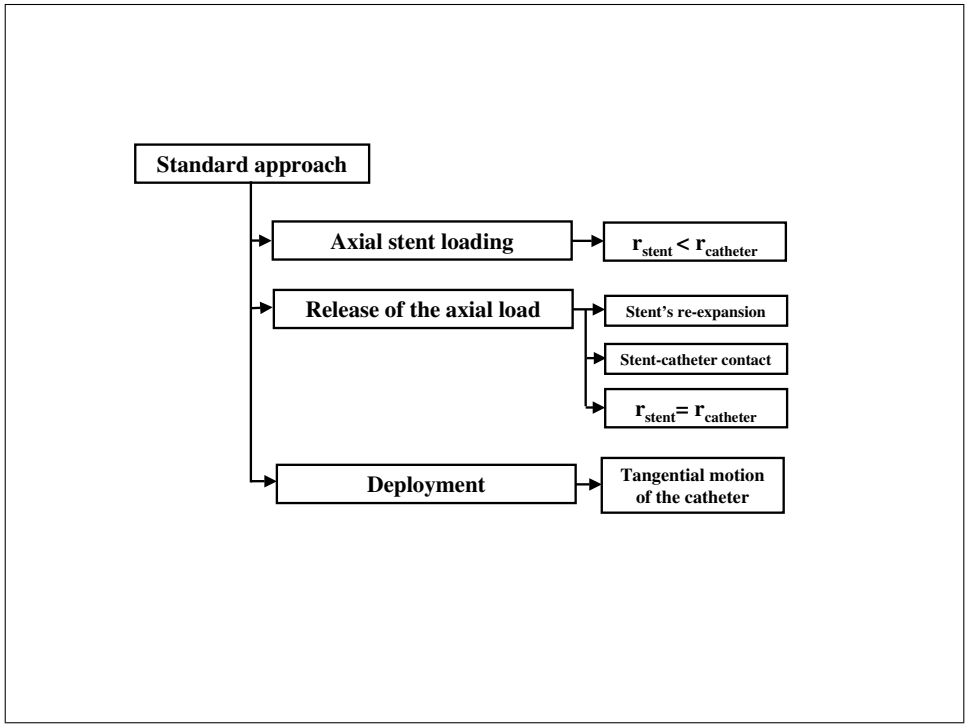

Figure 4.3: Steps in the numerical simulations of stent free expansion (standard approach).

4.2.1 Interaction between surfaces in ABAQUS standard

The stent-catheter interaction, as many other engineering problems, involves the contact between two different bodies: the stent and the catheter. Of course the contact analysis is one of the most interesting parts of F.E. simulations but it also involves non banal computational aspects. In this section we provide a brief overview of the parameters and the capabilities of ABAQUS standard (ABQ/STD) used in our simulations.

In a contact analysis, the first step is characterized by the definition of the contact pair surfaces; in our case they are the inner surface of the catheter and the wires of the stent. We hypothesize that the contact between the stent wires and the catheter takes place in the outer-nodes of the stent model, i.e. the nodes in contact with an imaginary cylindrical surface that has the same diameter as D_{e0}. Once the contact pair surfaces are chosen, it is necessary to define the surface discretization, the contact formulation and the tracking approach. We assume that the tangential motion between the bodies is frictionless.

Discretization of contact pair surfaces

The contact discretization is the way to define the locations and the conditions applied on each surface in the contact analysis. Two options are available: node-to-surface or surface-to-surface approach. Since the structure of the stent model, where a surface is not defined, it is necessary to choose the node-to-surface interaction. With this discretization one node of the slave interface (point s) (see Fig.4.4) interacts with a projection point in the other interface (point c), the master one. So in each contact condition involves a single slave node (point s) and a group of master node in the neighborhood of the projection point (m_1 and m_2). When the gap function gets zero, the contact takes place.

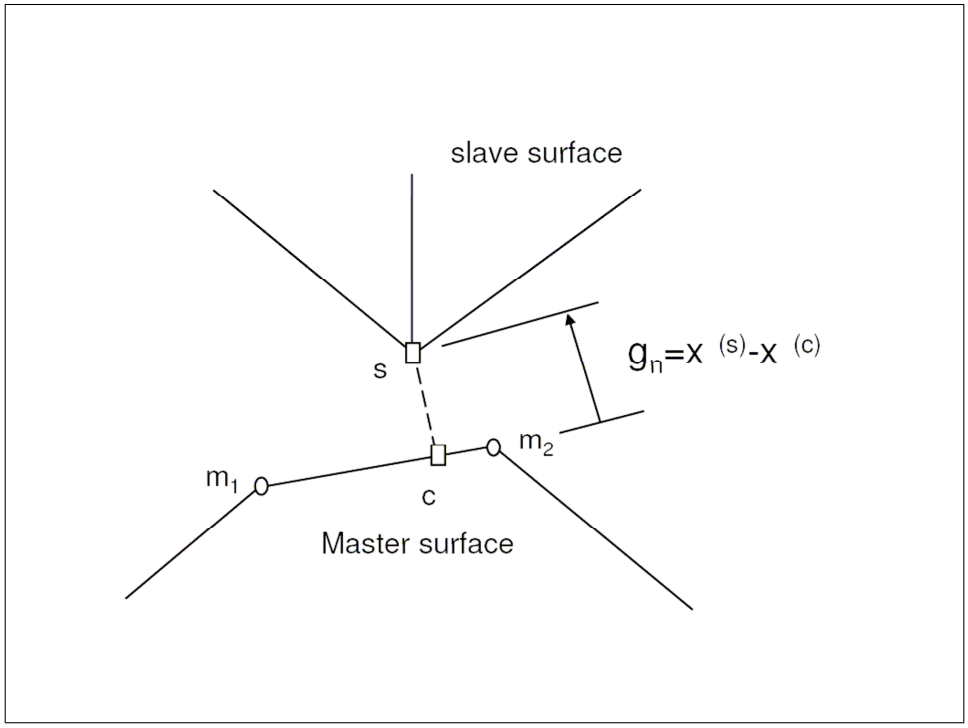

Figure 4.4: Node-to-surface approach.

Contact tracking approach

In the contact analysis is necessary to take into account the relative motion of the surfaces of the contact pairs. In ABQ/STD there are two tracking approaches:

- finite-sliding tracking approach assumes an arbitrary relative motion of the contacting surfaces;
- small-sliding tracking approach assumes a small relative motion of the contacting surfaces.

Finite-sliding contact is the most general tracking approach and allows for arbitrary relative separation, sliding, and rotation of the contacting surfaces. For finite-sliding contact the connectivity of the currently active contact constraints changes upon relative tangential motion of the contacting surfaces. The finite-sliding, node-to-surface contact formulation requires that master surfaces have continuous surface normals at all points. Convergence problems can result if master surfaces that do not have continuous surface normals are used in finite-sliding, node-to-surface contact analysis; slave nodes tend to get stuck at points where the master surface normals are discontinuous.

The small-sliding approach reduces to an infinitesimal-sliding and rotation approach, in which it is assumed that both the relative motion of the surfaces and the absolute motion of the contacting bodies are small [66].
In our case, we should use the finite-sliding approach since the axial and radial large displacements which the stent experiences when it deploys out of the catheter. It is necessary to specify at this point that to simulate only the static contact between the stent and the inner surface of the catheter the small sliding approach is appropriate. In our simulation, we define as static the stent-catheter contact which not involves tangential relative motion between the two bodies.

Master surface and slave surface

Since we modeled the catheter surface as a rigid-element based surface it must be chosen as the master surface. The stent interface is based on the outer node subset, so it is a node-based surface and it can only act as the slave surface.

4.2.2 Results

The simulations using the standard approach did not converge because severe contact over closure. An over closure takes place when during the contact analysis a node of a surface of the contact pair penetrates the other surface (Fig. 4.5). It happens when the gap function g is less then zero. In our simulations the severe over closures lead to numerical problems during the stent deployment thus during the relative tangential motion of the bodies.

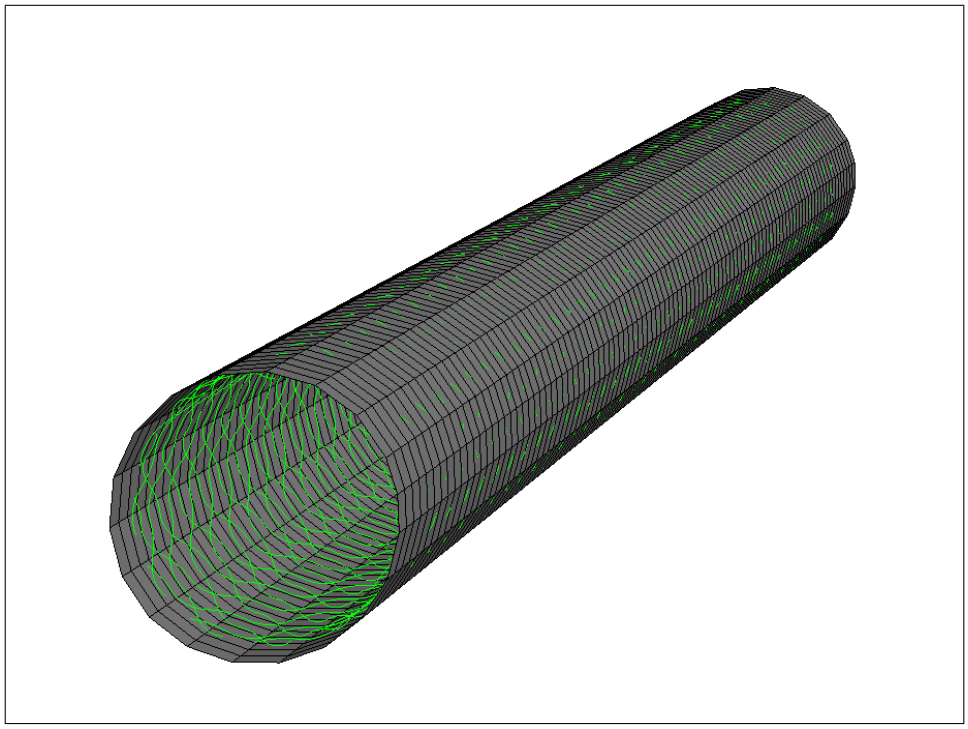

Figure 4.5: Stent-catheter interaction using standard approach.

Because of the complex structure of the stent model, many severe over closures were present in the analysis and we were not able to solve this numerical problem using the capabilities available. Therefore, we propose an other approach.

4.3 An innovative approach using BCs

The standard strategy to model the wire stent expansion involves a very complex contact problem characterized by numerical instabilities and long (unpractical) simulation times. In order to avoid this computational problem the stent expansion is modeled as a displacement driven process mimicking reality. Keeping in mind the hypothesis that the contact between the stent and the catheter takes

place in the outer-nodes of the stent model, the idea is to implement the action that the catheter imposes on the stent radius. The idea can be resumed as follows:

- the outer node set is split in n subsets;
- on each subset a radial boundary condition (BC) imposes an initial radial reduction of the subset (r_{stent}==$r_{catheter}$);
- step by step, the BCs are released and the stent expands (see Fig.4.6).

.

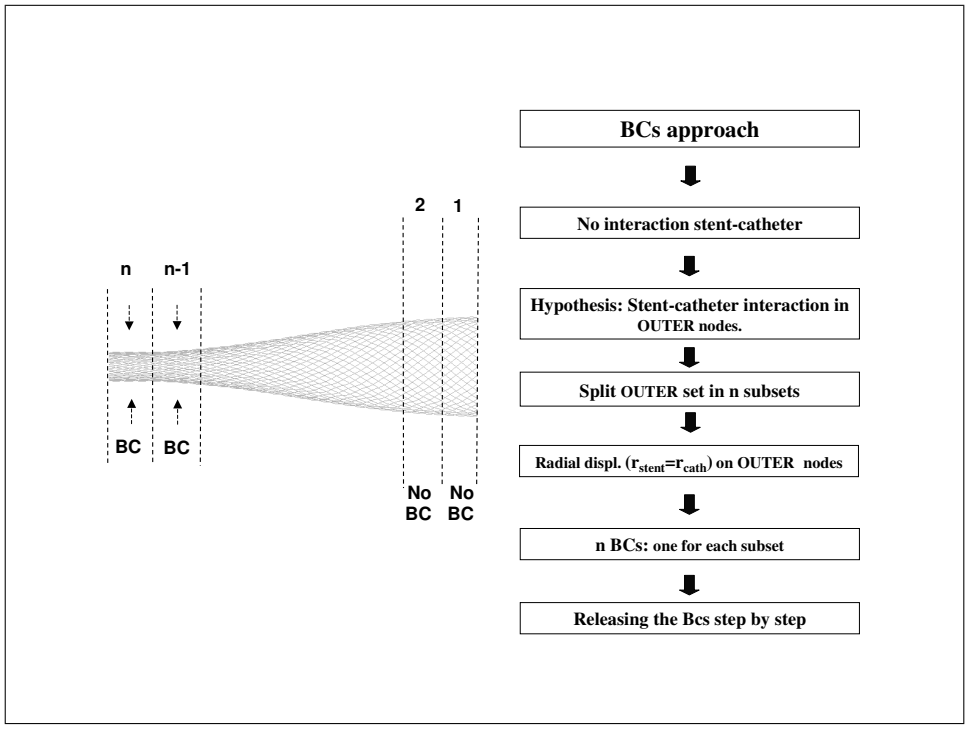

Figure 4.6: Steps in the numerical simulations of stent free expansion (innovative approach).

4.3.1 Results

The simulations of the wire stent deployment have been performed using the methodology previously described and have been validated by comparison with experimental data reported by Wang and Ravi-Chandar (see section 3.2.2). We assume the mechanical properties of the stent materials (i.e. Phynox and Nitinol) defined in the section 3.4.2. A comparison of the shape of the stent exiting the catheter as predicted by the numerical simulations with the shape measured from a photograph of the stent partially released from the catheter is depicted in Fig. 4.7.
Clearly, the numerical simulations provide a good representation of the deformability of the stent. The small inconsistencies in the stent deformation of the non-completely deployed sections might be due to simulation approach. Furthermore, it can be noted that the elastic material properties (from Phynox and Nitinol) seem to have limited influence on the stent expansion behavior. This independence from the elastic moduli can be explained by the fact that the stent release can be considered as a linear elastic problem governed by imposed displacements.

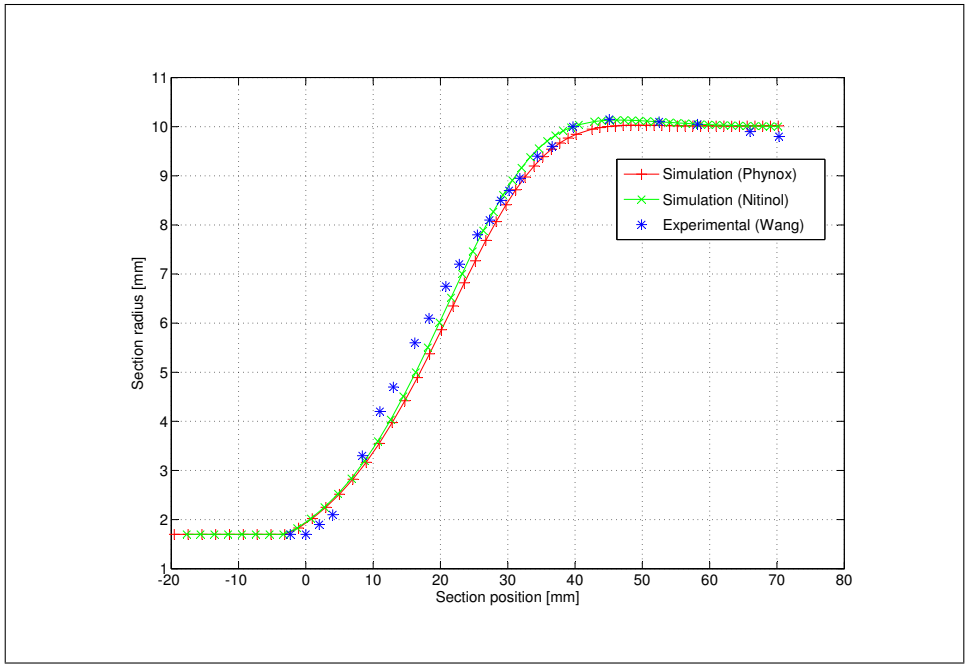

Figure 4.7: Comparison of the experimentally measured variation of the radius of the stent with position along the stent as it exits the catheter with the predictions of the numerical model.

This approach minimizes the computational cost of the simulations and provides a very good approximation of the stent shape as shown in Fig. 4.8.

4.3.2 Stent free expansion and von Mises stress

During the deployment an area of stress concentrations takes place. This area corresponds to the exit end of the catheter. The concentration of the stress is due to the high gradient of radial deformation that the stent experiences during the deployment. In fact the sections out the catheter have radius equal to r_0 and the sections inside the catheter have radius equal to $r_{catheter}$ as shown in Fig. 4.9.
In order to consider the possible plastic deformation provides by the stress concentration previously discussed, let us consider Phynox as an elasto-plastic material defined by the following engineering constants:

- E=220Gpa (Young's modulus);
- ν=0.33 (Poisson's ratio);
- σ_y=1578 (Yielding stress).

Taking into account the elasto-plastic response, the simulation shows residual plastic deformations (see Fig. 4.10.
The Fig. 4.11 shows the unrecoverable radial displacement of the stent due to the the plastic deformations after the deployment. By the radial displacement point of view, the stent can be split in the part:

- the part of the stent which has experienced plastic strain shows a light radial compression (i.e. negative residual radial displacement-blue color in the contour plot);

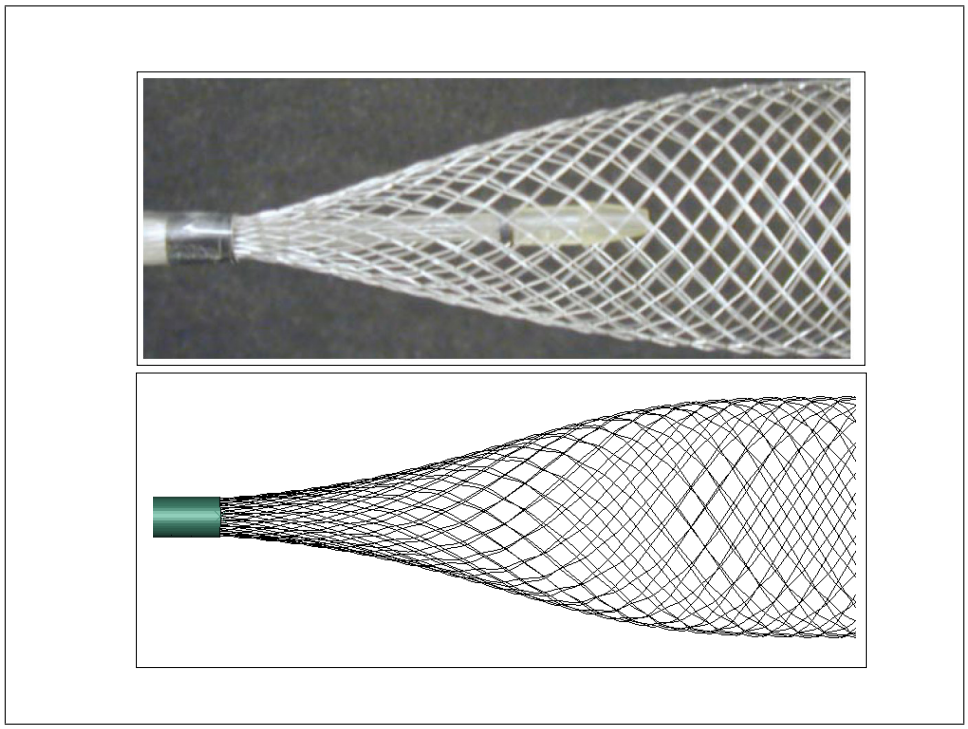

Figure 4.8: Shape of a wirestent as it exits out the catheter: on top) picture from Ravi-Chandar and Wang [63]; on bottom) F.E. model.

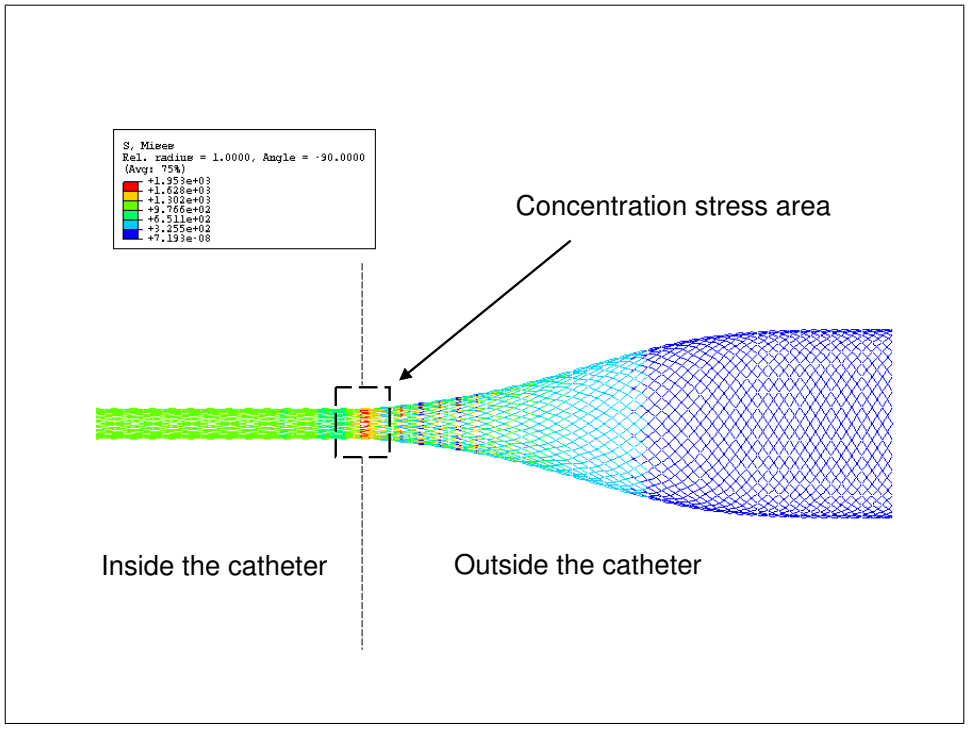

Figure 4.9: von Mises stress in stent during the deployment.

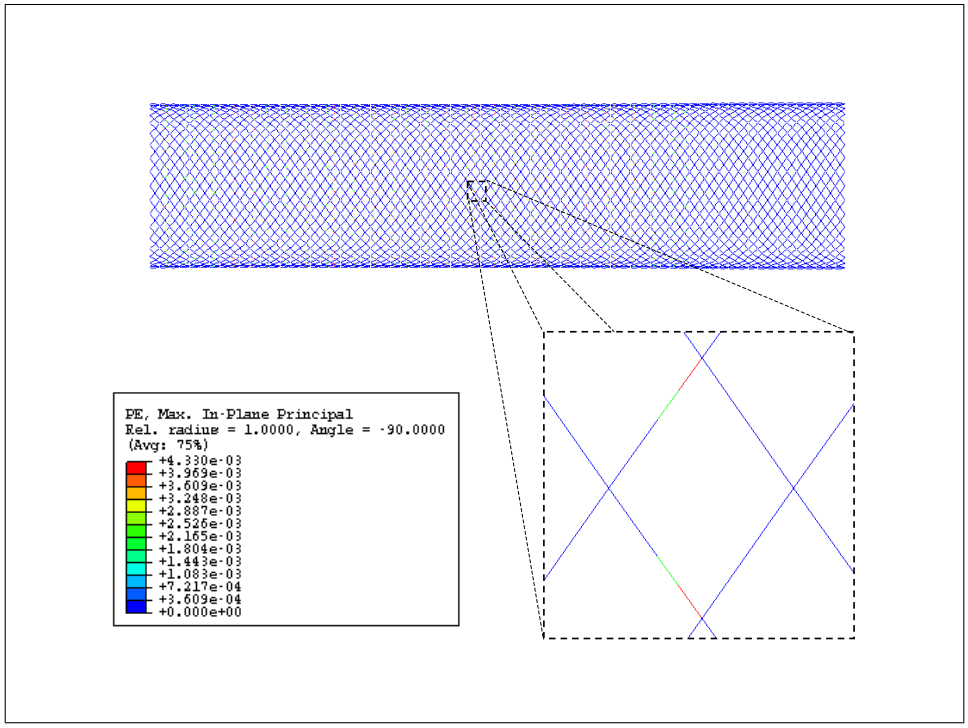

Figure 4.10: Plastic strain in stent after deployment.

- the other part, which has not experienced plastic deformation, is slightly over-expanded (i.e. positive residual radial displacement-red color in the contour plot).

Globally the stent shows a light residual axial stretch, as shown in Fig. 4.12 depicting the contour plot of the axial displacement after the deployment.
As shown in Fig. 4.13 and Fig. 4.14, there is a sudden increase of the stress as soon as the wire exits out the catheter (step 20). In the phynox stent it means to overcome the yield stress (see Fig. 4.13) instead in the nitinol stent the stress peak is far from the yielding stress threshold (see Fig. 4.14).
The main conclusions, considering the results of the stent deployment simulation, are:

- the analytical model or the simple simulation of the stent diameter reduction is not able to catch the stress concentration;
- the mechanical analysis of the wirestent can not leave out the stent free expansion;
- the use of Phynox provides unrecoverable deformations;
- the use of Nitinol can avoid the unrecoverable deformation thanks to its lower elastic modulus but also in this case it is super-elastic behavior is not exploited;
- the F.E. model and the innovative and experimentally validated simulation method are an very useful tool to understand the mechanics of this complex structure.

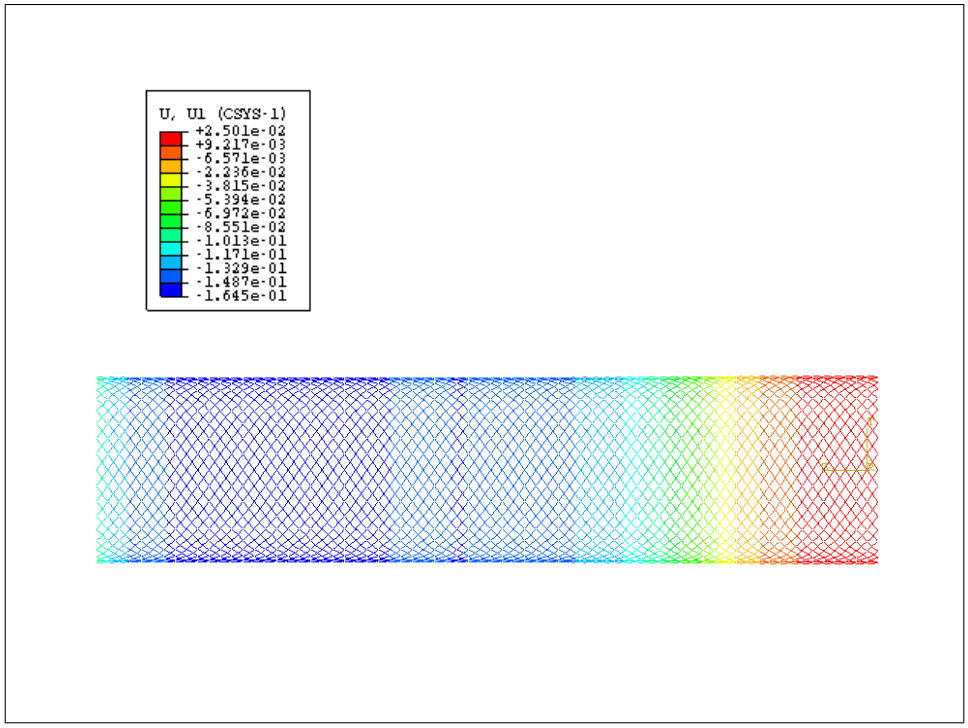

Figure 4.11: Contour plot of the stent radial displacement (U1) after deployment.

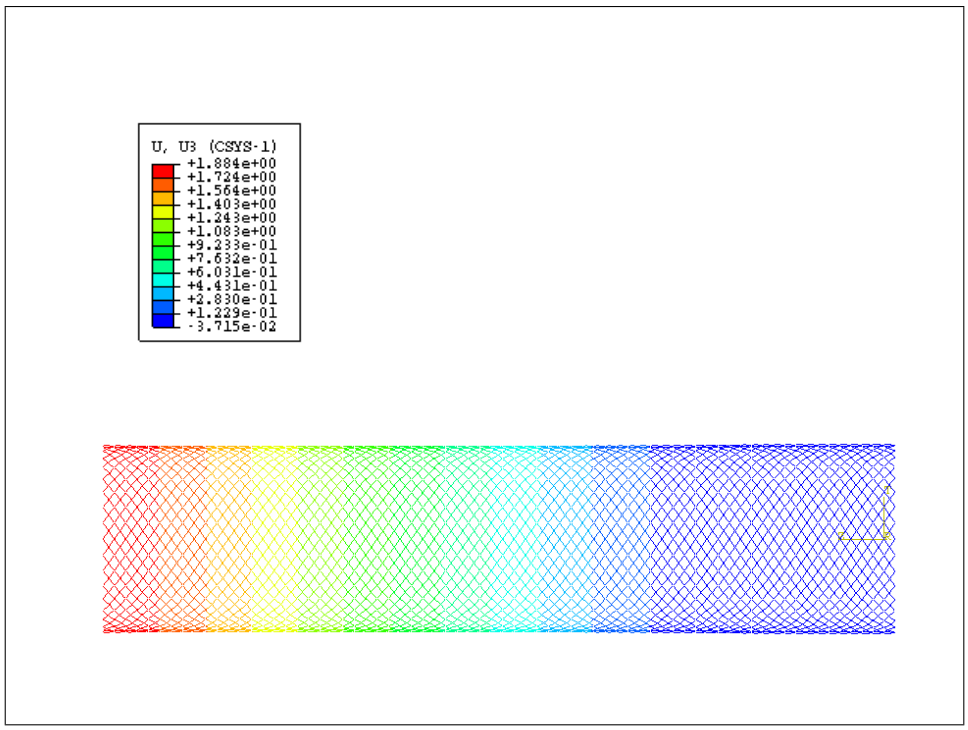

Figure 4.12: Contour plot of the stent axial displacement (u3) after deployment.

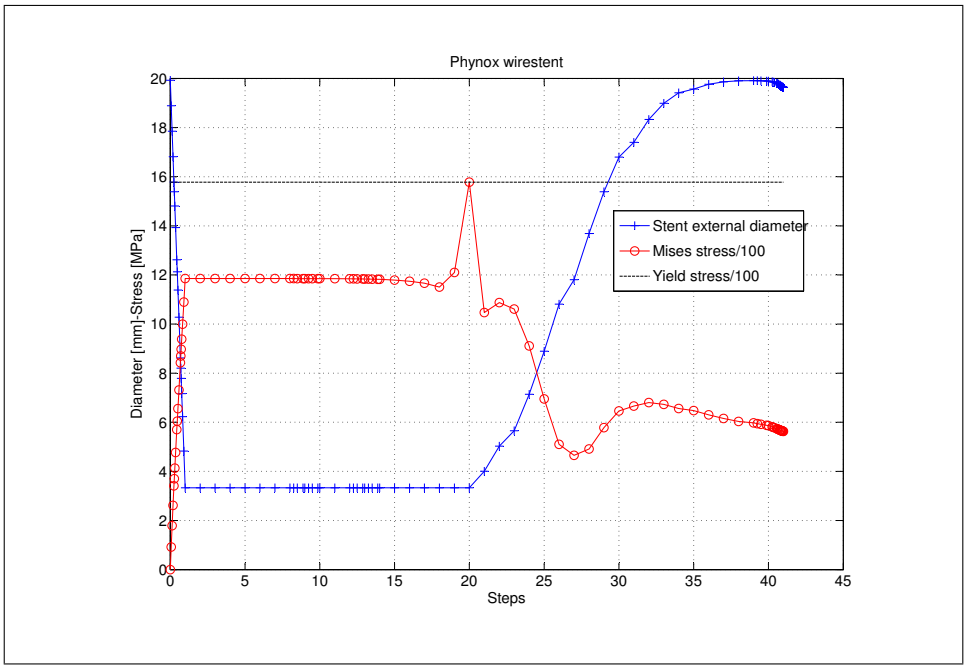

Figure 4.13: von Mises stress and diameter (node 9675) in phynox stent(b).

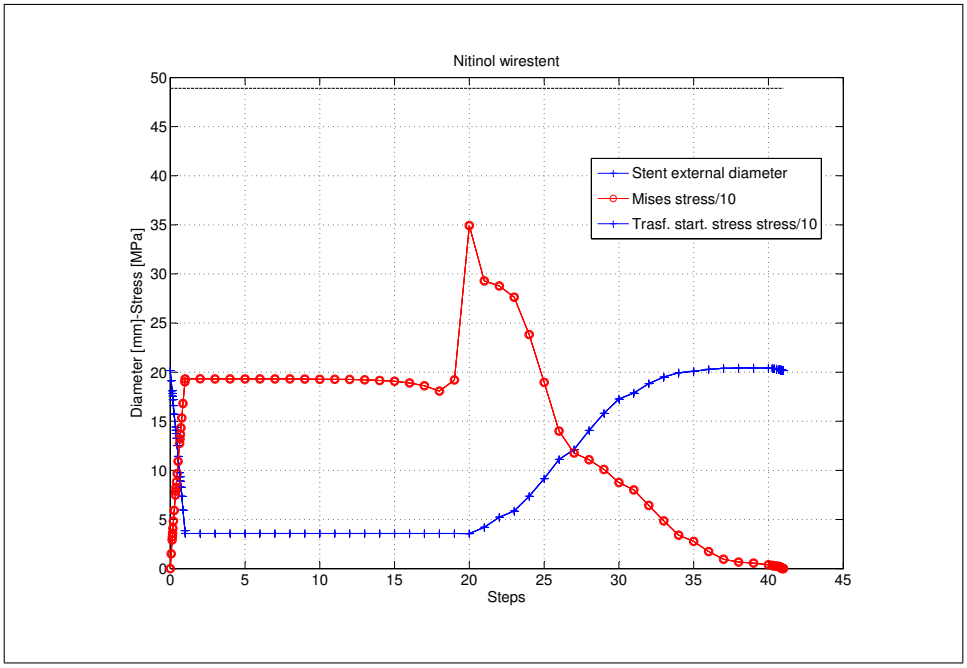

Figure 4.14: von Mises stress and diameter (node 9675) in nitinol stent(b).

Chapter 5

Stent vessel interaction

In this chapter we will discuss the numerical simulation of wire stent-vessel interaction. The goal of the F.E.A. of the coupled system stent-stenotic vessel is to evaluate the ability of the stent to open the stenotic vessel and to examine the contact stresses between the two bodies. Since available experimental studies clearly indicate the stent-artery mechanical interaction as one of the significant causes for the activation of restenosis mechanisms [24], the reduction of vessel injury can play a key role in the stent design. The F.E.A. has become an useful tool to investigate the stent design and its relation with the contact stresses. Many studies of this type are available in literature but most of them dealt with balloon-expanding stents. Most of them are also not validated. These investigations involve the stent, the vessel and the plaque; three different bodies with very different mechanical behavior and for this reason, the vessel and the plaque modeling is one of the more difficult task of biomechanics. A large amount of experimental data on the mechanical properties of vascular tissue is available in the literature. But it is not easy to obtain useful indications from these data since the low standardization of the experimental settings, the great variety of tissue typologies and the complex artery anatomic structure. Moreover much data is based on thoracic and iliac arteries [70]. Also the vessel geometry is not easy to create because in the stenting procedure the stent is in contact with a diseased vessel and this increases the complexity of the model. Due to the overall complexity, the constitutive modeling of arteries often requires significative approximations. So, mainly, the vessel tissue is considered as an isotropic, incompressible material modeled as an hyper-elastic material. To achieve a patient specific model that involves the complexity of the plaque-vessel structure a big effort is required, as shown in the exemplary study of Holpzafel [71]. In the current work a simplified vessel model is considered because we want to provide a stable method to perform numerical simulations between the wire stent and the (stenotic) vessel.

In the first part of this chapter, we will give an overview of the articles regarding F.E. simulations available in literature involving stent-vessel-plaque interaction focusing our attention on the useful data for the current analysis. In the second part, a brief resume of the numerical implementation of the hyper-elastic model in Abaqus Standard is given. Finally, in the third part, the obtained numerical results will be discussed.

5.1 Vessel modeling: previous works in literature

5.1.1 Auricchio et al.

Auricchio et al. [58] performed a F.E.A. to study the bio-mechanical interaction between a balloon expandable stent and a stenotic vessel. The Table 5.1 resumes the geometrical properties of the stenotic vessel model. They considered a straight artery segment with a plaque having a parabolic longitudinal profile (see Fig.5.1).

	Length [mm]	**Lumen diameter [mm]**	**Thickness [mm]**
Artery	26	3	0.75
Plaque	13	1.6 (53% stenosis)	0.7 (the maximum)

Table 5.1: Geometrical properties in artery-plaque model of Auricchio et al. [58]

Material constitutive equations

The constitutive response of a hyperelastic isotropic material is described introducing a strain energy U, function of the left Cauchy-Green tensor $\mathbf{B}$ through its invariants. The proposed model is interesting because it is able to catch good match of the experimental data with a very limited number of non-zero material constants.

An excellent fit was obtained with the experimental data using three constants for the plaque (C_{10},C_{02},C_{03}) and two for the artery (C_{10},C_{03})(see Table 5.2[1]). The experimental data are obtained by a previous work of Hayashi and Yosuke [72] in which they tested separately plaque and artery after dissection of a stenotic rabbit aorta in the passive state.

F.E.M. solver code: Abaqus.

Boundary conditions:

- hybrid 8-node brick elements (C3D8H);
- interaction between the stent and the artery/plaque: contact between deformable surfaces;
- contact conditions: finite sliding, no friction, with constrain enforced by a Lagrange multiplier method.

Constant	**Artery**	**Plaque**
C_{10}	0.019573 MPa	0.002176 MPa
C_{01}	0 MPa	0.00148 MPa
C_{30}	0.02976 MPa	0.013431 MPa

Table 5.2: Material constants for artery and the plaque model in Auricchio et al. [58].

[1] Values reviewed

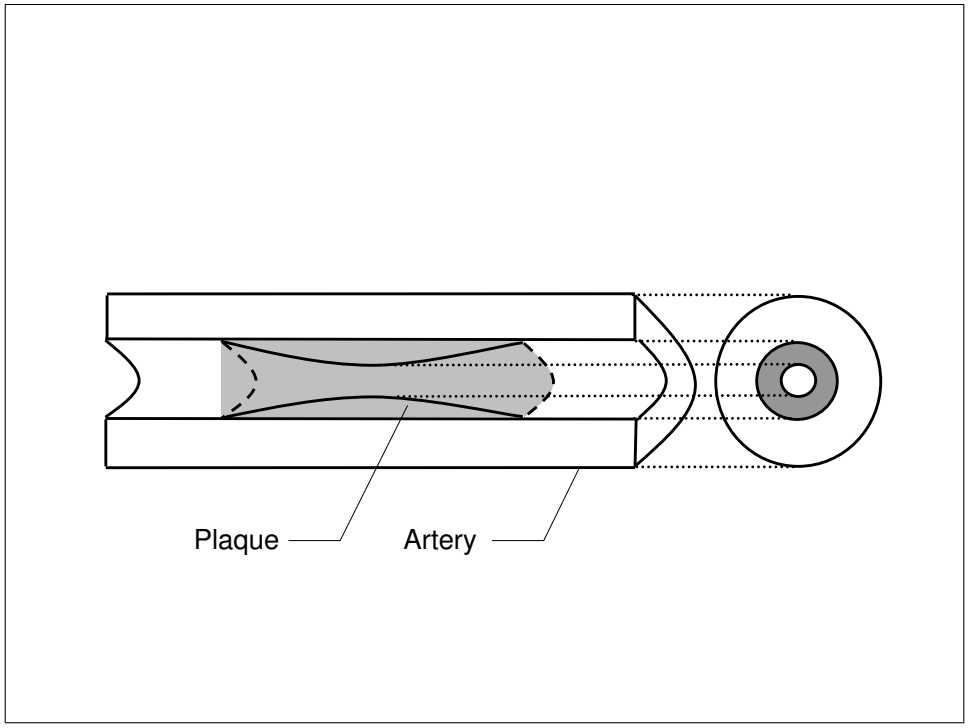

Figure 5.1: Symmetric stenosis by Auricchio et al. [58].

5.1.2 Lally et al.

In their work, Lally et al. [73] investigated levels of stresses provoked by two different stent designs within an atherosclerotic artery using the F.E. method. The geometry of the stenotic-artery model is defined by a straight cylinder with a localized crescent-shaped axisymmetric stenosis (see Table 5.3).

	Lumen diameter [mm]	**Thickness [mm]**
Artery	3	0.5
Plaque	2	1 (the maximum)

Table 5.3: Geometrical properties in artery-plaque model in Lally et al. [73]

Material constitutive equations

The constitutive equation of a hyper-elastic material is based on uni-axial and biaxial experiments on human femoral artery and porcine aortic vascular tissue [74]. The model of the arterial wall and stenotic plaque, were modeled using a 5-parameter third-order Mooney-Rivlin hyper-elastic constitutive equation.
The general polynomial form of the strain energy density function in terms of the strain invariants is:

$$W = \sum_{i=0,j=0}^{\infty} a_{ij} \left(I_1 - 3\right)_m \left(I_2 - 3\right)_n, a_{00} = 0 \tag{5.1}$$

using the hyperelastic model, the Cauchy stress, σ_{ij}, may be given in terms of the left Cauchy-Green tensor, B_{ij}, as:

$$\sigma_i j = -p + 2\frac{\partial W}{\partial I_1} B_i j - 2\frac{\partial W}{\partial I_2} B_i j^{-1} \tag{5.2}$$

, where I_1, I_1, I_3 are the invariants of B_{ij} and they are defined as follow:

$$I_1 = \lambda_1^2 + \lambda_2^2 + \lambda_3^2 \tag{5.3}$$

$$I_2 = \lambda_1^{(-2)} + \lambda_2^{(-2)} + \lambda_3^{(-2)} \tag{5.4}$$

$$I_3 = \lambda_1^2 \lambda_2^2 \lambda_3^2 \tag{5.5}$$

with λ_1, λ_2, λ_3 principal stretches. The tissue is defined incompressible so $I_3 = 1$. Therefore, the strain-density function is defined as follows:

$$W = a_{10}(I_1 - 3) + a_{01}(I_2 - 3) + a_{20}(I_1 - 3)^2 + a_{11}(I_1 - 3)(I_2 - 3) + a_{30}(I_1 - 3)^3 \tag{5.6}$$

Table 5.4 summarize the constants defining W^2.

F.E.M. solver code: Marc/Mentat.

Boundary conditions

An initial prestretch of 1.2 was applied in order to simulate the longitudinal *in vivo* lengthening of the coronary vessel. The contact between the stent and the stenotic vessel takes place in two steps:

- first step: the stent elements are deactivated and the vessel is expanded to a diameter greater than the expanded stent diameter by increasing the vessel internal pressure (to 13 MPa);
- second step: the elements of the stent are activated and the pressure on the inner lumen of the artery is gradually reduced to a value of 13.3 kPa (equal to mean blood pressure of 100 mmHg).

The contact between the vessel and the stent is assumed frictionless and the contact algorithm is implemented by the direct constraint method. Deformable-deformable contact was used to describe the contact between the contact bodies and both contact bodies were defined as analytical surfaces.

Constant	**Artery**	**Plaque**
a_{10}	0.0189 MPa	-0.49596 MPa
a_{01}	0.00275 MPa	0.50661 MPa
a_{20}	0.59043 MPa	3.6378 MPa
a_{11}	0.00275 MPa	1.19353 MPa
a_{30}	0 MPa	4.73725 MPa

Table 5.4: Material constants for artery and plaque model in Lally et al. [73].

	Length [mm]	Lumen diameter [mm]	Thickness [mm]
Artery	11.68	2.15	0.5
Plaque	3.68	1.25	0.45 (the maximum)

Table 5.5: Geometrical properties in artery-plaque model of Migliavacca et al. [76]

5.1.3 Migliavacca et al.

Migliavacca et al. [76] present some mathematical stent models and investigate the interaction of these stents with the vessel wall. Table 5.5 resumes the geometry of the modeled plaque and artery.

Material properties

To describe the mechanical behavior of both tissues, a hyper-elastic isotropic constitutive model is adopted. The constants of the model (see Table 5.6) are based on data reported by Salunke et al. [77]. Plaque and artery are discretized by means of linear hybrid brick elements.

F.E.M. solver code: Abaqus.

Boundary conditions

An axial pretensioning of 10% is applied to the vessel. A pressurization of the vascular wall (artery and plaque) of 100 mmHg was applied.

Constant	Artery	Plaque
C_{10}	0.019573 MPa	0.04 MPa
C_{02}	0 MPa	0.003 MPa
C_{03}	0.02976 MPa	0.02976 MPa

Table 5.6: Material constants for artery and the plaque in Migliavacca et al. [76].

5.1.4 Liang et al.

Liang et al. [68] investigated the biomechanical characteristics of ICSI (Intra-coronary stent implantation) by F.E.A., developing a three-dimensional model of the complete stenting system and self-defined constitutive models for the plaque and the balloon.

Model geometrical properties

The geometrical properties of the vessel model proposed by Liang et al. are reported in Table 5.7.

Material properties

As previously described, vessel tissue is often modeled as an isotropic hyperelastic material. However, hyperelastic constitutive models are not able to fully characterize the non-recoverable deformation of the interlining between plaques and arteries. Assuming both plaque and arteries as hyperelastic

[2] Values in errata corrige [75]

	Length [mm]	**Lumen diameter [mm]**	**Thickness [mm]**
Artery	7	2.5	0.5
Plaque	5	1.5	0.5

Table 5.7: Geometrical properties in artery-plaque model of Liang et al. [68].

materials, the recoil ratio of the stenotic artery will be 100% in PTCA. Therefore, the authors present a model of a coupled plaque-vessel system in which only the artery is assumed to be hyperelastic. The hyperelastic constitutive model of the artery is described by 5-term strain energy constants (C1-C5) (see Table 5.8) but there are no references for the experimental data. The authors assume that the interlining layer experiences a plastic deformation (such as the yielding of metals). They also assume that the unrecoverable deformations take place when the applied pressure is larger than 0.65 MPa. It is noted that this is clearly a limiting and somehow unrealistic assumption due to the lack of experimental data. The assumptions provide a sort a visco elastic model, as shown in Fig. 5.2.

Constant	C_1	C_2	C_3	C_4	C_5
	35.625 Pa	25.438 Pa	37.146 Pa	528.09 Pa	188.61 Pa

Table 5.8: Material constants for artery in Liang et al. [68].

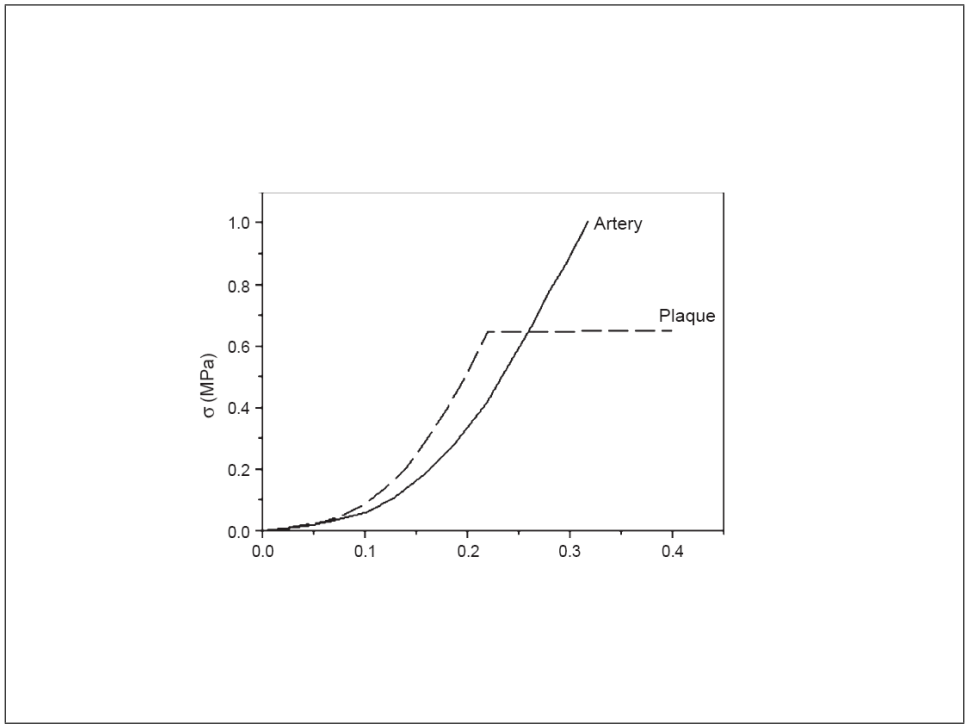

Figure 5.2: Stress-strain curve for artery and plaque model in Liang et al. [68].

5.2 Hyperelasticity in ABQ STD

In ABAQUS, the hyperelastic material model is isotropic and implements the behavior of nonlinear rubber-like materials. In this kind of materials, the compressibility is very little compared to their shear flexibility. So the assumption is that the volume change is only related to the thermal expansion. Therefore it is recommended to use hybrid elements in ABQ/STD. If a material is incompressible, the pressure cannot be computed from the displacement of the nodes, thus in hybrid elements an additional degree of freedom provides the pressure stress in the element directly. The isotropic assumption is based on re-orientation of the molecules of the elastomeric material when it is stretched. Moreover hyperelastic materials are described in terms of a strain energy potential, U(ϵ) because the development of isotropy follows the straining. The strain energy potential can be formulated as a function of the strain invariants; thus to define the hyperelastic constitutive equation, we have used polynomial form, following the common approach in the works previously discussed. In this form U(ϵ) is defined as:

$$U(\epsilon) = \sum_{i+j=1}^{N} C_{ij}(\bar{I}_1 - 3)^i(\bar{I}_2 - 3)^j + \sum_{i=1}^{N} \frac{1}{D_i}(J^{el} - 1)^{2i} \tag{5.7}$$

Where N is a material parameter, C_{ij} and D_i are temperature-dependent material parameters, J^{el} the elastic volume ratio. $\bar{I}_1$ and $\bar{I}_2$ are the first and the second deviatoric strain invariants defined as:

$$\bar{I}_1 = \bar{\lambda}_1^2 + \bar{\lambda}_2^2 + \bar{\lambda}_3^2 \tag{5.8}$$

$$\bar{I}_2 = \bar{\lambda}_1^{-2} + \bar{\lambda}_2^{-2} + \bar{\lambda}_3^{-2} \tag{5.9}$$

The deviatoric stretches are defined as $\bar{\lambda}_i = J^{-1/3}\lambda$, where J is the total volume ratio and λ_i are the principal stretches. It should be noted the other formulations such as the Mooney-Rivlin or the neo-Hookean one can be considered as particular cases of the polynomial model [66].

5.3 Wire stent deployment in a stricture: the procedure in the reality

In order to perform a F.E.A. of the wire stent-vessel interaction, it is necessary to have a clear idea about the stenting procedure of this kind of devices. In reality, the stenting procedure using self-expanding wire stent requires a deployment system to improve the insertion and the device positioning. In many cases, a PTA is performed previously to open the stricture and to help the stent deployment and its task. As example, let us consider the case of malignant tracheobronchial stricture in which a covered wire stent is used as palliative [78]. The stent introducer set consists of a sheath, a breathing tube, a pusher catheter and a guiding balloon catheter. The deflated balloon catheter is passed through a breathing tube, and then both are passed through a pusher catheter. These three devices are pushed into the sheath, with half of the balloon out of the sheath. From the opposite end, a stent was passed over the balloon catheter and breathing tube and then compressed to be loaded between the breathing tube and the distal end of the sheath. Clearly, it shows the complexity of deployment system and the several mechanical conditions that the wire stent experiences when it is inserted in this system. The Fig. 5.3 shows the diagram of the technical steps in tracheal stent placement. Tracheal Stent Placement Technique consists of five main steps:

- a straight graduated sizing catheter is passed over the guide wire to the distal part of the stricture to measure the length of the stricture (see Fig. 5.3(1));

- an angioplasty balloon catheter is passed over the guide wire to a position over the stricture and the balloon is slowly inflated to resize the stricture (see Fig. 5.3(2));
- the proximal part of the stent is lubricated with a water-soluble lubricant. The stent is then compressed and loaded onto the introducer set then the whole introducer set is passed over the guide wire into the trachea and advanced until the distal tip of the stent reaches a position slightly beyond the stricture (see Fig. 5.3(3));
- the pusher catheter is held in place with one hand while the sheath is slowly withdrawn in a continuous motion with the other hand. The stent deploys and is released within the stricture (see Fig. 5.3(4));
- after the sheath, the pusher catheter, and the breathing tube are removed, conventional radiography is performed to verify the position of the stent (see Fig. 5.3(5)).

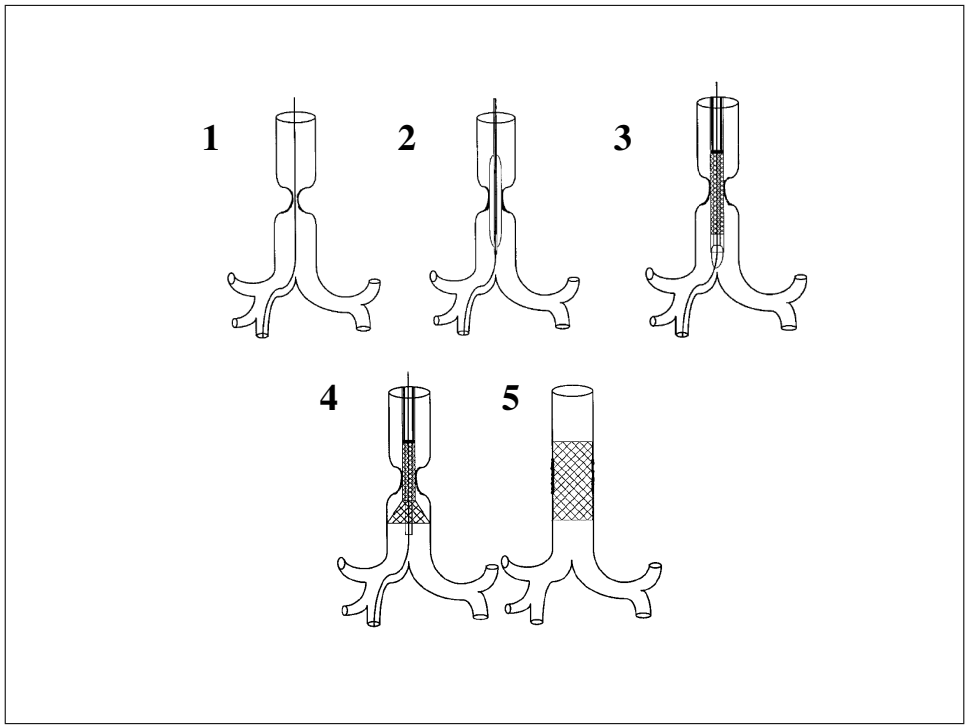

Figure 5.3: Diagram of the technical steps in tracheal stent placement in Song et al. [78].

5.4 F.E.M. simulation

Before discussing the adopted methodology in the following simulations, it is necessary to emphasize that the main goal of our investigation is to achieve a stable method to avoid numerical problems involved in the contact analysis (as much as possible). This is an essential step to perform further parametric analysis of the vessel-stent interaction. In our simulations, we adopt the hyperelastic material model proposed by Lally et al. (see Section 5.1.2). The vessel is modeled as a straight cylinder and the plaque is not included in the model. The interaction is defined by small-sliding

tracking approach using hard contact method. The interaction is defined between the stent node-based surface (outer-node set) and the inner surface of the cylindrical vessel. Frictionless relative tangential behavior is assumed. One end of the vessel is fixed by BCs which allow only radial displacement of the nodes defining the section. In the other end, an initial axial displacement is applied to prestretch the vessel.

5.4.1 Direct approach: stent-vessel interaction

The first attempt to perform the interaction between a stenotic vessel and the wire stent is based on the following approach:

- the diameter of the wire stent is first reduced to simulate the stent insertion into the catheter;
- applying the deployment procedure based on the BCs (see Chapter 4), the stent expands and the contact with the vessel takes place.

The Fig. 5.4 shows the scheme of the simulation following the direct approach.

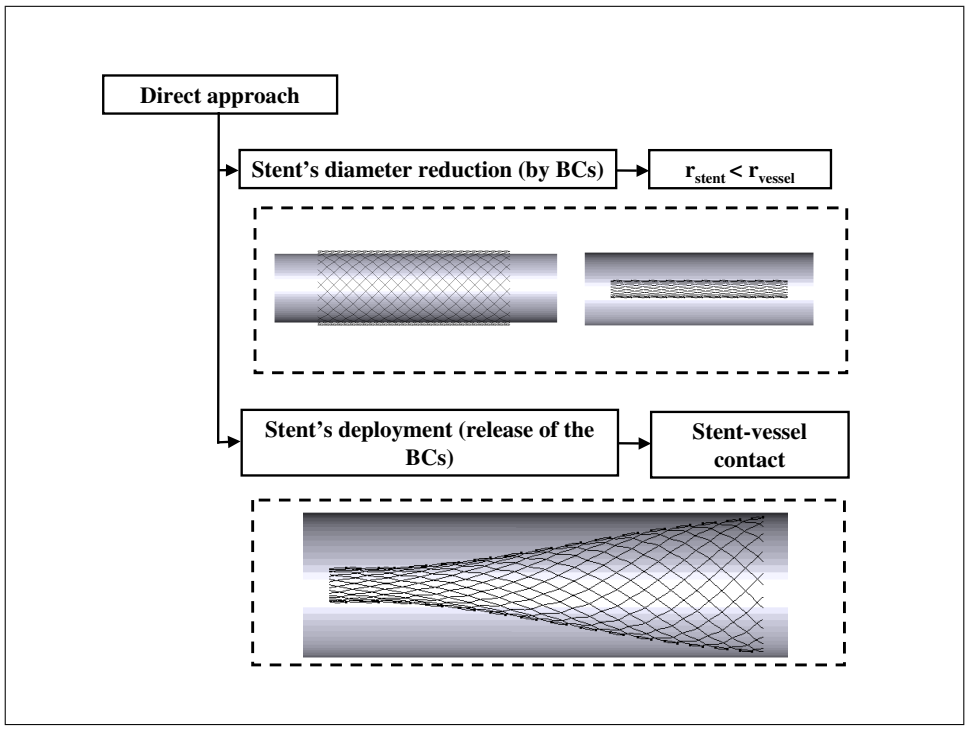

Figure 5.4: Main steps of the stent-vessel interaction (direct approach).

In this approach we use the features of ABAQUS that allows elements to be activated or deactivated during the analysis. So, during the stent diameter reduction, the stent-vessel interaction is not active but in the next step the interaction is activated and contact takes place.

Results

The simulations performed with the direct approach failed because **Severe Discontinuity Iterations (SDIs)**. To solve this kind of error it is necessary to understand the algorithm used by ABQ/STD

to solve the contact problem [66]. This algorithm is based on the Newton-Raphson technique. The Fig. 5.5 shows the main steps in the contact logic of ABQ/STD, **p** is the contact pressure and **h** the penetration of the slave node in the master surface.

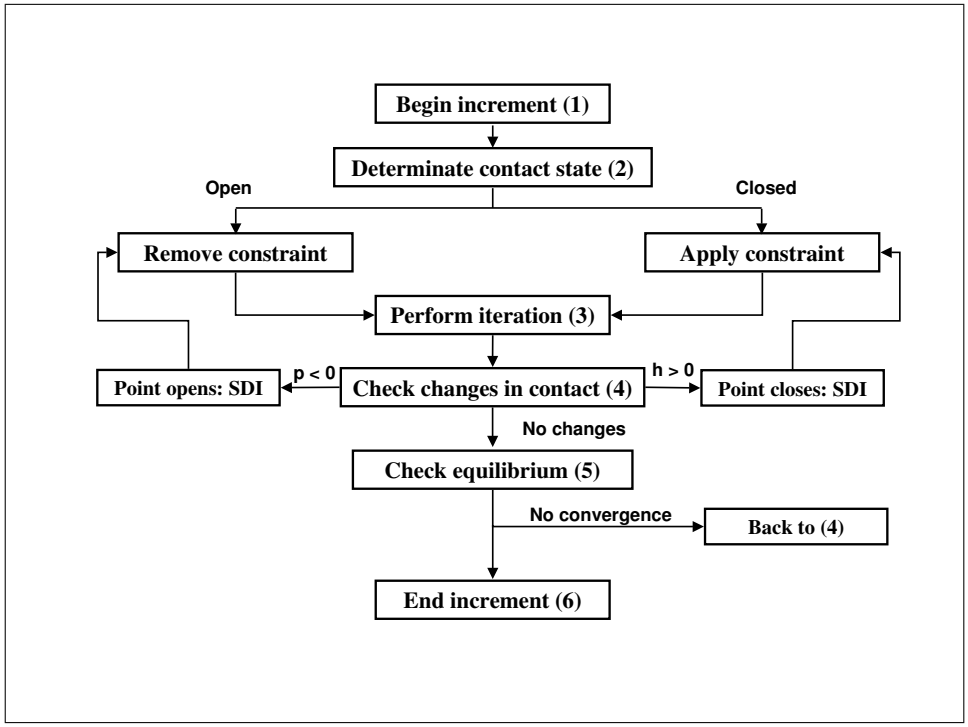

Figure 5.5: Contact logic.

The contact logic can be briefly resumed in the following steps:

- when a new increment starts (1), the state of all contact interactions is checked to assess if a node is open or closed (2);
- a constraint is applied if a node is closed instead the constraint is removed in the node that changes from open to closed;
- the code refreshes the configuration by a new iteration (3);
- after this iteration, the code checks the status of the slave nodes (4) to assess if an open one has become closed or vice versa; if the code find a contact change, it labels the interaction as **SDI** and the equilibrium is not carried out;
- when there are no more SDI, the equilibrium is checked (5);
- the increment ends when the convergence is achieved.

So the interactions can be split in equilibrium iterations and in SDIs allowing to understand the nature of the contact problem. In our simulations the SDIs could be due to iterative radial displacement of the vessel wall when it is in contact with the expanding stent. This displacement provides a sort of chattering and does not allow a stable contact between the interfaces and so SDIs take place. A possible solution for this problem could consist of fixation of the vessel surface during the stent

deployment. This is a common strategy to achieve a stable contact between the interfaces as suggested in the Abaqus manual [66]. Unfortunately, this approach provides overconstraints over the nodes of the vessel because they are also involved in the contact. For this reason we used the strategy proposed by Lally et al. [73].

5.4.2 An alternative approach: contact sequence inversion

As proposed by Lally et al. (see section 5.1.2), it is possible to perform a preopening of the vessel by an inner pressure increase and then perform the stent-vessel contact using the elastic equilibrium between the two bodies. Thus, the stent acts like a scaffold for the vessel. The Fig. 5.6 shows the scheme of the simulation following the direct approach.

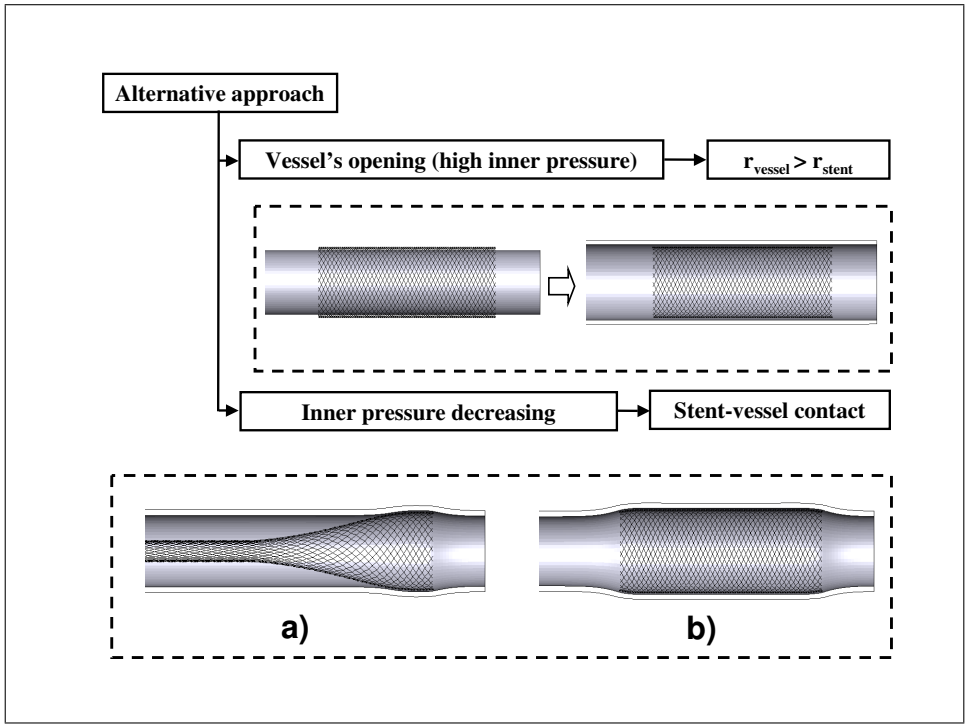

Figure 5.6: Main steps of the stent-vessel interaction (alternative approach).

However, also using this alternative approach some problems, related to the severe overclosures, remain. Therefore, we use the automatic stabilization of rigid body motions in contact problems based on the stiffness of the underlying elements. This option is available in ABQ/STD and it provides viscous damping for the relative motions of the contact pair at all slave nodes. It should be noted that the automatic stabilization damping is applied only for the duration of step in which it is defined. In order to specify a scale factor for the default damping coefficient, we have considered a toy test. The goal of the test is to simplify the problem of the contact between of surface defined by wires (the stent interface) and a solid continuum surface (the vessel interface). Thus, a rectangular body, discretized by 8-node linear bricks (C3D8), is pushed against a rectangular web of beams. The web is discretized by 3-d beam elements. The Fig. 5.7 shows the achieved contact between the web and the solid body using a scale factor of 10.

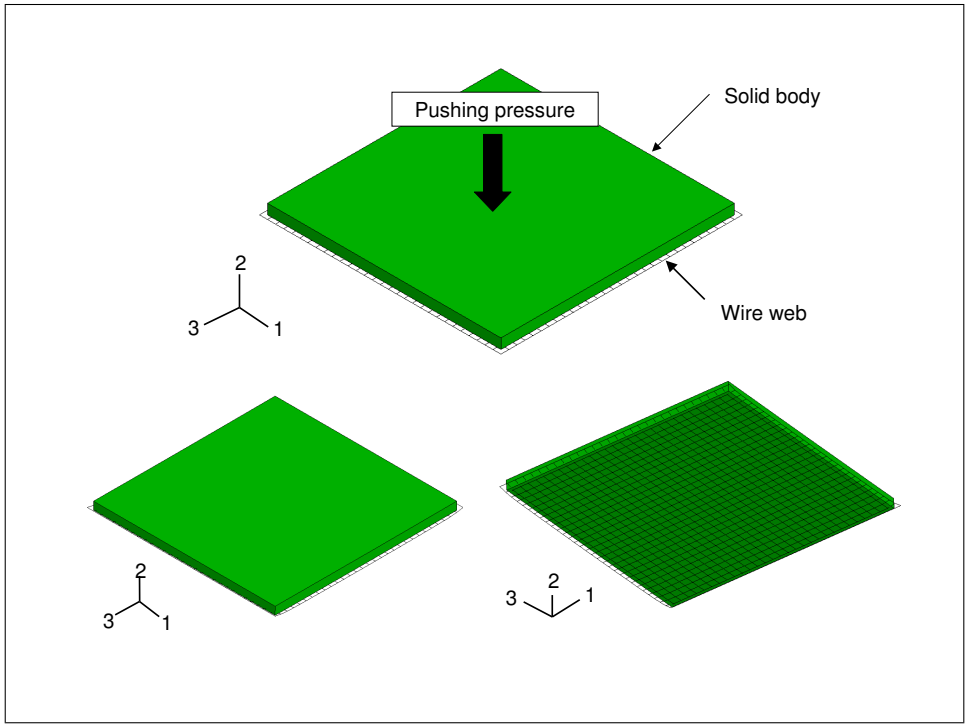

Figure 5.7: Example of contact defined by contact controls.

Results

Fig. 5.8-5.10 shows the obtained shape of the deformed the vessel under the action of the partially/-totally deployed stent by applying the contact control. The geometrical properties of the vessel and the stent model are reported in Table 5.9. The stent consists of 48 wires and has a pitch angle of 25°.

	Length (L)[mm]	**Initial diameter (D_0)[mm]**	**Thickness (Th)[mm]**
Vessel	40	6	0.6 (10% of D_0)
Wirestent	20	8	–

Table 5.9: Geometrical properties of stent-vessel model.

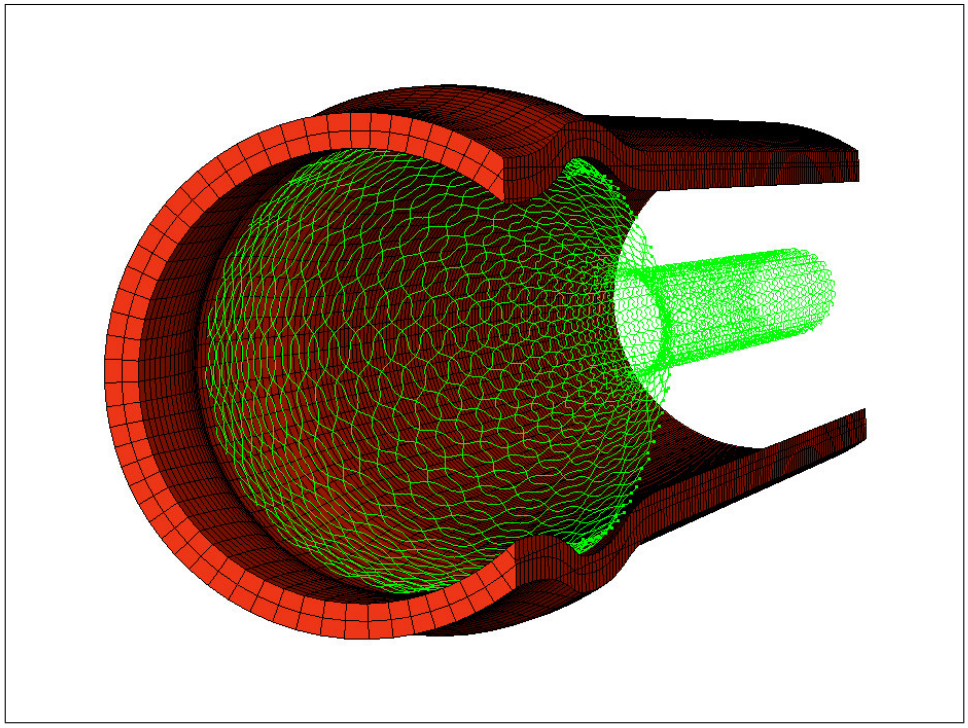

Figure 5.8: Vessel and slightly deployed stent.

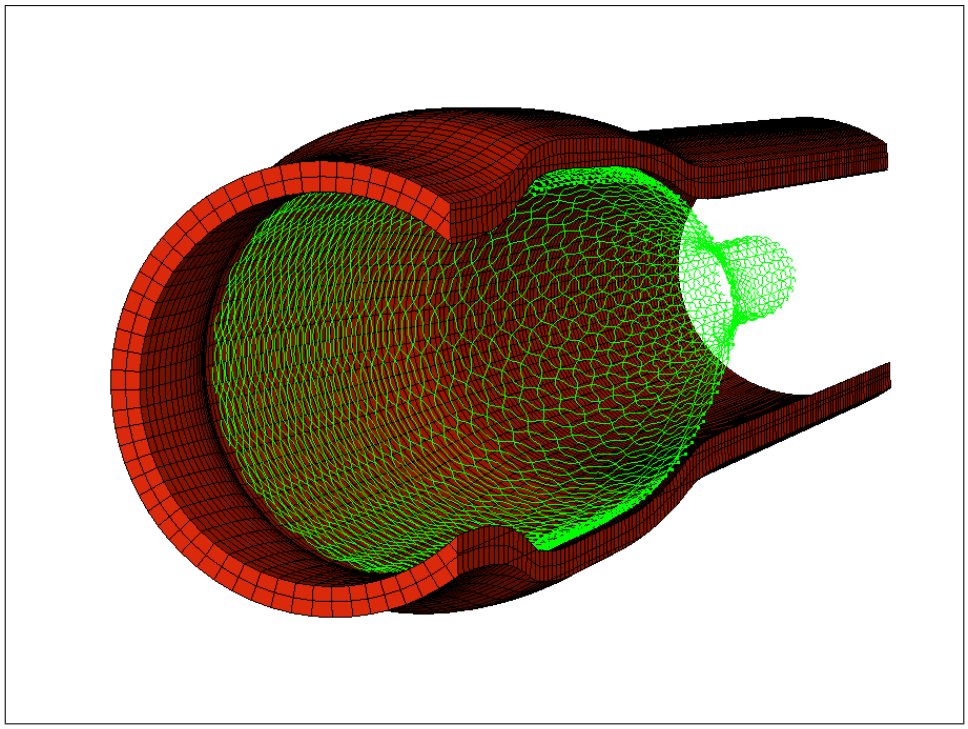

Figure 5.9: Vessel and semi-deployed stent.

Fig. 5.11 shows the contour plot of the Mises stresses (S.Mises) in the vessel wall and its radial

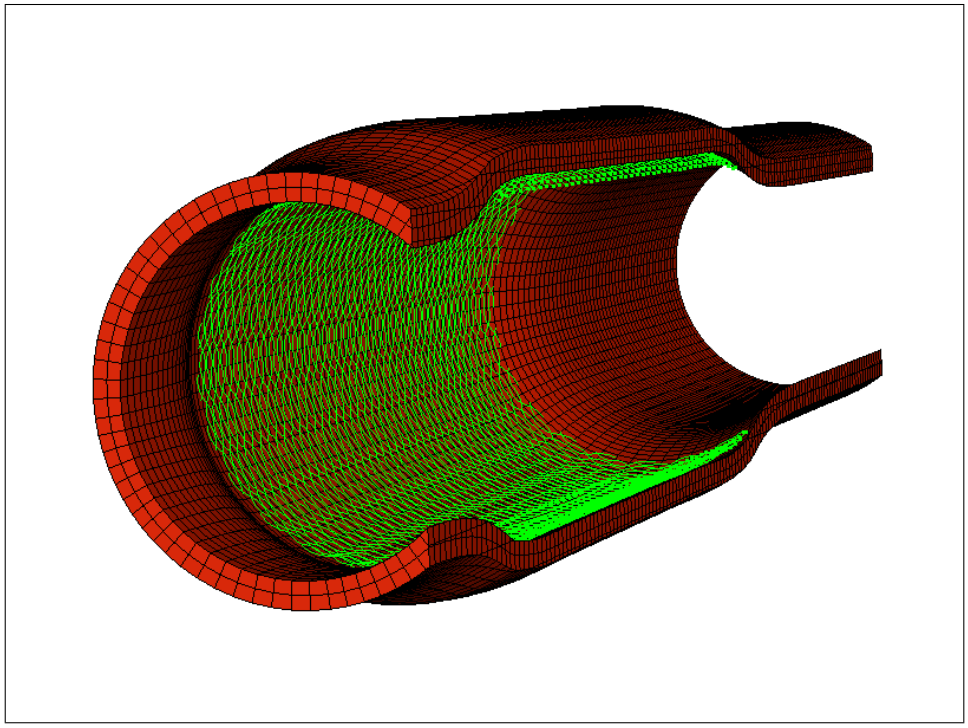

Figure 5.10: Vessel and deployed stent.

displacements (U1). A stress concentration, provided by the local deformation, appears in the region near to the stent end. In the area of the high radial expansion, the vessel diameter is increased from 6 mm to 7.7 mm.
If we observe the same variable, considering the contact between the vessel and the semi-deployed stent shown in Fig. 5.12, the stress of the vessel wall is increased and there is an over radial expansion ($diameter_{vessel} > diameter_{open-stent}$). It happens because during the reduction phase of the vessel diameter, the vessel surrounds the stent and, with its action, it does not allow the relative tangential movement of the wires so it leads a sort of compression of the stent.
The phenomenon of axial compression appears clearly when the stent is completely deployed (see Fig. 5.13). In fact, both stent ends are compressed and the stent is a bit shorter than in the open-air configuration.
The results provide two main indications:

1. it is possible to perform the investigated contact using ABQ/STD but it requires many efforts to solve all numerical problems involved;

2. the obtained results are not useful to assess accurately the stress in the vascular wall; they are only a starting point for more accurate investigations.

It is necessary to take into account the computational effort required for this kind of simulations; in fact the step in which the contact is defined requires more than 300 increments, since the small tracking approach. Thus, all the following elements can offer help to perform a more accurate contact simulation:

- a reduction of the vessel length; only the part that will be in contact with the stent can be modeled;

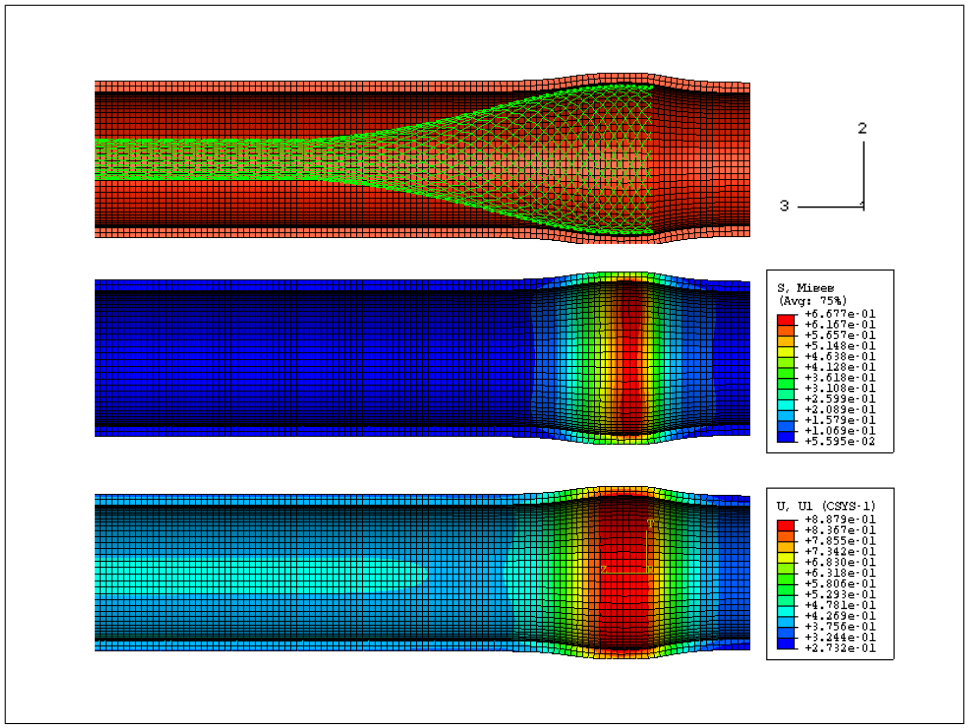

Figure 5.11: Mises stresses and radial displacement in the vessel wall in contact with the slightly deployed stent.

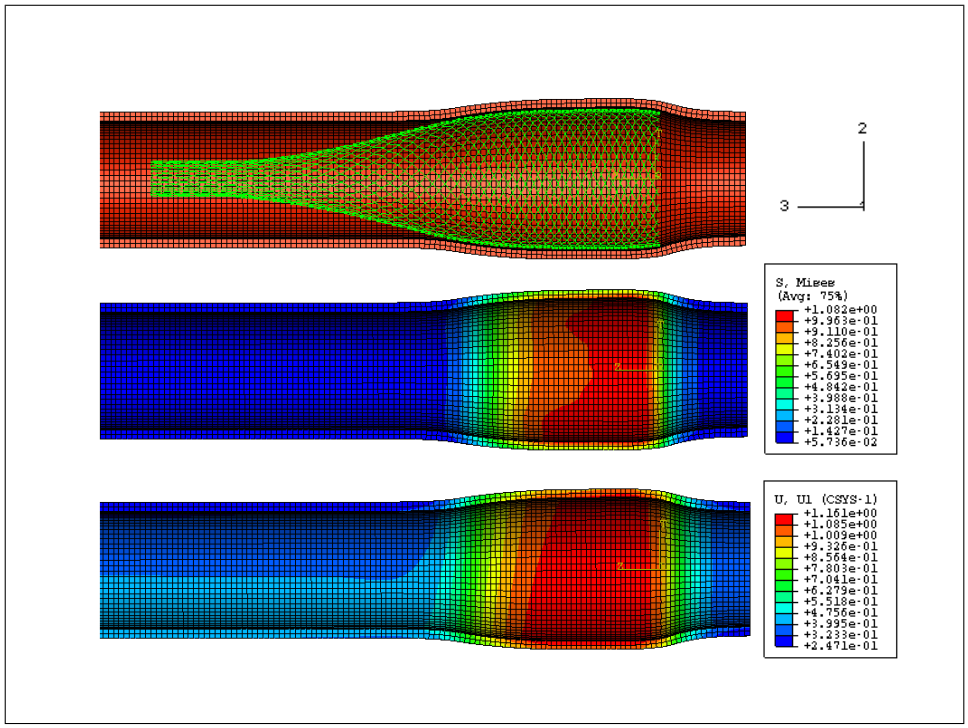

Figure 5.12: Mises stresses and radial displacement in the vessel wall in contact with the semi-deployed stent.

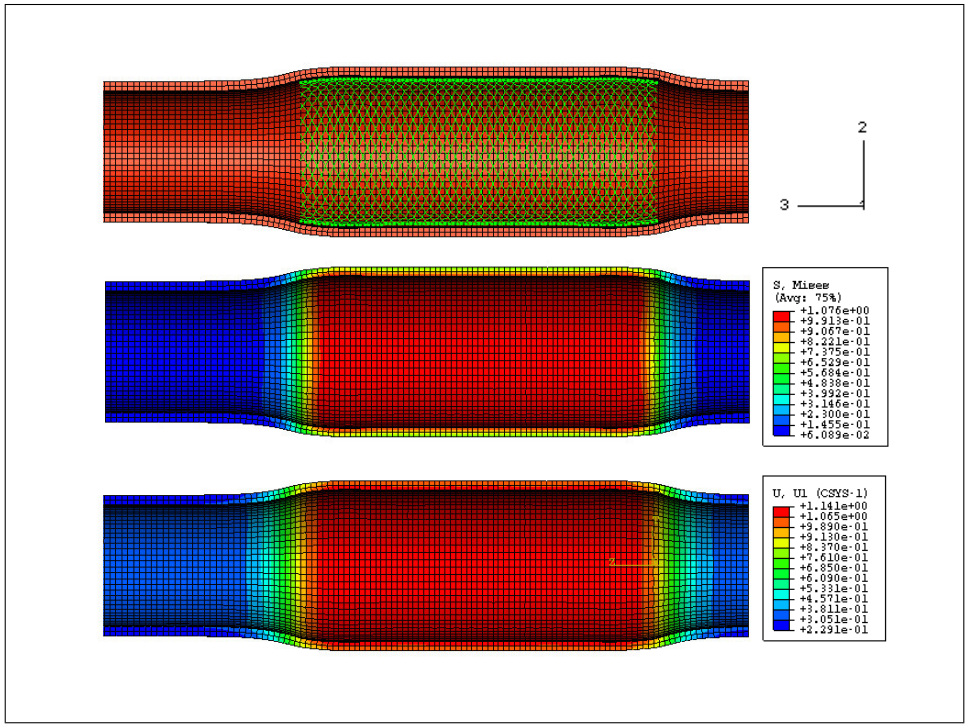

Figure 5.13: Mises stresses and radial displacement in the vessel wall in contact with the totally deployed stent.

- a finer mesh to catch the stress over the thickness of vascular wall;
- the use of explicit module that provides more stable methods for the contact analysis.

It is clear that a lot of work is still required seen the approximations done for the material model of the vessel and the simple geometry proposed.

Chapter 6

Conclusions and further scenarios

In this work we present the investigation of the mechanical behavior of the self-expanding bare braided wirestent by Finite Element Analysis (F.E.A.).

The geometrical model of the wirestent is built using pyformex, an open source program developed at Ghent University. Thanks to pyFormex, a complex geometrical and finite element models of wire stents can quickly be built.

In this study an innovative and analytically confirmed virtual benchmark test is described to evaluate the stress state of the stent wires when the stent diameter of the braided Wallstent® is reduced to several catheter sizes. The use of different stent materials has been simulated. The results have highlighted the usefulness of the built model. It seems possible to reduce the actually used catheter size from 10 French (i.e. 3.4 mm) to 9 French (i.e. 3 mm) for this stent design without (pseudo-) plastically deforming the stent. Such a catheter size reduction would increase in-situ lesion access, but could decrease the ease of the actual stent delivery (i.e. higher force necessary to release the stent out of the catheter).

Subsequently, an original and experimentally validated methodology to analyze the free expanding stent exiting the catheter is developed. The results show a stress concentration that the elastic material properties (from phynox and nitinol) have no influence on the stent expansion behaviour but plastic unrecoverable deformations can occur when an elasto-plastic wire material is used.

It may concluded that the developed Finite Element model and the proposed virtual benchmarks provide an useful tool to investigate the geometrical and mechanical properties of self-expanding braided wire stents with arbitrary geometry and arbitrary material. The developed pyFormex modeling strategy is a solid base for further study of the mechanical behavior of braided wire stents in real life conditions (e.g. patient-specific stent vessel interaction) and might be useful in the quest for the perfect braided stent.

Bibliography

[1] R. Wyttenbach, A. Gallino, M. Alerci, F. Mahler, L. Cozzi, M. Di Valentino, J.J. Badimon, V. Fuster, and R. Corti. Effects of percutaneous transluminal angioplasty and endovascular brachytherapy on vascular remodeling of human femoropopliteal artery by noninvasive magnetic resonance imaging. *Circulation*, 110:1156–1161, 2004.

[2] M. Cejna, S. Thurnher, H. Illiasch, W. Horvath, P. Waldenberger, K. Hornik, and J. Lammer. Pta versus palmaz stent placement in femoropopliteal artery obstructions: A multicenter prospective randomized study. *Journal of Vascular and Interventional Radiology*, 12:23–31, 2001.

[3] F. Pozzi Mucelli, M. Fisicaro, L. Calderan, M. Malacrea, C. Mazzone, L. Cattin, S. Scardi, and R. Pozzi Mucelli. Percutaneous revascularization of femoropopliteal artery disease: Pta and pta plus stent. results after six years' follow-up. *La Radiologia Medica*, 105:339–349, 2003.

[4] Brown University division of Biology and Medicine: `http://www.nhlbi.nih.gov`.

[5] A. C. Morton, D. Crossman, and J. Gunn. The influence of physical stent parameters upon restenosis. *Pathologie Biologie*, 52:196–205, 2004.

[6] F. Flueckiger, H. Sternthal, G.E. Klein, M. Aschauer, D. Szolar, and G. Kleinhappl. Strength, elasticity and plasticity of expandable metal stents: in vitro studies with three types of stress. *Journal of Vascular and Interventional Radiology*, 5:745–750, 1994.

[7] J. Harnek, E. Zoucas, U. Stenram, and W. Cwikiel. Insertion of self-expandable nitinol stents without previous balloon angioplasty reduces restenosis compared with pta prior to stenting. *CardioVascular and Interventional Radiology*, 25(5):430–436, 2002.

[8] Carlos E. Ruiz. Use of intravascular stents in children with congenital heart disease, outside of the pulmonary arteries. *Journal of Interventional Cardiology*, 11(5):449–458, 1998.

[9] W. Schmidt, Andresen R., P. Behrens, and K. P. Schmitz. Comparison of mechanical properties of peripheral self-expanding nitinol and balloon-expandable stainless-steel stents. *CIRSE-Barcelona-Spain*, 2004.

[10] T.W. Duerig and M. Wholey. A comparison of balloon- and self-expanding stents. *Minimally Invasive Therapy and Allied Technologies*, 2002.

[11] P. Theriault, P. Terriault, V. Brailovski, and R. Gallo. Finite element modelling of a progressively expanding shape memory stent. *International Journal of Cardiology*, 39:2837–2844, 2006.

[12] D. Aliabadi, F.V. Tilli, T. R. Bowers, V. Gangadharan, A.D. Berman, and R.D. Safian. Tracheobronchial wallstents for degenerated saphenous vein bypass grafts. *Catheterization and Cardiovascular Diagnosis*, 42:335–338, 1997.

[13] E. Therasse, V.L. Oliva, P. Lafontaine, E. andPerreault, M.F. Giroux, and G. Soulez. Balloon dilation and stent placement for esophageal lesions: Indications, methods, and results. *Radiographics*, 23:23–89, 2003.

[14] I. Borisch, M. D. Okka, W. Hamer, N. Zorger, S. Feuerbach, and J. Link. In vivo evaluation of the carotid wallstent on three-dimensional contrast materialenhanced mr angiography: Influence of artifacts on the visibility of stent lumina. *Journal of Vascular and Interventional Radiology*, 16:669–677, 2005.

[15] A.R. Assali, S. Sdringola, A. Moustapha, M. Rihner, A.E. Denktas, M.A. Lefkowitz, M. Campbell, and R.W. Smalling. Endovascular repair of traumatic pseudoaneurysm by uncovered self-expandable stenting with or without transstent coiling of the aneurysm cavity. *Catheterization and Cardiovascular Interventions*, 53:253–258, 2001.

[16] E. M. Walser. Stent placement for tracheobronchial disease. *European Journal of Radiology*, 55:321–330, 2004.

[17] N. Suzuki, B. P. Saunders, S. Thomas-Gibson, C. Akle, M. Marshall, and S. Halligan. Colorectal stenting for malignant and benign disease: Outcomes in colorectal stenting. *Disease of the Colon & Rectum*, 47(7):1201–1207, 2004.

[18] S. Resnick, V. Rome, and R. Vogelzang. Use of a partially deployed wallstent to act as an inferior vena cava filtration device during coil embolization of a high-flow arteriovenous fistula. *Journal of Vascular and Interventional Radiology*, 17:369–372, 2006.

[19] L. Ingles and C. Rabbia. *Stent vascolari*. Edizioni Minerva Medica, 1995.

[20] Kubota Yoshitsugu et al. Covered wallstent for palliation of malignant common bile duct stricture: prospective muilticenter evaluation. *Digestive Endoscopy*, 17(3):218–223, 2005.

[21] Website Boston Scientific: `http://www.bostonscientific.com/`.

[22] R. Reyes, J.M. Carreira, F. Gude, E. Gorriz, L. Gallardo, M.D. Pardo, and M. Hermida. Long-term follow-up of iliac wallstents. *CardioVascular and Interventional Radiology*, 27:624–631, 2004.

[23] R. Rerknimitr, P. Naprasert, P. Kongkam, and P. Kullavanijaya. Trimming a metallic biliary stent using an argon plasma coagulator. *CardioVascular and Interventional Radiology*, 30:534–536, 2006.

[24] R.S. Schartz and K.C. Huber. Restenosis and the proportional neointimal response to coronary artery injury: results in a porcine model. *Journal of the American College of Cardiology*, 19:267–274, 1992.

[25] R. Kornowski, M.K. Hong, F.O. Tio, O. Bramwell, H. Wu, and M. B. Leon. In-stent restenosis: contributions of inflammatory responses and arterial injury to neointimal hyperplasia. *Journal of the American College of Cardiology*, 31:224–230, 1998.

[26] Issel Anne L. Lim. Biocompatibility of stent materials. *MIT Undergraduate Research Journal*, 11, 2004.

[27] Murthy Y. V. Use of stainless steel in medical applications. *Materials & Processes from Medical Devices Conference, 2003 - asminternational.org*, 2003.

[28] Carlo Di Bello. *Biomateriali: introduzione allo studio dei materiali per uso biomedico.* Patron Editore, 2004.

[29] B. W. Nolan, M. L. Schermerhorn, R. J. Powell, E. Rowell, M.F. Fillinger, E.F. Rzucidlo, M.C. Wyers, D. Whittaker, R. M. Zwolak, D. B. Walsh, and J. L. Cronenwett. Restenosis in gold-coated renal artery stents. 42, 2005.

[30] K. Kolandaivelu and E. R. Edelman. Environmental influences on endovascular stent platelet reactivity: an in vitro comparison of stainless steel and gold surfaces. 70A, 2004.

[31] Phynox™ is a trademark of Imphy SA, Paris, France.

[32] Elgiloy® is a registered trademark of Elgiloy Limited Partner-ship, Elgin, IL.

[33] C. O. Clerc, M. R. Jedwab, D. W. Mayer, P. J. Thompson, and J. S. Stinson. Assessment of wrought astm f1058 cobalt alloy properties for permanent surgical implants. *Journal of Biomedical Material Research*, 38:229–234, 1997.

[34] P. Poncin, C. Millet, and J. Chevy. Comparing and optimizing co-cr tubing for stent applications. *Materials & Processes for Medical Deviices Conference*, 2004.

[35] A. Kastrati, J. Mehilli, J. Dirschinger, F. Dotzer, H. Schhlen, F. J. Neumann, M. Fleckenstein, C. Pfafferott, M. Seyfarth, and A. Schmig. Intracoronary stenting and angiographic results strut thickness effect on restenosis outcome (isar-stereo) trial. *Circulation*, 103:2816–2821, 2001.

[36] C. Di Mario, Griffiths H., O. Goktenin, N. Peeters, J. Verbist, M. Bosisers, K. Deloose, B. Heublein, R. Rohde, Kasese V., C. Ilsley, and R. Erbel. Drug-eluting bioabsorbable magnesium stent. *Journal of Interventional Cardiology*, 17(6):391–395, 2004.

[37] W. J. Van der Giessen, A. M. Lincoff, R.S. Schwartz, H. M. M. Van Beusekom, P. W. Serruys, D. R. Holmes, S. G. Ellis, and E. J. Topol. Marked inflammatory sequelae to implantation of biodegradable and nonbiodegradable polymers in porcine coronary arteries. *Circulation*, 94:1690–1697, 1996.

[38] H. Tamai, K. Igaki, E. Kyo, K. Kosuga, A. Kawashima, S. Matsui, H. Komori, T. Tsuji, S. Motohara, and H. Uehata. Initial and 6-month results of biodegradable poly-l-lactic acid coronary stents in humans. *Circulation*, 102:399–404, 2000.

[39] R. Waksman, R. Pakala, P.K. Kuchulakanti, R. Baffour, D. Hellinga, R. Seabron, F.O. Tio, E. Wittchow, S. Hartwig, C. Harder, R. Rohde, B. Heublein, A. Andreae, K.H. Waldmann, and A. Haverich. Safety and efficacy of bioabsorbable magnesium alloy stents in porcine coronary arteries. *Catheterization and Cardiovascular Interventions*, 68:607–617, 2006.

[40] W. J. Buehler, J. V. Gilfrich, and R. C. Wiley. Effect low temperature phase changes on the mechanical properties of alloys near composition ti-ni. *Journal of Applied Physics*, 34:1475–1477, 2006.

[41] Website Oulu University Library: `http://herkules.oulu.fi/`.

[42] Website Memry: `http://www.memry.com/`.

[43] Website Nitinol Devices and Components: `http://www.nitinol.com`.

[44] Wenyi Yan, Chun HuiWang, Xin Ping Zhang, and Yiu-Wing Mai. Effect of transformation volume contraction on the toughness of superelastic shape memory alloys. *Smart Material and Structure*, 11:947–955, 2002.

[45] Mohammed Es-Souni, Es-Souni Martha, and H. Fischer-Brandies. Assessing the biocompatibility of niti shape memory alloys used for medical applications. *Analytical and Bioanalytical Chemistry*, 381:557–567, 2005.

[46] J. Rhyanen. Biocompatibility evaluation of nickel-titanium shape memory metal alloy. 1999. Ph.D. Thesis (Oulu University, Oulu).

[47] T. Duerig and A. Pelton. An overview of superelastic stent design. *Materials Science Forum Vols.*, pages 1–8, 2002.

[48] D.U. Stoeckel, A.U. Pelton, and T.U. Duerig. Self-expanding nitinol stents: material and design considerations. *European Radiology*, 14(2):292–301, 2004.

[49] T.U. Duerig, A.U. Pelton, and D.U. Stoeckel. The use of superelasticity in medicine. *Metall(Germany)*, pages 569–574, 1996.

[50] A.R. Pelton, X.Y. Gong, and T.W. Duerig. Fatigue testing of diamond shaped specimen. *Proceedings of the International Conference on Shape Memory and Superelastic Technologies (Pacific Grove, California, 2003)*, 2003.

[51] S.M. Barrans, Q. Xu, and E.M. Ghurbal. Designing nitinol components using abaqus. *ABAQUS UK Users Group Conference*, 2001.

[52] M. A. Quidwai and D. C. Lagoudas. Numerical implementation of a shape memory allot thermomechanical constitutivemodel using return mapping algorithms. *International Journal for Numerical Methods in Engineering*, 47:1123–1168, 2004.

[53] F. Auricchio and R.L. Taylor. Shape memory alloys: Modeling and numerical simulations of the finite-strain superelastic behavior. *Computer Methods in Applied Mechanics Engineering*, 143:175–194, 1996.

[54] F. Auricchio, R.L. Taylor, and J. Lubliner. Shape-memory alloys: macromodelling and numerical simulations of the superelastic behaviour. *Computer Methods in Applied Mechanics Engineering*, 146:281–312, 1997.

[55] L. Petrini, F. Migliavacca, P. Massarotti, S. Schievano, G. Dubini, and F. Auricchio. Computational studies of shape memory alloy behavior in biomedical applications. *Journal of Biomechanical Engineering*, 127:716–725, 2005.

[56] Hibbit, Karlsson, and Sorensen. Abaqus inc.

[57] J. Lubliner. A simple model of generalized plasticity. *International Journal of Solids and Structures*, 28:769–778, 1991.

[58] F. Auricchio, M. Di Loreto, and E. Sacco. Finite-element analysis of a stenotic artery revascularization through a stent insertion. *Computer Methods in Biomechanics and Biomedical Engineering*, pages 1–15, 2001.

[59] F.D. Whitcher. Simulation of in vivo loading conditions of nitinol vascular stent structures. *Computers and Structures*, 64(5):1005–1011, 1997.

[60] A.M. Wahl. *Mechanical Springs, 2nd edition*, pages 241–254. McGRAW-HILL BOOK COMPANY, 1963.

[61] M. R. Jedwab and Clerc C. O. A study of the geometrical an mechanical properties of a self-expanding metallic stent - theory and experiment. *Journal of Applied Biomaterials*, 1993.

[62] R. Wang and K. Ravi-Chandar. Mechanical Response of a Metallic Aortic Stent-Part I: Pressure-Diameter Relationship. *Journal of Applied Mechanics*, 71:697, 2004.

[63] R. Wang and K. Ravi-Chandar. Mechanical Response of a Metallic Aortic Stent-Part II: A Beam-on-Elastic Foundation Model. *Journal of Applied Mechanics*, 71:706, 2004.

[64] Kim Van Loo. Modellering en simulatie van zelfexpandeerbare draadstents. 2006. Masterthesis, Universiteit Gent.

[65] B. Verhegghe. `http://pyFormex.berlios.de/`.

[66] Hibbit, Karlsson, and Sorensen. Abaqus manual 6.5.

[67] A.R. Pelton, J. DiCello, and S. Miyazaki. Self-expanding nitinol stents: material and design considerations. *Minimally Invasive Therapy and Allied Technologies*, 9(1):107–118, 2000.

[68] D.K. Liang, D.Z. Yang, M. Qi, and W.Q. Wang. Finite element analysis of the implantation of a balloon-expandable stent in a stenosed artery. *International Journal of Cardiology*, 104, 2005.

[69] Website U.S. Food and Drug Administration (center for Devices and radiological Health)-WALLSTENT® Venous Endoprosthesis with Unistep™ Plus Delivery System (12 mm - 16 mm Venous Endoprostheses) – P980033: `http://www.fda.gov/cdrh/pdf/p980033.html`.

[70] G.A. Holzapfel, G. Sommer, and P. Regitnig. Anisotropic mechanical properties of the tissue components in human atherosclerotic plaques. *Journal of Biomechanical Engineering*, 126:657–665, 2004.

[71] G.A. Holzapfel, R. Eberlein, Wriggers P., and H.W. Weizsacker. Large strain analysis of soft biological membranes: Formulation and finite element analysis. *Computer Methods in Applied Mechanics and Engineering*, 132:46–61, 1996.

[72] K. Hayashi and Yosuke. Imai. Tensile property of atheromatous plaque and an analysis of stress in atherosclerotic wall. *Journal of Biomechanics*, 1997.

[73] C. Lally, F. Dolan, and P.J. Prendergast. Cardiovascular stent design and vessel stersses: a finite element analysis. *Journal of Biomechanics*, 2005.

[74] P.J. Prendergast, C. Lally, S. Daly, A.J. Reid, and T.C. Lee. Analysis of prolapse in cardiovascular stents: A constitutive equation for vascular tissue and finite-element modelling. *Journal of Biomechanical Engineering*, 2003.

[75] Erratum to cardiovascular stent design and vessel stresses: A finite element analysis [journal of biomechanics 38 (2005) 15741581]. *Journal of Biomechanics*, 2006.

[76] F. Migliavacca, S. Schievano, G. Ricciardi, and G. Dubini. Does numerical simulation reflect really the mechanical behaviour of a stent? *ESVB-2005,New Technologies in Vascular Biomaterials, Fundamental About Stent*, 2005.

[77] N.V. Salunke, L.D.T Topoleski, J.D. Humphrey, and W.J. Mergner. Compressive stress-relaxation of human atherosclerotic plaque. *Journal of Biomedical Material Research*, 2001.

[78] Ho-Young Song, Tae Sun Shim, Sung-Gwon Kang, Gyoo-Sik Jung, Do Yun Lee, Tae-Hyung Kim, Sangsoo Park, Young Moo Ahn, and Woo Sung Kim. Endovascular repair of traumatic pseudoaneurysm by uncovered self-expandable stenting with or without transstent coiling of the aneurysm cavity. *Radiology*, 213:905–912, 1999.

[79] G. Fischer, H. H. Kramer, J. Stieh, P. Harding, and O. Jung. Transcatheter closure of secundum atrial septal defects with the new self-centering amplatzer septal occluder. *European Heart Journal*, 20:541–549, 1999.

[80] T. Duerig, A. Pelton, and D. Stockel. An overview of nitinol medical applications. *Materials Science and Engineering*, A273-275:149–160, 1999.

[81] Website SMA Cofin 2002: `http://www.unipv.it/dms/auricchio/cofin_02/index.htm`.

[82] Website Creganna Medical Devices: `http://www.creganna.com`.

[83] Website ASM international- Material Information Society: `http://www.asminternational.org`.

[84] Endostab™ is a trademark of ENDOSMART Gesellschaft fr innovative Medizintechnik mbH ,Stutensee, Germany.

Appendix A

Materials

A.1 Cold work

A material is considered to be cold worked if its grains are in a distorted condition after plastic deformation is completed. All the properties of a metal that are dependent on the lattice structure are affected by plastic deformation or cold working. The following properties are affected by cold work significantly:

- Tensile Strength;
- Hardness;
- Yield Strength;
- Ductility.

Tensile strength, yield strength and hardness are increased, while ductility is decreased. Although both strength and hardness increase, the rate of change is not the same. Hardness generally increases most rapidly in the first 10 percent reduction (cold work), whereas the tensile strength increases more or less linearly. The yield strength increases more rapidly than the tensile strength, so that, as the amount of plastic deformation is increased, the gap between the yield and tensile strengths decreases. This is important in certain forming operations where appreciable deformation is required. As shown in Fig. A.1, for example, the load must be above the yield point to obtain appreciable deformation but below the tensile strength to avoid failure. If the gap is narrow, very close control of the load is required.
The cold work act on the size of the grains within a material. It has an effect on the strength of the material. The boundary between grains acts as a barrier to dislocation movement and the resulting slip because adjacent grains have different orientations. Since the atom alignment is different and slip planes are discontinuous between grains. The smaller the grains, the shorter the distance atoms can move along a particular slip plane. Therefore, smaller grains improve the strength of a material. The size and number of grains within a material is controlled by the rate of solidification from the liquid phase.

Overview of nitinol medical applications

Nowadays, since its unique mechanical properties, its good compatibility and high corrosion resistance, Nitinol has a wide range of medical applications. In this section, we propose a brief review of the main applications, highlighting the mechanical aspects involved in the performance of each device. In fact we do not want to provide a extremely complete review of Nitinol medical application but just underline the capability of this material and its usefulness in the field of medical devices. Finally we will focus the attention on Nitinol stents.

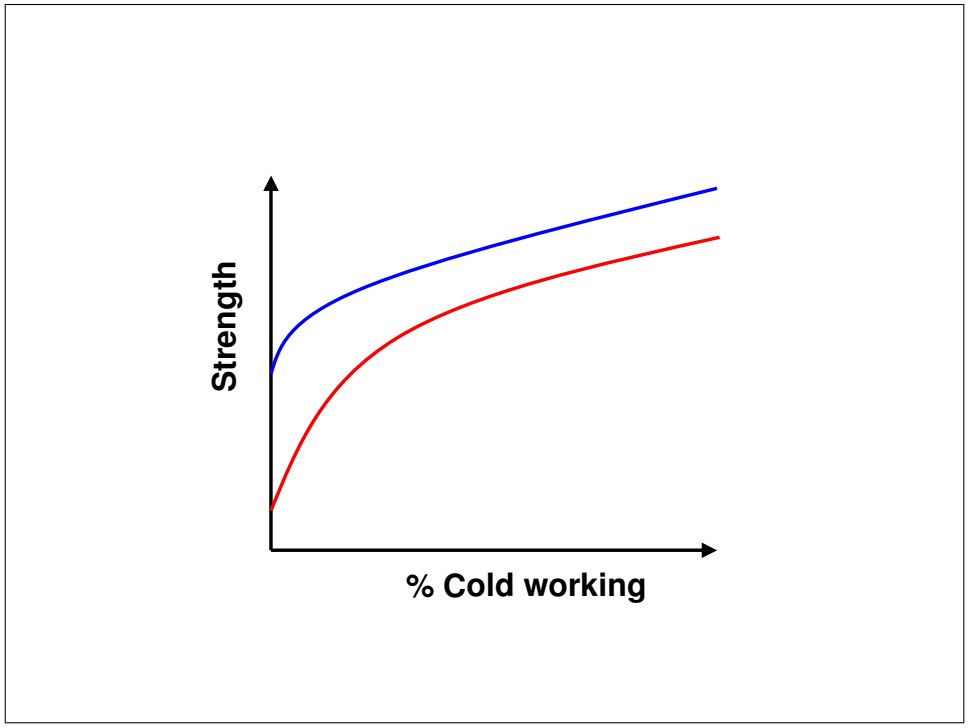

Figure A.1: Effect of cold working on tensile and yield strength of copper.

Since the actual medical procedures require less and less non-invasive approaches, the use of Nitinol and of its flexibility is very useful in complex operations performed by trocars[1] or percutaneous approach. For example, the atrial septal defect occlusion system (ASDOS) is a complex device which involves the concept of elastic deployment performed by features of Nitinol[79] (see Fig. A.2).
The nitinol SME effect is the basis of Simon vena cava filter's deployment (see Fig. A.3). The goal of this device is to filter blood clots in the vena cave vein. It employs nitinol allowing it to be introduced in a straight form via a small sheath when cooled by saline solution flow through the catheter. It transforms instantly into its predetermined filter shape at body temperature in fact the bloodstream promotes the heating of the filter that returns to its former shape. The SMA thermal deployment is used also in orthopedic applications. The bone fracture can be treated applying nitinol bones plates. They accelerate the bone healing process cause thanks to their shape memory effect, when heated these plates tend to recover their former shape, exerting a constant force that tends to join parts separated by fractures (see Fig. A.4(a)). The shape memory vertebrae spacer is another example of application of nitinol in the orthopedic field. This device is compressed in martensitic phase assuming a reduced shape to allow an easier insertion between the vertebrae. When it is inserted in the body, it recovers its original shape applying a compressive constant load on the vertebrae (see Fig. A.4(b)).
Another important mechanical feature of Nitinol is the kink resistance. Medical devices as catheters, angioplasty guidewires, biopsy forceps (see Fig. A.5(a)), medical shafts, take advantage of the nitinol kink resistance improving their ability to maintain its cross sectional profile during compressive deformation. When kink resistance is high, the physician can rely on the device shaft to negotiate difficult routes without fracturing or breaking[82]. For example, in laparoscopic surgery a flexible, steer able tip for an endoscopic camera can avoid changing the camera system during an operation. Fig. A.5(b)

[1] small portals into the body.

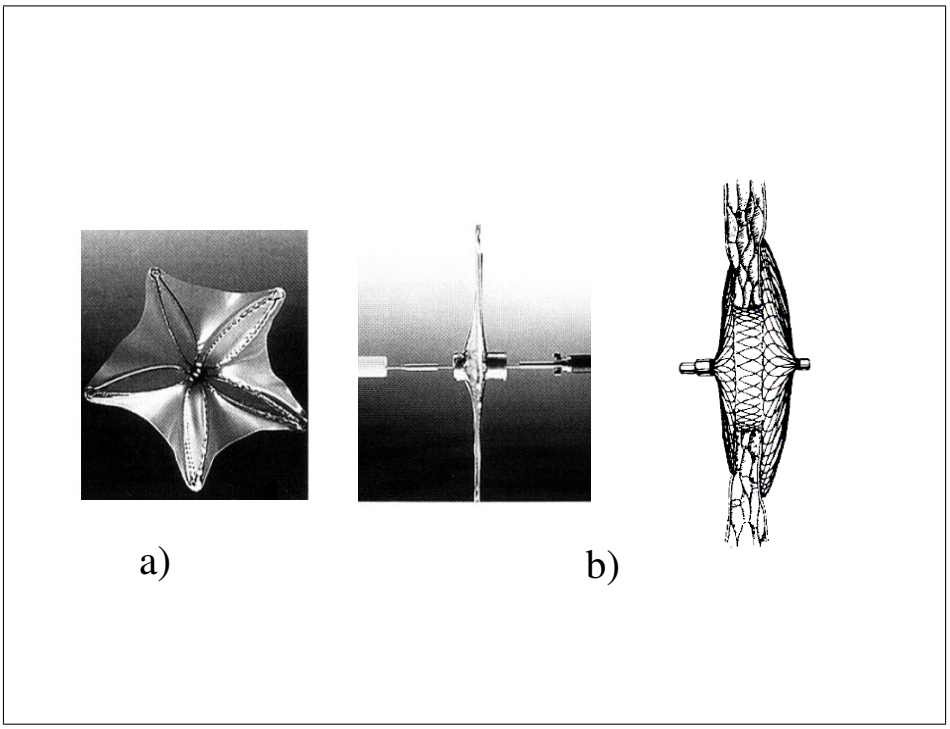

Figure A.2: a) The ASDOS includes nitinol wires in a polyurethane film; b) the two umbrellas are screwed together to form a patch in order to occlude the atrial defect[80][79].

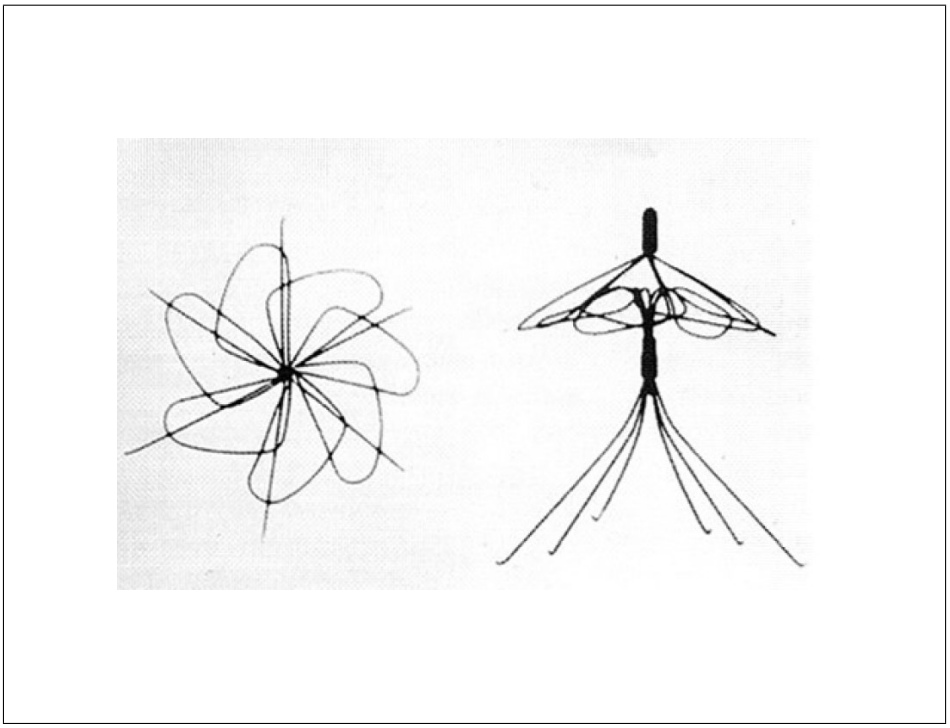

Figure A.3: The Simon vena cava filter[80].

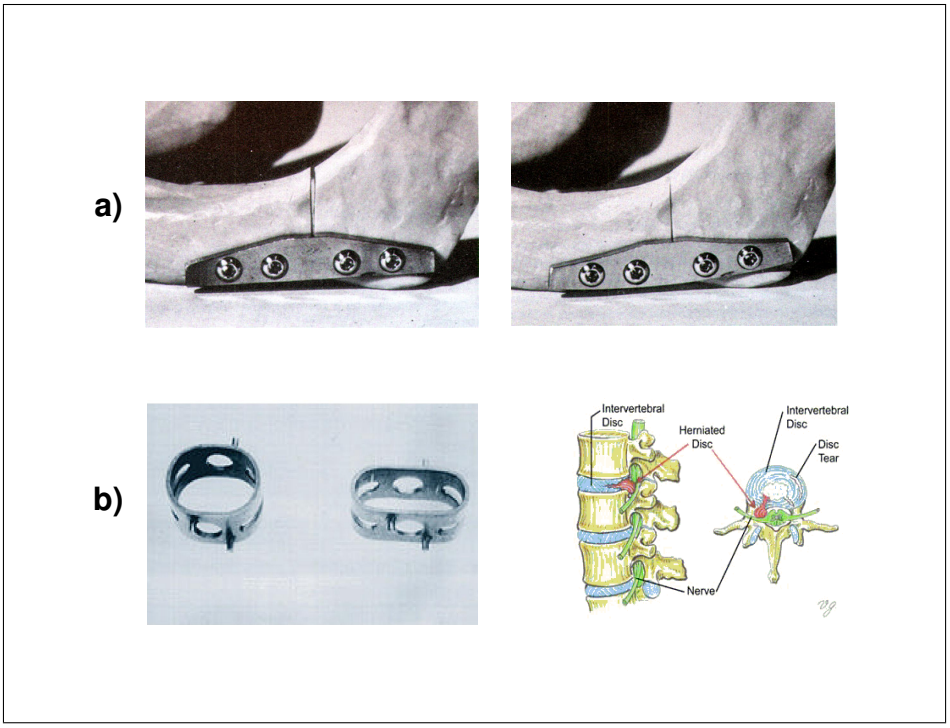

Figure A.4: Orthopedic nitinol applications: a)bone plates; b) spinal vertebrae spacer[81].

shows the flexible distal tip made of NiTi and the steerable endoscopic camera. The aim of this device is to have a short tip, which can be deflected up to 90 in one direction but still be rather stiff in all other directions. The use of Nitinol allows to reduce the induced tension at the bending zones and consequently to increase bending cycles[83].
The superelastic nitinol provides also a constant unloading stresses over large strains. This feature is used by orthodontic archwire; in fact the nitinol wires are able to move with the teeth providing a constant force over a very wide range of teeth's displacement (see Fig. A.6(a)). Instead using other materials (i.e. Stainless steel), the force relaxes with the teeth displacement. The endoscopic stabilizer for bypass surgery with a joint like behavior is another example of a flexible, superelastic unit is made of NiTi. During bypass operations on the beating heart, stabilizers must be used causing a localized immobilization of the heart. Thus, the stabilizer must be rigid enough to immobilize the vascular section desired. ENDOSTAB™[84] is developed, using the effect of the constant force (see Fig. A.6(b)).
Very interesting it is also the medical use of porous NiTi. As shown in Fig. A.7, the human bone structure is very similar to the structure of a porous NiTi foam. In addition, the NiTi foam provide also a strain capability of about 3-4% so this could be the ideal material for bone implants (i.e. dental pins or hip implants). Infact the material can easily adapt to the huge amount of movement inside the bones during the body movement. Of course, many investigations are required to understand the biocompatibility of this material[83].

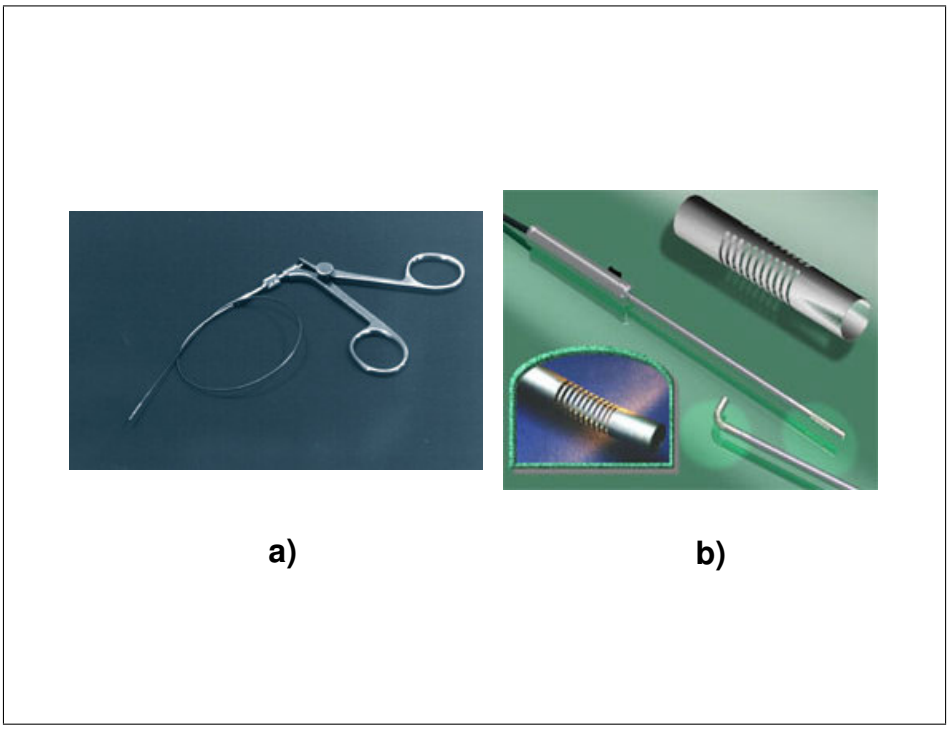

Figure A.5: Nitinol kink resistance application: a)biopsy forceps[81]; b) tip for endoscopic camera[83].

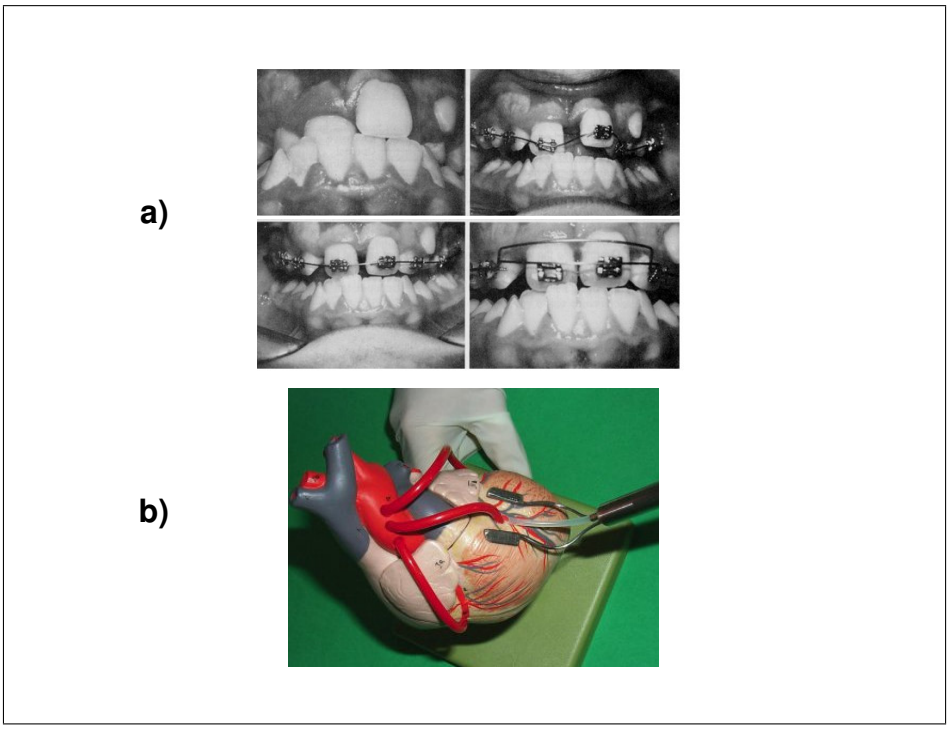

Figure A.6: Nitinol constant stress application: a)Orthodontic archwires for the correction of tooth malposition[81]; b)Endostab ™[84].

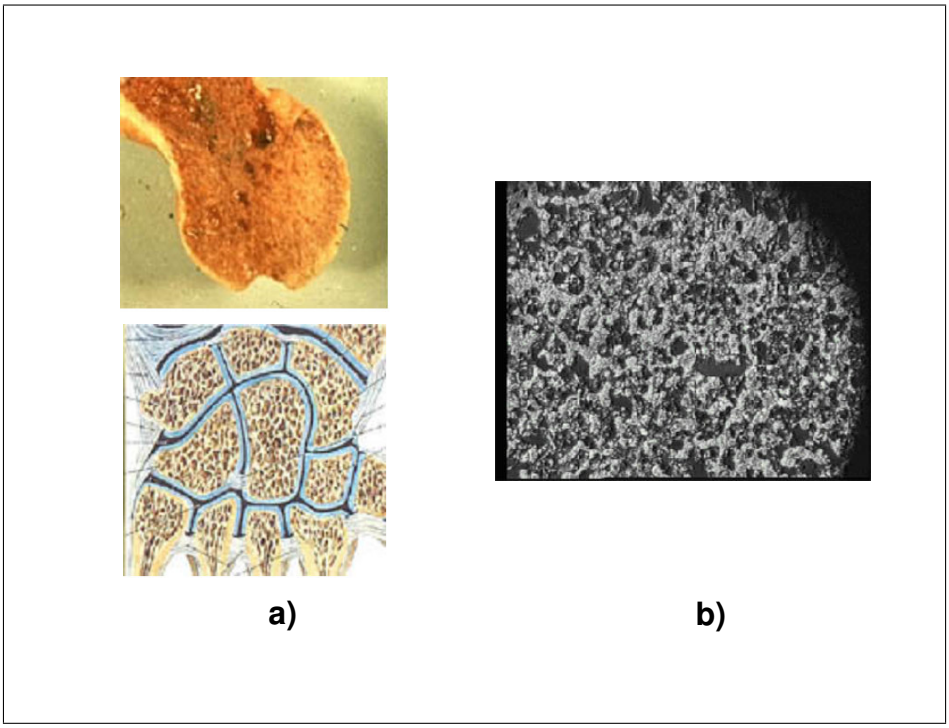

Figure A.7: a) bone structure; b) Nitinol foam structure[83].

Appendix B

von Mises stress

B.1 Transverse shear stiffness

Using the Umat for nitinol superelastic, the transverse shear stiffness must be defined. So when we use the UMAT for nitinol, we will define the transverse shear stiffness as follows:

- $K_{\alpha 3}$=kGA with $\alpha = 1, 2$;

where **G** is the elastic shear modulus or moduli and **A** is the cross-sectional area of the beam section and **k** is a constant. For circular section **k** is defined as 0.89[66]. In our simulations, since the stent wire diameter is 0.17 μm (see Table 3.1), the circular cross-section area is 0.0227 mm^2 and the shear modulus **G** of the Nitinol is 13488 MPa, K_{13} and K_{23} result 272.5.

B.2 Beam element cross-section orientation

The orientation of a beam cross-section is defined in terms of a local, right-handed axis system.

The orientation of a beam cross-section is defined in ABAQUS in terms of a local, right-handed (t,n_1,n_2) axis system, where:

- t the tangent to the axis of the element, positive in the direction from the first to the second node of the element;
- n_1 and n_2 are basis vectors that define the local 1- and 2-directions of the cross-section.

n_1 is referred to as the first beam section axis and n_2 is referred to as the normal to the beam as shown in Fig. B.1.

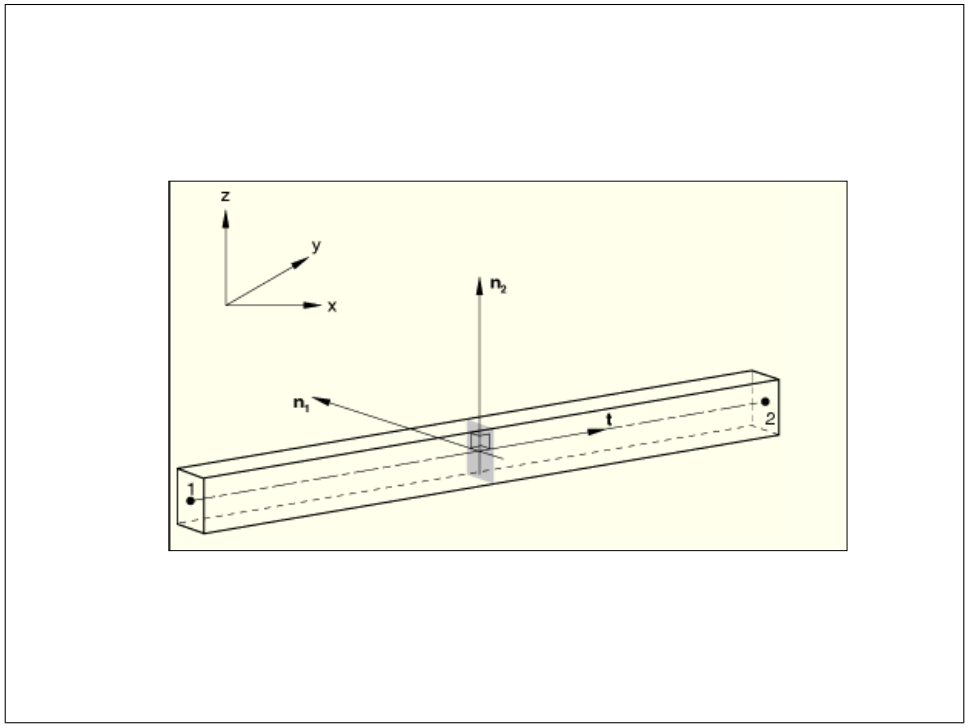

Figure B.1: Beam element cross-section orientation in Abaqus[66].

In our simulations we use 3-D beam element For beams in space the approximate direction of must be defined directly as part of the beam section definition or by specifying an additional node off the beam axis as part of the element definition. This additional node is included in the element's connectivity list.

If an additional node is specified, the approximate direction of is defined by the vector extending from the first node of the element to the additional node.

If is defined directly for the section and an additional node is specified, the direction calculated by using the additional node will take precedence.

If the approximate direction is not defined by either of the above methods, the default value is (0.0, 0.0, 1.0).

This approximate n_1-direction may be used to determine the n_2-direction (discussed below). Once the n_2-direction has been defined or calculated, the actual n_1-direction will be calculated as n_2 X t, possibly resulting in a direction that is different from the specified direction.

Since in the preprocessing, the additional node in the element is not defined, we use the default value.

The Fig. B.2 shows the tangent orientation of the beam elements in the wirestent model when the default value of n_1 is adopted.

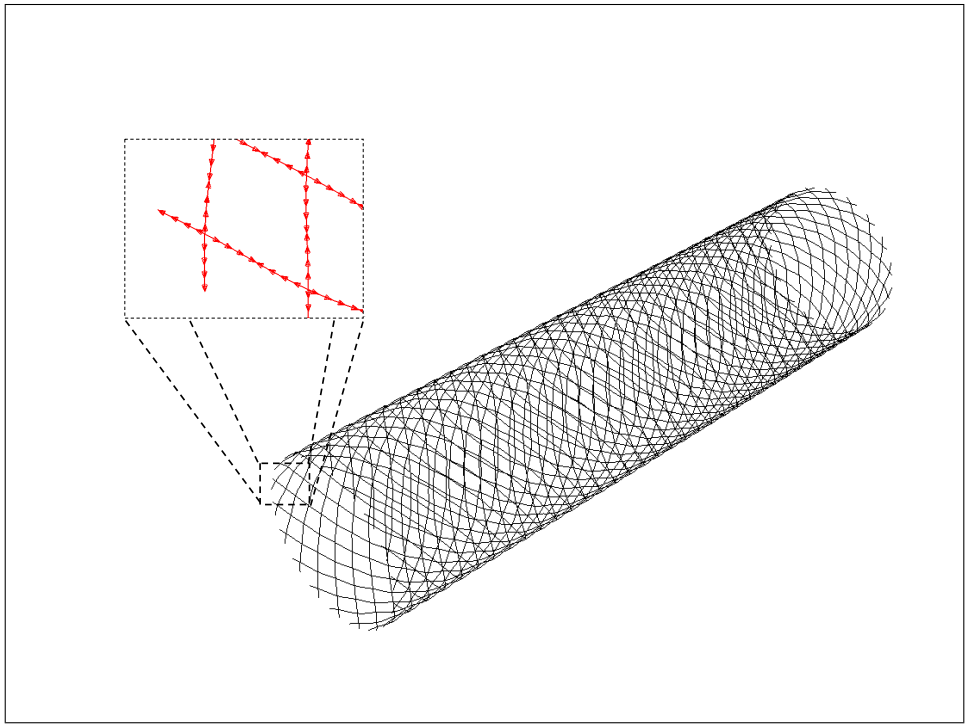

Figure B.2: Beam element cross-section orientation in Abaqus[66].

The tangent orientation highlights a wrong relative orientation of the local coordinate system of beam elements. This drawbacks could be the cause of the contact problem but further investigation in this direction are required. To avoid this problem an extra node has to be defined during the py Formex preprocessing when the geometry of stent (and consequently the nodes position in space) is created.

Beam element cross-section orientation

The beam section behavior is defined in terms of the response of the beam section to stretching, bending, shear, and torsion. It may or may not require numerical integration over the section and can be linear or nonlinear (as a result of nonlinear material response).

In Abaqus standard two types of beam section are available:

- beam section;
- beam general section.

When a beam section integrated during the analysis is used, ABAQUS integrates numerically over the section as the beam deforms, evaluating the material behavior independently at each point on the section. This type of beam section should be used when the section nonlinearity is caused only by nonlinear material response.

Instead when a general beam section is used, ABAQUS precomputes the beam cross-section quantities and performs all section computations during the analysis in terms of the precomputed values. This method combines the functions of beam section and material descriptions (a material definition is not needed). A general beam section should be used when the beam section response is linear or when

it is nonlinear and the nonlinearity arises from more than just material nonlinearity, such as in cases when section collapse occurs.

Since the nitinol has a very non linear mechanical response, it is necessary to use an ad hoc built subroutine (Umat in ABQ/STD) to implement its mechanical behavior. Consequently it requires to use a beam section integrated during the analysis. The input file usage required for nitinol umat in 3-D (for a beam with circular cross section having radius r=0.085) is:
*Beam Section, elset=WIRES, material=ABQ_super_elastic_1,section=CIRC
0.085
0.,0.,-1.
*transverse shear stiffness
272.5,272.5,0.25

B.3 Open-coiled helical springs with large deflection

In this section, we will provide the equations proposed by the spring's theory by Wahl (Chapter 20[60]).

When an open-coiled helical spring is subject to an axial tension giving a large deflection, there is a tendency for the coils to undwind; in other words, one end of the spring tends to rotate with respect to the other about the spring axis. If this rotation can take place freely and without restraint, we have the condition of ana axially loaded spring as shown in Fig. B.3(a).

If, hovewer, the ends are prevented from rotation by friction (as usually the case in compression springs) or by clamping, end moments acting about the axis of the coil are set up which tend to prevent this rotation. For this reason it is necessary to distinguish two cases:

- ends free to rotate;
- ends fixed against rotation.

The discussion will be limitated to the round wires.

B.3.1 Springs with ends free to rotate

Calculation of the stress

Let us consider the open-coiled helical spring with axial load showed in Fig. B.3.

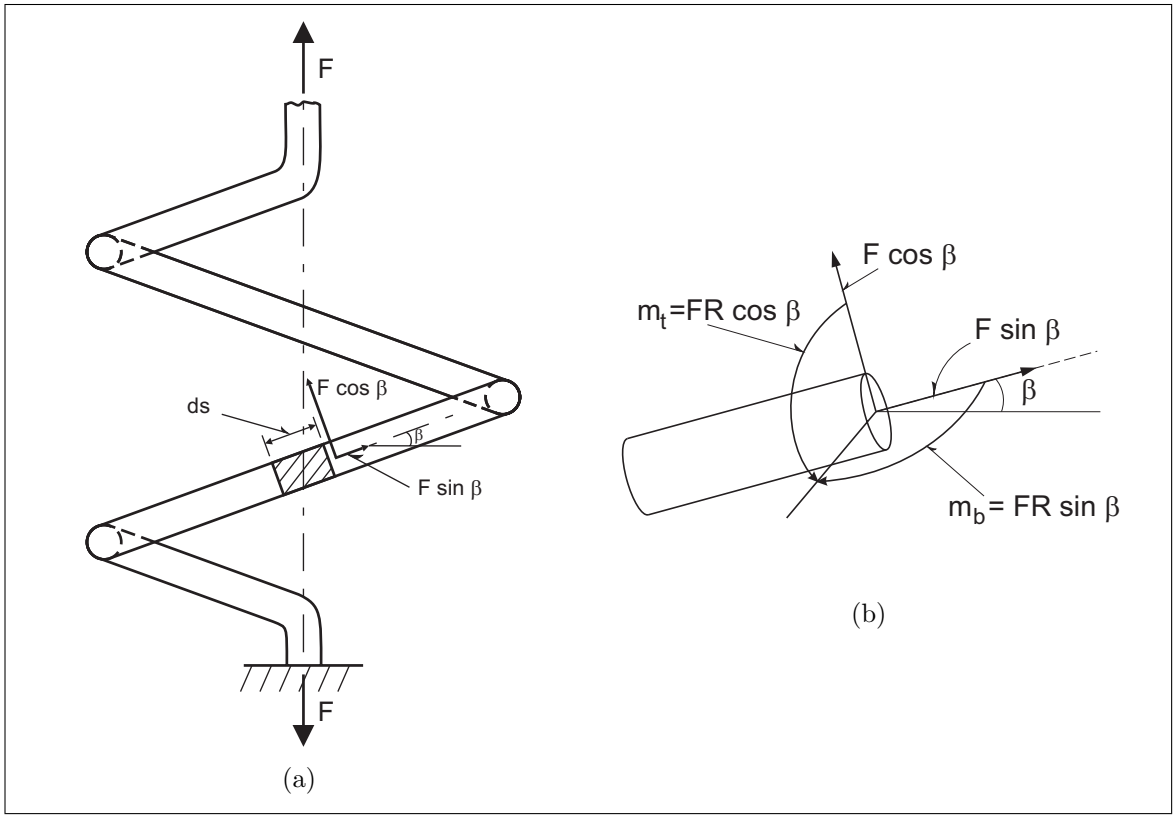

Figure B.3: Open-coiled helical spring with axial load[60].

If β is the helix or pitch angle and r the current coil radius after deflection, the force and the moments acting on the element A of length dS (see Fig. B.3(b)) will be:

- a bending moment $Fr\ sin\ \beta$;
- a twisting moment $Fr\ cos\ \beta$;
- a shear force $F\ cos\ \beta$;
- a tension force $F\ sin\ \beta$;

So the shear stress τ due to the twisting moment $F\ cos\ \beta$ and the bending moment σ due to the bedning moment $F\ sin\ \beta$ will be:

$$\tau = \frac{16Frcos\beta}{\pi d^3} \tag{B.1}$$

$$\sigma = \frac{32Frcos\beta}{\pi d^3} \tag{B.2}$$

$$\tag{B.3}$$

Calculation of the deflection

The variation from the initial pitch angle β_0 to the current pitch angle β, during the spring deflection due to the axial load, leads a change in the curvature and twist of the spring:

$$\Delta\kappa = \frac{\cos^2\beta}{R} - \frac{\cos^2\beta_0}{R_0} \tag{B.4a}$$

$$\Delta\theta = \frac{\sin\beta\,\cos\beta}{R} - \frac{\sin\beta_0\,\cos\beta_0}{R_0} \tag{B.4b}$$

The bending moment m_b causing the change in curvature must be equal to the flexural rigidity multiplied by the change in curvature $\Delta\kappa$:

$$m_b = -F\,R\sin\beta = -EI\left(\frac{\cos^2\beta}{R} - \frac{\cos^2\beta_0}{R_0}\right) \tag{B.5}$$

Where E is the Youngs modulus and I the inertia of the cross-section. Thus, F can be defined as:

$$F = F_b = \frac{EI}{R\sin\beta}\left(\frac{\cos^2\beta}{R} - \frac{\cos^2\beta_0}{R_0}\right) \tag{B.6}$$

The same approach can be followed to obtain F form the change $\Delta\theta$ of the spring's twist, so:

$$m_t = F\,R\cos\beta = GI_p\left(\frac{\sin\beta\,\cos\beta}{R} - \frac{\sin\beta_0\,\cos\beta_0}{R_0}\right) \tag{B.7}$$

$$F = F_t = \frac{GIp}{R\cos\beta}\left(\frac{\sin\beta\,\cos\beta}{R} - \frac{\sin\beta_0\,\cos\beta_0}{R_0}\right) \tag{B.8}$$

Where GI_p is the torsional rigidity of the round wire.

B.3.2 Springs with ends fixed against rotation

Calculation of the deflection

Where the spring ends are fixed (i.e. there is no rotation about the axis of the spring during deflection), it is necessary to take into account the moment acting tat the spring ends which prevents the coils form unwinding. Considering the Fig. B.3 and Fig. B.4, if a moment M_0 and a load F are acting on the spring simultaneously, the bending and the twisting moments m_b and m_t acting on the wire will be:

$$m_b = M_0\cos\beta - F\,R\,\sin\beta \tag{B.9}$$

$$m_t = M_0\sin\beta + F\,R\,\cos\beta \tag{B.10}$$

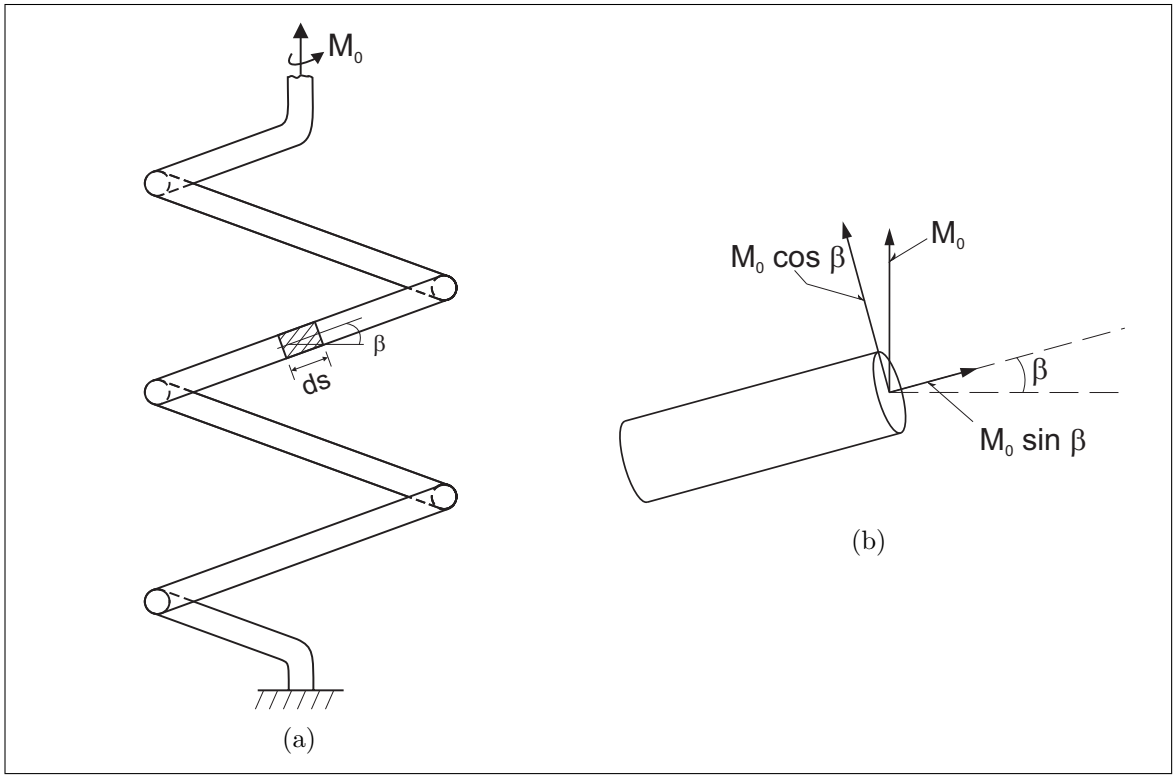

Figure B.4: Open-coiled helical spring with axial load[60].

As previously discussed for the spring withe end free to rotate the change in curvature $\Delta\kappa$ and in twist $\Delta\theta$ will be:

$$\Delta\kappa = \frac{m_b}{EI} = \frac{\cos^2\beta}{R} - \frac{\cos^2\beta_0}{R_0} \tag{B.11}$$

$$\Delta\theta = \frac{m_t}{GI_p} = \frac{\sin\beta\,\cos\beta}{R} - \frac{\sin\beta_0\,\cos\beta_0}{R_0} \tag{B.12}$$

Substituing B.9 and B.10 in Eqs. B.11 and B.12 F and M_0 will be:

$$F = \frac{GI_p\cos\beta}{R}\left(\frac{\sin\beta\cos\beta}{R} - \frac{\sin\beta_0\,\cos\beta_0}{R_0}\right) - \frac{EI\sin\beta}{R}\left(\frac{\cos^2\beta}{R} - \frac{\cos^2\beta_0}{R_0}\right) \tag{B.13}$$

$$M_0 = GI_p\sin\beta\left(\frac{\sin\beta\,\cos\beta}{R} - \frac{\sin\beta_0\,\cos\beta_0}{R_0}\right) + EI\cos\beta\left(\frac{\cos^2\beta}{R} - \frac{\cos^2\beta_0}{R_0}\right) \tag{B.14}$$

Calculation of Equivalent Stress

The same procedure followed incase of ends free to rotate can be followed.

B.4 von Mises criterion

The von Mises stress is a stress quantity that is proportional to the the strain energy density associated with a change in shape (with a zero volume change) at a material point is the von-Mises stress which

is defined by:

$$\sigma_{VM} = \frac{1}{\sqrt{2}}\sqrt{(\sigma_x-\sigma_y)^2+(\sigma_y-\sigma_z)^2+(\sigma_z-\sigma_x)^2+6(\tau_{xy}^2+\tau_{yz}^2+\tau_{zx}^2)} \quad \text{(B.15)}$$

The von Mises stress is a scalar measure of the stress state (the normal and shear stresses) at any point within a body.

B.5 Matlab script for Phynox

Script B.1: mc_picture/appendix–3/Phynox_085.m

```
%-------------------------------------------------------------------------
%---------- Stress equivalent stresses in Phynox stent wire --------------
%-------------------------------------------------------------------------

%loading of workspace

clear all                               %current workspace cleaning
load('Phynox_085.mat')                  %loading of the workspace with the data from FEM

%stent geometrical properties

n=36;                                   %number of wires
d=0.17;                                 %wire diameter
D0=diam_avg_phynox(1,2);                %initial stent average diameter

%stent material properties

%inertia
I=pi*d^4/64;
Ip=2*I;                 %polar inertia

%phynox material properties
ni=0.33;
E=220000;
G=E/(2*(1+ni))

%pitch angle: input of the analytical model
beta_degree_p_b_c=[34:1:89];        %pitch angle (deg.)
beta_p_b_c=beta_degree_p_b_c./57.2;  %pitch angle (rad)
beta0_p_b_c=beta_p_b_c(1,1);%34     %initial pitch angle

%Analytical model
D_p_b_c=(D0*cos(beta_p_b_c))./cos(beta0_p_b_c); %costraint due to the wire friction in
      the crossing points
r_p_b_c=D_p_b_c/2;                                  %current radius
r0=D0/2;                                            %initial radius
F1_p_b_c=G*Ip.*((cos(beta_p_b_c).*sin(beta_p_b_c)./r_p_b_c)-(sin(beta0_p_b_c)*cos(
     beta0_p_b_c)/r0));
F2_p_b_c=E.*I.*((cos(beta_p_b_c).^2./r_p_b_c)-cos(beta0_p_b_c)^2/r0);
Mt_p_b_c=F1_p_b_c;                                  %twisting moment
Mb_p_b_c=F2_p_b_c;                                  %bending moment
tau_p_b_c=(16.*Mt_p_b_c)/(pi*d^3);                  %shear stress
sigma_p_b_c=(32.*Mb_p_b_c)/(pi*d^3);                %bending stress
sigma_VNM_p_b_c=sqrt(sigma_p_b_c.^2+3.*(tau_p_b_c.^2)); %von Mises equivalent stress

%stress treshold according von Mises criterion
sigmay=1578;                                    %yield stress
t_p_b_c=diam_avg_phynox(:,1);
vector=ones(length(t_p_b_c));
tresca_limit=sigmay/2.*vector;
VNM_limit=sigmay.*vector;                       %treshold

```

```
51 %plots
52
53 close all
54 %Von Mises (nodes:2895,6677,9573,13682,17452) comparison analytical and FEM
55 figure (1)
56 plot(diam_avg_phynox(:,2),Mises_p_b_c_220(:,2),'r+-')
57 hold on
58 plot(D_p_b_c,sigma_VNM_p_b_c,'bx-')
59 hold on
60 plot(diam_avg_phynox(:,2),VNM_limit,'k--')
61 title('Comparison:Von Mises equivalent stress in phynox stent wire')
62 grid on
63 legend('F.E.M','analytical','maximum allowable stress')
64 xlabel('Stent diameter,De [mm]')
65 ylabel('Equivalent stress [MPa]')
```

B.6 Matlab script for Nitinol

Script B.2: mc_picture/appendix–3/Niti_085_timo.m

```
1  %-------------------------------------------------------------------------
2  %---------- Stress equivalent stresses in Nitinol stent wire -------------
3  %-------------------------------------------------------------------------
4
5  %workspace loading
6  clear all                                %current workspace cleaning
7  load('Niti_085_timo.mat')                %loading of the workspace with FEM data
8
9  %stent geometrical properties
10 n=36;                                    %number of wires
11 d=0.17;                                  %wire stent diameter
12 D0=diam_avg_niti(1,2);                        %initial average stent diameter
13                                          %we impose that the initial average
14                                          %diameter is the same
15
16 %stent material properties
17
18 %inerzia
19 I=pi*d^4/64;
20 Ip=2*I;
21
22 %Nitinol material properties
23
24 ni=0.33;
25 E_n=35877;
26 G_n=E_n/(2*(1+ni))
27
28 %Pitch angle: the input of the analytical model
29
30 beta_degree_n_b=[34:1:89];          %pitch angle (deg.)
31 beta_n_b=beta_degree_n_b./57.2;     %pitch angle (rad.)
32 beta0_n_b=beta_n_b(1,1);            %initial pitch angle (34 )
33
34 %analytical model
35
36 D_n_b=(D0*cos(beta_n_b))./cos(beta0_n_b); %costraint due to the wire friction in the
       crossing points
37 r_n_b=D_n_b/2;                             %current average radius
38 r0=D0/2;                                   %initial average radius
39 F1_n_b=G_n*Ip.*((cos(beta_n_b).*sin(beta_n_b)./r_n_b)-(sin(beta0_n_b)*cos(beta0_n_b)/
       r0));
40 F2_n_b=E_n.*I.*((cos(beta_n_b).^2./r_n_b)-cos(beta0_n_b)^2/r0);
41 Mt_n_b=F1_n_b;                             %twisting moment
42 Mb_n_b=F2_n_b;                             %bending moment
```

```
43  tau_n_b=(16.*Mt_n_b)/(pi*d^3);              %equivalent shear stress
44  sigma_n_b=(32.*Mb_n_b)/(pi*d^3);            %bending stress
45  sigma_VNM_n_b=sqrt(sigma_n_b.^2+3.*(tau_n_b.^2)); %von Mises equivalent Stress
46
47  %treshold according von Mises' criterion
48
49  sigmay_niti=489;                             %yield stress
50  t_n_b=diam_avg_niti(:,1);
51  vector_n_b=ones(length(t_n_b),1);
52  VNM_limit_n_b=sigmay_niti.*vector_n_b;       %strees treshold
53
54
55  %plots
56
57  close all
58
59  %comparison Von Mises data from FEM and analytical
60  figure (1)
61  plot(diam_avg_niti(:,2),Mises_niti_35877(:,2),'r+-')%data from FEM
62  hold on
63  plot(D_n_b,sigma_VNM_n_b,'bx-')                %analytical model
64  hold on
65  plot(diam_avg_niti(:,2),VNM_limit_n_b,'k--')
66  hold on
67  title('Comparison:Von Mises equivalent stress in Nitinol stent wire')
68  grid on
69  legend('F.E.M','analytical','maximum allowable stress')
70  xlabel('Stent diameter [mm]')
71  ylabel('Equivalent stress [MPa]')
```